Quantitative modeling of nitrogen cycling along the river continuum:

Streambed sediments, reservoirs, and isotopes

by

Zahra Akbarzadeh

A thesis
presented to the University of Waterloo
in fulfillment of the
thesis requirement for the degree of
Doctor of Philosophy
in
Earth Sciences

Waterloo, Ontario, Canada, 2018

Examining Committee Membership

External Examiner	Dr. Sergei Katsev Professor Large Lakes Observatory & Department of Physics University of Minnesota, Duluth
Supervisor	Dr. Philippe Van Cappellen Professor, Canada Excellence Research Chair Department of Earth and Environmental Sciences University of Waterloo
Co-supervisor	Dr. Fereidoun Rezanezhad Assistant Professor Department of Earth and Environmental Sciences University of Waterloo
Internal-external Member	Dr. William Taylor Distinguished Professor Emeritus Department of Biology University of Waterloo
Internal Member	Dr. Nandita Basu Associate Professor Department of Earth and Environmental Sciences University of Waterloo
Other Member(s)	Dr. Anniet Laverman Chargé de Recherche Centre national de la recherche scientifique University of Rennes

Author's Declaration

This thesis consists of material all of which I authored or co-authored: see Statement of Contributions included in the thesis. This is a true copy of the thesis, including any required final revisions, as accepted by my examiners.

I understand that my thesis may be made electronically available to the public.

Statement of Contribution

This thesis consists of co-authored papers. As first author of each paper, I was primarily responsible of the study design and its execution. The following summarizes the contributions of the co-authors of each chapter.

Chapter 2

Philippe Van Cappellen (PVC), Anniet Laverman (AL), and I designed the study. Babak Shafei (BS) developed the first version of the early diagenetic model, which I then expanded by incorporating a comprehensive nitrogen reaction network. Anniet Laverman (AL), Mélanie Raimonet (MR), and Eric Viollier (EV) designed and implemented the fieldwork and the incubation experiments in France. I wrote the paper with help of PVC, Fereidoun Rezanezhad (FR), AL and MR.

Chapter 3

I designed the study with input from PVC and AL. I developed the computer code and run the simulations. I wrote the chapter with input from PVC.

Chapter 4

Taylor Maavara (TM) and I developed the nitrogen reservoir model. I performed the research and analyzed the data with help from PVC and TM. PVC, TM and I wrote the paper.

Abstract

The vast release of anthropogenically produced reactive nitrogen (N) into the environment, by agricultural activities, energy production and municipal wastewater, has led to a variety of consequences for atmospheric, terrestrial, and aquatic ecosystems and human health. In particular, elevated loadings of N have been documented in many rivers worldwide. However, the fate of this reactive N in the different biogeochemical compartments of the river system is yet to be fully investigated. Elevated concentrations of N in the river system influence the interactions at the sediment-water interface (SWI), which can significantly impact the water quality and primary productivity in the river system and receiving water bodies.

In addition, humans have impacted the N cycling in rivers by dam construction. The damming of rivers represents one of the most profound human interventions in the freshwater cycle, with substantial implications for water security, energy production, biodiversity and aquatic ecosystem functioning. River damming, on the rise during the last 60 years, shows no sign of abating in the coming decades. However, since the beginning of the 20th century, the geographical locations of the new dams have increasingly spread to the rapidly developing parts of the world, in particular, Southeast Asia and South America.

This thesis aims to simulate the biogeochemical cycling of N along the river continuum across different scales so as to quantitatively predict the modifications caused by anthropogenic activities. At the local to regional scale, the role of bottom sediments in the nitrite budget of a European river system, impacted by urban and agricultural activities, is investigated using an early diagenesis model. At the global scale, the changes in the past, present and future riverine fluxes of N due to river damming are estimated and analyzed.

To describe the fate of reactive N in streambed sediments, a comprehensive reactive-transport model is developed. The model explicitly represents the production and consumption of nitrite, a

reactive intermediate in the N cycle, through nitrification, denitrification, dissimilatory nitrate reduction to ammonium (DNRA) and anammox. Although nitrite is typically considered to be a short-lived compound, elevated concentrations of it have been observed at relatively high concentrations in freshwaters aquatic systems, raising concerns due to its toxicity for humans, animals and plants.

Among other impacted rivers, nitrite accumulation has been observed in the Seine, a N polluted river with high agricultural and urban inputs in France, raising questions about its sources and fate. The early diagenetic model is employed to assess the role of sediments in releasing nitrite to the overlying water or removing it at two different sampling locations and two different times of the year. Four datasets collected in summer and fall, upstream and downstream of the largest wastewater treatment plant (WWTP) serving the Paris conurbation area, are used to test the model. The datasets include pore water profiles plus benthic exchange fluxes of nitrate, nitrite and ammonium at the SWI, measured during core incubation experiments. The model results emphasize the major role of the WWTP for the nitrite budget in river, not only due to the direct release of nitrite through effluent discharges, but also by supplying the high loads of labile organic carbon (C) that enhance heterotrophic activity in the sediments.

In the next step, the reactive-transport model is expanded by incorporating the N isotopic compositions of nitrate, nitrite, ammonium and organic N, and accounting for the isotopic fractionations along the N transformation pathways. The model is used to simulate the temporal variation in isotopic composition of N species under non-steady state conditions at the SWI during incubation experiments. A sensitivity analysis is performed, by applying different scenarios, to provide insight into the main controls on the nitrite isotopic compositions at the SWI. The results highlight the major role of oxygen on the variations of the isotopic values of N species and illustrate the effects of different N transformations on the isotopic compositions of N species at the SWI. The model will be applied in

upcoming sediment incubation experiments with Seine River sediments that will be carried out by our French colleagues.

Finally, I assess the impacts of damming on the global riverine nitrogen fluxes by estimating N burial in sediments of dam reservoirs and gaseous emissions through denitrification. Moreover, I estimate global N fixation in reservoirs as a source of new N to these systems. A process-based N mass balance model is developed to represent the biogeochemical cycling of N in reservoirs. Using Monte Carlo simulations, the model is scaled up to generate a virtual database of dams. From this dataset, I derive two global relationships between N elimination in reservoirs, by either denitrification or burial, and the hydraulic residence time. These relationships are then combined with N loads to rivers obtained from the Global-NEWS model and N fixation fluxes calculated for dams included in databases for existing and future reservoirs. The results demonstrate that, globally, denitrification and burial in dam reservoirs exceed N fixation, and dam reservoirs therefore act as a sink of N worldwide. I estimate that denitrification and burial in reservoirs eliminated 7% of N loading to the global river network in the year 2000. This percentage is predicted to double by 2030, mainly because of the current boom in dam building.

This thesis provides new tools to make more detailed assessments of the role of bottom sediments in the nitrite budget of rivers and give insights on the processes that affect the direction and magnitude of the nitrite fluxes at the SWI. Additionally, I present the first estimation of global N fixation in dam reservoirs. By coupling my results to those of the earlier work on phosphorus (P), I further show that dams increase the N:P ratio of riverine discharge, thereby reducing the magnitude of N limitation for primary production in receiving lentic and coastal marine environments. This information should be taken into consideration when developing strategies to lessen the impacts of cultural eutrophication.

Acknowledgements

First of all, I would like to thank my supervisor, Philippe Van Cappellen, for his insightful comments, ideas, and immense knowledge. This journey would not have been completed without his guidance and support.

For all their helpful comments and encouragement, I would like to thank my co-supervisor, Fereidoun Rezanezhad, and committee members, Nandita Basu, Sherry Schiff, and Hans Dürr, and especially Anniet Laverman, who has been a true mentor. In addition, I would like to express my thanks to William Taylor and Sergei Katsev for agreeing to be part of my examination committee.

The support of Ecohydrology Research Group friends must also be acknowledged. I am indebted to Helen who walked me through first steps of my PhD. To Taylor, Tatjana, Bhaleka, Bijen, Tariq, Bingjie, Stephane, Maddy, Mahyar, Geertje, Christina, Chris, Steph, Erin, Adrian, Igor, and Katya, I am grateful for your support and encouragement.

I particularly wish to thank my amazing friends, Amy for all her care and generosity, Nazli for all the joy and laughter she brought into my life, Fatemeh and Maria for their thoughtfulness, kindness, and support, and Nastaran and Maryeh for being awesome friends.

On a more personal level, the constant affirmation of my parents sustained me during this degree. Thanks so much for those weekly Skype sessions Maman and Baba. And thanks to my sisters, Mahboobeh and Maryam, and my brother, Ali, for always being there for me.

Finally, I wish to thank the Canada Excellence Research Chair program for funding this research.

Table of Contents

List of Tables

List of Figures

Chapter 1

Introduction

1.1 N cycling and anthropogenic effects

Nitrogen (N), a critical nutrient required for all forms of life, is essential for food security for the ever-growing human population (Erisman et al., 2013). While different forms of N exist in atmospheric, terrestrial, and marine systems, only limited forms of N are available to organisms for direct uptake (Galloway et al., 1995). Humans have altered the N cycle tremendously by increasing the release of bioavailable N into environment through agricultural activities and fossil fuel combustion (Galloway et al., 2004). Humans have also increased the mobility of N from land to coastal areas. Significant amounts of anthropogenically mobilized N in watersheds are transported to ground and surface waters, ending up in lakes and coastal marine areas and leading to eutrophication, hypoxia and even anoxia (Seitzinger et al., 2010).

Dam construction in particular changes N transport from land to coastal areas (Van Cappellen and Maavara, 2016). Damming has been accelerating over the last few decades. Today's number of hydroelectric dams will double by 2030 when ongoing and planned dam construction is completed (Zarfl et al., 2015). Closing of a dam raises the water residence time in the section of the river that becomes the reservoir, and decreases turbulence, thereby promoting the in-reservoir biogeochemical cycling of N. In turn, this leads to N removal by sedimentary burial in the reservoir, plus gaseous emissions to the atmosphere, primarily through denitrification. The overall effect of damming will therefore be changes in the magnitude and speciation of N fluxes in river basins (Harrison et al., 2009; Tomaszek and Koszelnik, 2003).

Studies show that the loading of N has increased over time at local (e.g., individual small watersheds and river systems) to global scales (Green et al., 2004). This excess N has major implications for both human and ecosystem health. For instance, excess reactive N lowers air quality and may impair drinking water and food safety beyond recommended levels. Moreover, it intensifies acidification and eutrophication in aquatic ecosystems, and contributes to climate change and global warming when nitrous oxide (N_2O) forms by incomplete fossil fuel combustion and fertilizer production. Additionally, the

application of industrial fertilizer to soils, plus increased hypoxia and anoxia in surface waters, promotes the formation of nitrous oxide. Another impact of excess reactive N on climate change is the formation of ground level ozone due to emissions of NOx and volatile organic carbon and stratospheric ozone depletion (Erisman et al., 2013).

1.2 N cycling in rivers

Surface waters receive notable fractions of the reactive N produced and mobilized by anthropogenic activities (Galloway et al., 2004; Seitzinger et al., 2005). Elevated loadings of N have been documented in many rivers worldwide (Green et al., 2004; Liu et al., 2012; Schlesinger et al., 2006). However, the fate of N related to specific anthropogenic perturbations in the river system remains to be fully investigated. In this study, we focus on N cycling in two important biogeochemical compartments of the river system: N cycling in stream sediments at the regional scale, and N cycling in dam reservoirs at the global scale. **Figure 1.1** represents that how riverine N fluxes may be modified by interactions with the sediments. The reaction formulations of the various processes of **Figure 1.1** are presented in **Table 1.1**.

1.2.1 N cycling in river sediments

Benthic processes can have a significant impact on the water quality of aquatic systems (Han et al., 2014; Paraska et al., 2014; Thouvenot et al., 2007), and can affect the availability of inorganic nutrients by acting as an important source for phytoplankton growth (Han et al., 2014). At the water-sediment interface (SWI), inorganic N species may be transferred to the oxic water column or buried into anoxic sediment layers. Inorganic N species undergo different processes depending on the environment they diffuses into. Microbial oxidation and reduction of N species in the water column and sediments, coupled to exchange processes across the sediment water interface (SWI), determine the fate of N species in the river system. If the system cannot eliminate the excess amount of inorganic N, the result is eutrophication (Yu et al., 2012). Benthic models, which simulate the physical, chemical and biological processes in near surface sediments, are called early diagenetic models (Boudreau, 2000; Paraska et al., 2014)

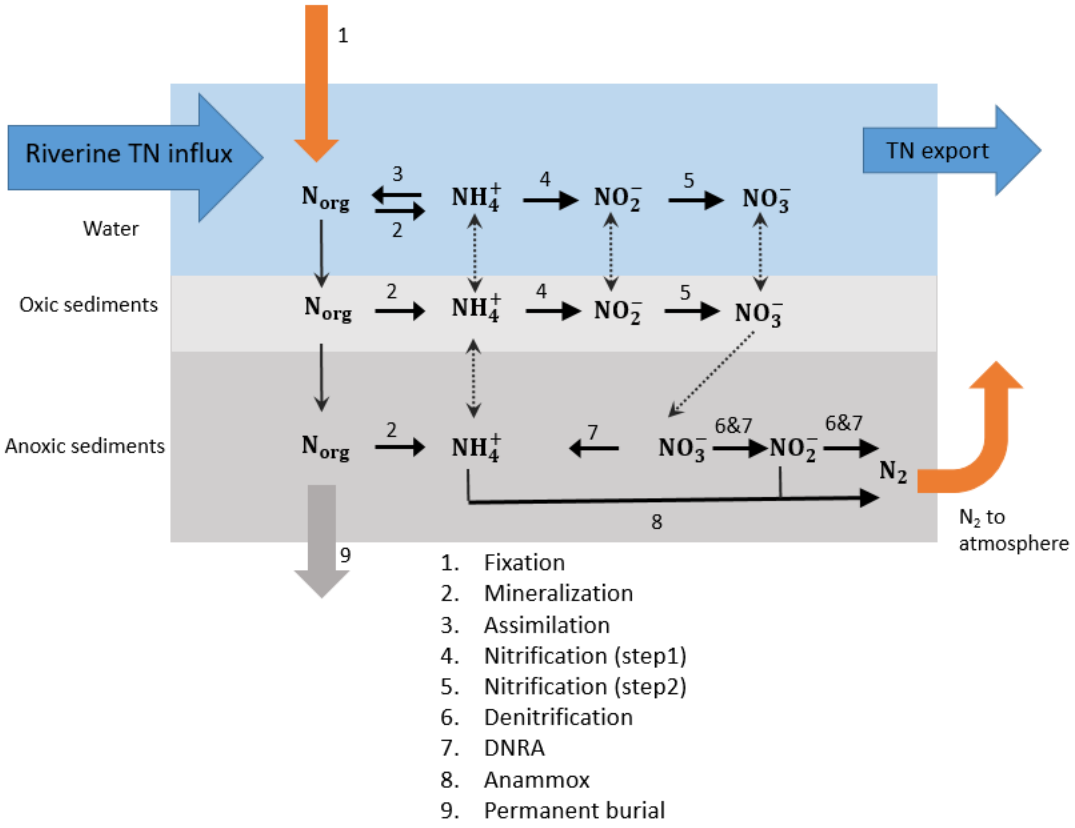

Figure 1.1. The N cycle in streams and bottom sediments. The dashed arrows indicate diffusional fluxes. The figure was modified after Thamdrup and Dalsgaard (2008). While burial and denitrification remove nitrogen permanently from a river system, N fixation adds nitrogen to it.

Numerical modeling of sediment early diagenesis models started with the work of Berner (1980) and was developed further by, among others, (Van Cappellen et al., 1993; Wang and Van Cappellen, 1996; Boudreau, 2000, 1997). The most important driver of the reactions in early diagenetic models is the deposition of organic matter at the SWI. Early diagenetic models differ in their conceptualizing of the decomposition of sedimentary organic matter. The most common approach is to use the multi-G model, in which organic matter is divided into discrete pools based on its degradability. Early diagenetic models also vary in treating the system as being either at steady state, in which changes occur slowly over a long time, or in non-steady state, when the response of the system upon a perturbation occurs dynamically over a short

time (Van Cappellen et al., 1993). Different compartments of a sediment may reach steady state conditions at different time scales. To determine if the steady state assumption can be applied or not, we focus on the time scale over which the distribution of a specific species of interest changes (Paraska et al., 2014).

Many researchers have used reactive transport models to analyze multicomponent data collected from marine and lacustrine sediments, but few have applied them to riverbed sediments. In a review of 83 early diagenetic modeling studies published since 1996, Paraska et al., (2014) found just four studies on river sediments (Devallois et al., 2008; Massoudieh et al., 2010; Trinh et al., 2012; Van Den Berg et al., 2000). Therefore, the modeling of benthic processes in freshwater river sediments is still an open field of research.

1.2.1.1 Nitrite in early diagenetic models

Nitrite, an intermediate species produced during nitrification, denitrification and dissimilatory nitrate reduction to ammonium (DNRA), is known to be highly toxic to human and aquatic life (Philips et al., 2002). In exposed humans, primarily infants, it may cause methemoglobinemia, which interferes with the blood's ability to transport oxygen. The maximum level of nitrite for drinking water set by the US Environmental Protection Agency is 1 ppm. In aquatic ecosystems, if the nitrite level rises above a certain low limit, many lifeforms are negatively impacted: according to the European Union guideline, the nitrite limit for rivers supporting salmonid fish is 0.003 mg $N\text{-}NO_2^- L^{-1}$. Even though nitrite is usually assumed to be a short-lived intermediate in the N cycle in oxic waters, accumulation of nitrite in rivers and streams has been reported in the literature. In particular, relatively high nitrite concentrations have been reported in various urbanized rivers, for instance the Lahn River in Germany (von der Wiesche and Wetzel, 1998), rivers of Northern Ireland (Kelso et al., 1997), and the Seine River in France (Garnier et al., 2006; Raimonet et al., 2015; Raimonet et al., 2017). The potential causes of the nitrite build up in these studies include release from sediments, lower rates of the second step of nitrification rather than the first, as well as anthropogenic sources.

Table 1.1. Reaction formulae of N transformation processes in the microbial N cycle.

process	Formulation	Reference
N Fixation	$\mathbf{N_2} + 8H^+ + 8e^- \rightarrow \mathbf{2NH_3} + H_2$	(Thamdrup, 2012)
Nitrification (step1)	$\mathbf{NH_4^+} + 1.5O_2 \rightarrow \mathbf{NO_2^-} + H_2O + 2H^+$	(Akbarzadeh et al., 2018)
Nitrification (step2)	$\mathbf{NO_2^-} + 0.5O_2 \rightarrow \mathbf{NO_3^-}$	(Akbarzadeh et al., 2018)
Anammox	$\mathbf{NH_4^+} + \mathbf{NO_2^-} \rightarrow \mathbf{N_2} + 2H_2O$	(Akbarzadeh et al., 2018)
Aerobic respiration[a]	$(CH_2O)_{org} + \mathbf{y(NH_3)_{org}} + z(H_3PO_4)_{org} + O_2 + (2z\text{-}y)HCO_3^- \rightarrow \mathbf{yNH_4^+} + zHPO_4^{2-} + (1\text{-}y+2z)CO_2 + (1\text{-}y+2z)H_2O$	(Akbarzadeh et al., 2018)
Denitrification[b]	$(CH_2O)_{org} + \mathbf{y(NH_3)_{org}} + z(H_3PO_4)_{org} + \mathbf{0.8NO_3 \rightarrow 0.4\ (1\text{-}\alpha\text{-}\beta)N_2} + \mathbf{yNH_4^+} + \mathbf{0.8\alpha NO_2^-} + \mathbf{0.4\ \beta N_2O} + zHPO_4^{2-} + (0.8\text{-}\ 0.8\alpha + y\text{-}2z)\ HCO_3^- + (0.2\text{-}y+2z+\ 0.8\alpha)CO_2 + (0.6\text{-}y+2z\text{-}\ 0.8\alpha\text{-}0.4\ \beta)H_2O + (0.8\alpha\ \text{-}0.4\ \beta)H_2$	(Akbarzadeh et al., 2018)
Dissimilatory iron (hydr)oxide reduction	$(CH_2O)_{org} + \mathbf{y(NH_3)_{org}} + z(H_3PO_4)_{org} + 4Fe(OH)_3 \rightarrow 4Fe^{2+} + \mathbf{yNH_4^+} + zHPO_4^- + (8+y\text{-}2z)HCO_3^- + (2z\text{-}y\text{-}7)CO_2 + (3+y\text{-}2z)H_2O$	(Wang and Van Cappellen, 1996)
Dissimilatory sulfate reduction	$(CH_2O)_{org} + \mathbf{y(NH_3)_{org}} + z(H_3PO_4)_{org} + 0.5SO_4^{2-} \rightarrow 0.5H_2S + \mathbf{yNH_4^+} + zHPO_4^{2-} + (1+y\text{-}2z)HCO_3^- + (2z\text{-}y)CO_2 + (2z\text{-}y)H_2O$	(Wang and Van Cappellen, 1996)
DNRA[c]	$(CH_2O)_{org} + \mathbf{y(NH_3)_{org}} + z(H_3PO_4)_{org} + \mathbf{0.5NO_3^-} \rightarrow \mathbf{((0.5\text{-}\ \delta)\ + y)NH_4^+} + \mathbf{0.5\ \delta NO_2^-} + zHPO_4^- + (y\text{-}2z)HCO_3^- + (1\text{-}y+2z)CO_2 + (0.33\text{-}y+2z)H_2O + \delta H_2$	(Akbarzadeh et al., 2018)
Assimilation	$\mathbf{yNH_4^+} + zHPO_4^{2-} + (1\text{-}y+2z)CO_2 + (1\text{-}y+2z)H_2O \rightarrow (CH_2O)_{org} + \mathbf{y(NH_3)_{org}} + z(H_3PO_4)_{org} + O_2 + (2z\text{-}y)HCO_3^-$	

[a] y and z are the molar N:C and P:C ratios of the degrading organic matter.

[b] α and β are the percentages of nitrite and nitrous oxide leakage during denitrification respectively.

[c] δ is the percentage of nitrite leakage during dissimilatory nitrate reduction to ammonium (DNRA).

Nitrite is often neglected in existing early diagenetic models that represent N transformations. A few studies have used modeling to analyze porewater profiles of nitrite. For example, Stief et al. (2002) and Meyer et al. (2008) used inverse reaction-transport modeling to extract the depth distributions of nitrite production and consumption from measured nitrite pore water profiles in a freshwater mesocosm experiment and in estuarine sediment, respectively. However, this type of modeling cannot predict how the rate distributions change under varying boundary conditions and transport regimes. Some researches have applied box modeling approaches to estimate nitrite exchanges between streambed sediments and the overlying river (e.g., Aissa- Grouz et al., 2015; Raimonet et al., 2015; Vilmin et al., 2014), or to simulate nitrite production and consumption in sediments incubation experiments (e.g., Babbin and Ward, 2013). Such models, however, are unsuitable for analyzing porewater profiles because they cannot predict spatial distributions. Dale et al. (2011) developed an early diagenetic model and used it to examine data from a Baltic coastal marine site. Of all existing models, theirs is closest to ours because it includes nitrite as a reactive species and represents nitrification, denitrification, DNRA and anammox.

1.2.1.2 Nitrite in the Seine River, France

Seine River is a human-impacted river system in France, influenced by high N loads from diffuse agricultural and urban activities, as well as nonpoint sources, mainly from wastewater treatment plants (WWTPs). Among the latter, the Seine Aval (SAV) WWTP is the largest one located 70 km downstream from Paris, a large metropolitan city of 12 million inhabitants. SAV WWTP is a major source of N pollution to the Seine river, with daily releases of 41.2±23.6 t $N\text{-}NO_3$, 2.4±2.4 t $N\text{-}NO_2$, and 15.3±20.5 t $N\text{-}NH_4$ (Aissa-Grouz et al., 2015).

Until the late 1990s, the major water quality problem of the Seine River downstream of Paris was the release of high loads of organic matter into the river, leading to a huge ammonium production, and consequently high nitrification and anoxic conditions in the river. However, with the modification of the SAV WWTP in 2007 and 2011, and the introduction of nitrification (which eliminates almost all of the ammonium in effluent discharges) and denitrification (responsible of removing 70% of nitrate in effluent

discharges) processes, currently the major N-related environmental issue in the Seine River downstream of Paris is high nitrite concentrations, up to the levels exceeding the limit set by the European Water Framework Directive for good environmental status. SAV WWTP is indeed a major source of nitrite to the Seine River, however, nitrite concentrations persist tens of kilometers downstream of the WWTP in spite of the fully oxic conditions of the river (Aissa-Grouz et al., 2015; Raimonet et al., 2015)

The persistence of nitrite has been investigated in several studies, mainly focusing on the rates and kinetics of the two steps of the nitrification process. For instance, Raimonet et al., (2017) investigated the kinetics of the first and second step of nitrification in the water column of the Seine River and concluded that the low ammonia and nitrite oxidation rates as well as high river flow rates are the possible reasons explaining why nitrite persists along the Seine river for tens of kilometers downstream of the SAV WWTP. In another study, Aissa-Grouz et al., (2015) reported that the large numbers of nitrite oxidizing microorganism released by the WWTP do not grow in the river environment, therefore, nitrite released by the WWTP lasts in the river system. Despite all these studies, the assessment of the role of the sediments in the nitrite budget of the Seine River system remain to investigate, which we address in this study.

1.2.2 N cycling in dam reservoirs

The number of dams has increased significantly over the last 60 years and is going to continue to rise due to the economic, environmental and social benefits they provide for humans. Among these benefits are water storage, irrigation, flood mitigation, energy production, river navigation and waste management (Poff and Hart, 2002). However, alteration of river flow regimes and interruption of river continuity by damming can dramatically influence water temperature, sediment transport to coastal areas, and wildlife, consequently affecting the biogeochemical cycling in dam reservoirs.

By increasing the water residence time and reducing the turbulence in the reservoir, dams are expected to increase nutrient particle settling. As shown by Maavara et al. (2015, 2014), dams decrease global riverine fluxes of Silicon (Si) and phosphorus (P) by trapping these elements in reservoir sediments. However, the effects on N can differ from those of Si and P, because of N fixation. Nitrogen fixation can

act as a source of N to reservoirs (Cook et al., 2010; Horváth et al., 2013; Howarth et al., 1988; Jankowski et al., 2012). Thus, the overall role of reservoirs on riverine N fluxes along the land to ocean aquatic continuum is made more complicated because of N fixation. Few studies, however, have assessed the global importance of nitrogen fixation in dam reservoirs.

1.2.2.1 Denitrification and N burial

Because dams slow down water velocity and promote particle settling, their construction has led to trapping of nutrient particles in sediment and decreased the riverine sediment load to coastal areas (Dai et al., 2009; Gupta et al., 2012; Vörösmarty et al., 2003). Reservoirs have a larger areal burial rate than natural lakes because, in general, reservoirs have a larger catchment area to surface area ratio. Researchers rarely measure the burial rate of N in reservoirs directly. Knoll et al. (2014) who directly measured the areal rate of N burial in Midwestern US reservoirs, reported that the rate varies between 5 and 115 $gNm^{-2}y^{-1}$. Most importantly, the cumulative effects of N burial in reservoirs at the global scale needs further investigation.

Denitrification in sediments of reservoirs and lakes can be an important sink of bioavailable N. Denitrification is promoted where plenty of organic carbon and nitrate are available under anoxic conditions, such as in the top layers of sediments. Denitrification rates measured in individual lakes and reservoirs fall in the range of 0.01 to 108 $gNm^{-2}y^{-1}$; however, global estimations of denitrification fluxes in reservoirs are not available. The few studies that have been done on the global scale estimations of N removal in reservoirs do not distinguish between denitrification and burial (Beusen et al., 2015; Harrison et al., 2009; Wollheim et al., 2008)

1.2.2.2 On the importance of N fixation in dam reservoirs

To grow, phytoplankton on average take up N and P at the Redfield molar ratio of 16:1. If the N:P ratio in an aquatic system is greater than 16:1, algal primary production tends to P limited and, if it is lower, it tends to be N limited. When the system is N limited, it has surplus P, which is not accessible for planktonic growth. However, N fixation can make up for the surplus P available for primary productivity by adding

labile N ready for phytoplankton to use. Biological N fixation reduces the atmospheric N_2 to ammonium, which is immediately incorporated into the biomass of the microorganisms (Thamdrup, 2012) (see **Table 1.1**)

Generally, heterocystous cyanobacteria perform N fixation in lakes and reservoirs, since they outcompete other phytoplankton groups under N limiting conditions (Levine and Schindler, 1999). The areal rate of N fixation in individual lakes and reservoirs have been estimated in the range 0-17.5 $gNm^{-2}y^{-1}$. In freshwater systems, N fixation is regulated by several factors, including light, temperature and water column stability. Primarily, however, it is stimulated by low external input of reactive N, relative to that of reactive P (Levine and Schindler, 1999; Nõges et al., 2008; Pinto and Litchman, 2010; Schindler et al., 2008; Vrede et al., 2009).

Generally, the rate of N fixation is higher in eutrophic ecosystems because nutrients are abundantly available for primary producers to build biomass. Often the N:P supply ratio to eutrophic systems are lower than for oligotrophic system (Scott et al., 2009). The latter authors report that the transition zones of reservoirs are hot spots of N fixation because of the availability of light and nutrient. Usually N fixation is promoted in summer, when the temperature is high and eutrophic reservoirs often experience thermal stratification. For instance, Horváth et al., (2013) report that in the Kis-Balaton reservoir in Hungary, N fixation in summer months is three time higher than the N supplied by riverine inflow. Generally, N fixation can substantially contribute to the annual N budget of reservoirs. Although sparse literature data are available on N fixation in individual reservoirs worldwide, globally, quantifying the contribution of N fixation to the total N input to reservoirs is data limited.

1.2.2.3 N export in the Global-NEWS model

The spatially explicit Global-NEWS (Global Nutrient Export from Watersheds) model predicts the export of nutrients to coastal zones. In terms of N species, Global-NEWS encompasses three forms of N: dissolved inorganic nitrogen (DIN), dissolved organic nitrogen (DON) and particulate nitrogen (PN). We

use the catchment-specific yields predicted by the Global-NEWS model to estimate river inputs of N to reservoirs. Global-NEWS calculates the annual average N yields (kg m^{-2} yr^{-1}) of the three N species at the mouth of each watershed by considering biologically fixed N due to crop cultivation, non-point source N, fertilizers, manure, atmospheric N deposition, and legume cultivation, as well point source N (sewage) (Seitzinger et al., 2005).

1.3 Nitrogen isotopes

Nitrogen has two stable isotopes, ^{14}N, which constitutes the majority of naturally occurring N, and ^{15}N with an average abundance of 0.3663 percent. The two isotopes ^{14}N and ^{15}N differ due to the slight mass difference. Generally, the bonds between heavy isotopes are stronger and harder to break than bonds between light isotopes; therefore, in enzymatically catalysed reactions in the N cycle, the molecules having ^{14}N are preferred by microorganisms over those having ^{15}N. Consequently, the residual reactants become depleted in light isotopes, and the products become enriched with them. The dissimilatory processes in the N cycle, which shift N from one inorganic pool to another, are usually associated with stronger isotopic fractionations than assimilatory ones, in particular primary productivity that initiates the transfer of N through the food web (Casciotti, 2009; Kanta et al., 2014). Therefore, isotope compositions of N pools can be useful in identifying the sources of N and processes that are associated with a distinguishable isotopic fractionation.

Only very few reactive transport models address nitrite isotopic compositions in freshwater sediments under non-steady state conditions. The Rayleigh model is the most common modeling approach used in the literature to represent isotopic compositions in unidirectional closed or open systems (Casciotti, 2009). The Rayleigh model, however, is applicable only to individual isotope effects and unable to account for multiple processes that simultaneously influence both reactant and product pools. Time dependant 1 box models have been used to analyze measurements of dual isotopes of N and oxygen in the oceans (Casciotti and Buchwald, 2012; Granger and Wankel, 2016). The reactive transport process model of Rooze

and Meile (2016) estimates the N isotope effect of various N species including nitrite, but it does so only for steady state conditions in marine environments.

1.4 Thesis structure:

The overall objective of my thesis is to quantitatively describe the fate of reactive N along the river continuum. In particular, I quantify N cycling in two important biogeochemical compartments of a river network, bottom sediments and dam reservoirs. Sediments are an essential part of the functioning of the rivers system, and benthic exchanges across the SWI are strongly influenced by anthropogenic activities such as urbanization and agricultural runoff. Damming is an anthropogenic change that is imposed to the river system and has been accelerating in the last few decades.

1.4.1 Research Objectives

The following are the main research objectives of my research:

1. To investigate the benthic exchanges of nitrite at the SWI of stream sediments, and to evaluate the most important drivers that affect the magnitude and direction of these nitrite exchanges.
2. To predict and interpret the temporal variations in N isotopic compositions under non-steady state conditions during sediment core incubations.
3. To quantify the effect of river damming on the global riverine N fluxes by estimating the elimination and addition of reactive N in dam reservoirs worldwide.

1.4.2 Organization

This thesis includes five chapters associated with the research objectives identified above. Following the general Introduction (Chapter 1), the research portion of the thesis (Chapter 2 – 4) is organized as stand-alone manuscripts as follows.

In **Chapter 2**, I expand the reaction network for benthic N cycling in an existing early diagenetic computer code in order to explicitly include the reaction pathways producing and consuming nitrite. I use the model to interpret sediment data sets collected at two locations in the Seine River, one upstream, the

other downstream, of the largest WWTP of the Paris conurbation. The datasets in both locations consist of pore water profiles and benthic exchange fluxes of nitrate, nitrite and ammonium measured during core incubation experiments. The model explains the general trends of the measured pore water depth profiles and benthic fluxes. A sensitivity analysis provides insights into the main controls on the benthic exchange fluxes of nitrite.

In **Chapter 3**, I expand the existing diagenetic model of Chapter 2, by representing the N isotopic compositions of nitrate, nitrite, ammonium and organic N, and incorporating the isotopic fractionations along the N transformation pathways. We then use the model to investigate the temporal variations of isotopic composition of N species, including nitrate, nitrite and ammonium, under non-steady state conditions at the SWI. Applying a sensitivity analysis, I investigate the effects of different factors on N isotopic composition in freshwater sediments.

In **Chapter 4**, I quantify the role of damming in regulating riverine N fluxes using a process-based reservoir N mass balance model, which I scale up to all the river basins in the world. A virtual reservoir database is generated using Monte Carlo simulations, from which two global relationships between N elimination in reservoirs, by either denitrification or burial, and the hydraulic residence time are derived. I apply these equations to databases for existing and future reservoirs, and combine that information with nutrient loads obtained using the Global-NEWS model (Mayorga et al., 2010) and N fixation fluxes calculated from the degree of N limitation in the river inflows. I then present the spatially explicit estimates of N fixation, denitrification and N burial in reservoirs in the world's river basins at different time points. The Millennium Ecosystem Assessment (MEA) scenarios (Alcamo et al., 2005), implemented in Global-NEWS form the basis for the 2030 and 2050 estimates.

Chapter 2

Benthic nitrite exchanges in the Seine River (France): An early diagenetic modeling analysis

Modified from: **Zahra Akbarzadeh**, Anniet Laverman, Fereidoun Rezanezhad, Eric Viollier, Babak Shafei, and Philippe Van Cappellen. (2018) Benthic nitrite exchanges in the Seine River (France): An early diagenetic modeling analysis, *Journal of Science of the Total Environment*. 628–629, 580–593. doi:10.1016/j.scitotenv.2018.01.319

2.1 Summary

Nitrite is a toxic intermediate compound in the nitrogen (N) cycle. Elevated concentrations of nitrite have been observed in the Seine River, raising questions about its sources and fate. Here, we assess the role of bottom sediments as potential sources or sinks of nitrite along the river continuum. Sediment cores were collected from two depocenters, one located upstream, the other downstream, from the largest wastewater treatment plant (WWTP) servicing the conurbation of Paris. Pore water profiles of oxygen, nitrate, nitrite and ammonium were measured. Ammonium, nitrate and nitrite fluxes across the sediment-water interface (SWI) were determined in separate core incubation experiments. The data were interpreted with a one-dimensional, multi-component reactive transport model, which accounts for the production and consumption of nitrite through nitrification, denitrification, anammox and dissimilatory nitrate reduction to ammonium (DNRA). In all core incubation experiments, nitrate uptake by the sediments was observed, indicative of high rates of denitrification. In contrast, for both sampling locations, the sediments in cores collected in August 2012 acted as sinks for nitrite, but those collected in October 2013 released nitrite to the overlying water. The model results suggest that the first step of nitrification generated most pore water nitrite at the two locations. While nitrification was also the main pathway consuming nitrite in the sediments upstream of the WWTP, anammox dominated nitrite removal at the downstream site. Sensitivity analyses indicated that the magnitude and direction of the benthic nitrite fluxes most strongly depend on bottom water oxygenation and the deposition flux of labile organic matter.

2.2 Introduction

Humans have greatly modified the nitrogen (N) cycle, nearly doubling the inputs of bioavailable nitrogen to the environment (Gruber and Galloway, 2008). Excess nitrogen negatively impacts human and ecosystem health, causing eutrophication of aquatic ecosystems, decreasing air quality and contaminating drinking water supplies (Driscoll et al., 2003; Erisman et al., 2013; Ndegwa et al., 2008). The application of N-containing fertilizers and human wastewater release have been linked to the expansion of hypoxic and anoxic conditions in aquatic systems (Diaz and Rosenberg, 2008; Rabalais et al., 2010), while enhanced microbial nitrification and denitrification causes emission of nitrous oxide (N_2O), an important greenhouse gas (Crutzen et al., 2007).

Nitrate (NO_3^-) and nitrous oxide (N_2O) have received most attention as N contaminants. Strict nitrate water quality standards are in place in most developed countries (Oenema et al., 2011), while interest in N_2O emissions stems from concerns about accelerating climate change (e.g. Clough et al. 2006; Beaulieu et al. 2008; Rosamond et al. 2012). In comparison, relatively little research has been done on the intermediate species nitrite (NO_2^-). High nitrite concentrations in drinking water can cause serious illness in infants; shortness of breath and blue baby syndrome are some of the associated symptoms (Knobeloch et al., 2000). The maximum level of nitrite for drinking water set by the US Environmental Protection Agency is 1 ppm. Nitrite is also toxic to aquatic life (Cowling et al., 1998; Philips et al., 2002): according to the EU Water Framework Directive, the nitrite limit for good environmental status is 0.09 mg $N\text{-}NO_2^-$ L^{-1}.

Nitrite is a reactive intermediate produced and consumed in several redox pathways of the N cycle (Kelso et al., 1997; Mordy et al., 2010). It is produced during the first steps of nitrification and denitrification from ammonium (NH_4^+) and nitrate (NO_3^-), respectively. Under oxic conditions, nitrite oxidizers consume NO_2^- producing nitrate as part of the overall nitrification process. Under reducing conditions, nitrite can be transformed to N_2 gas during denitrification or anammox, or to ammonium via dissimilatory nitrate reduction to ammonium (DNRA). In addition to biotic transformations, nitrite is

chemically reactive (Udert et al., 2005). Thus, in general, nitrite concentrations in the environment are expected to be negligible. Nonetheless, accumulation of nitrite has been observed in rivers and streams. In particular, relatively high nitrite concentrations have been reported in various urbanized rivers, for instance the Lahn River in Germany (von der Wiesche and Wetzel, 1998), rivers of Northern Ireland (Kelso et al., 1997), and the Seine River in France (Garnier et al., 2006; Raimonet et al., 2015; Raimonet et al., 2017).

The Seine River receives large N inputs from diffuse agricultural and urban sources, as well as point sources, primarily waste water treatment plant (WWTP) discharges (Cébron and Garnier, 2005; Naeher et al., 2015; Raimonet et al., 2015; Raimonet et al., 2017). Downstream of the metropolitan area of Paris, the effluents from a very large WWTP, known by its acronym SAV (daily capacity of 1.7M m^3), greatly impact the river water quality (Vilmin et al., 2014). Nitrogen pollution in the past was dominated by ammonium, resulting in nitrification and even anoxia in the water column (Cébron and Garnier, 2005; Chesterikoff et al., 1992; Garban et al., 1995). Upgrades to the SAV WWTP, with the introduction of treatment by nitrification and denitrification in 2007 and 2011, respectively, considerably decreased N loading to the river: ammonium discharges dropped from 58±22 to 12±17 t N d^{-1} (Aissa-Grouz et al., 2015). Nitrate concentrations in the river have remained elevated, however, mainly because of agricultural activity in the surrounding area. In addition, even after the improvements, nitrite concentrations in the outflow of the WWTP have remained above European water quality standards (Raimonet et al., 2017).

With an estimated daily loading of around 2.4±2 tonnes NO_2-N (Aissa-Grouz et al., 2015), the WWTP is a major source of nitrite to the Seine River (Garnier et al. 2006; Raimonet et al. 2015). Surprisingly, elevated concentrations of nitrite persist for over 300 km downstream of Paris, despite fully oxic conditions along the river channel (Aissa-Grouz et al., 2015). Possible explanations include the sustained production of nitrite in the water column (Raimonet et al., 2015), or a continuous efflux of nitrite from streambed sediments. Benthic processes are known to have a significant impact on the water quality of aquatic systems in general (Han et al., 2014; Paraska et al., 2014; Thouvenot et al., 2007), and on the cycling of nitrogen in particular (Han et al., 2014). Fixed nitrogen is removed by sediments via permanent

burial of organic nitrogen and clay-bound ammonium, as well as through denitrification or anammox, which return dinitrogen gas to the atmosphere. Alternatively, dissolved inorganic nitrogen species can be recycled to the water column following mineralization of deposited organic matter (Thamdrup and Dalsgaard, 2008).

Here, we present a preliminary assessment of the potential role of benthic nitrite exchanges in the Seine River: pore water and benthic flux measurements on sediments collected upstream and downstream of the SAV WWTP are analyzed quantitatively by developing and applying an early diagenetic model that includes a comprehensive representation of the benthic N cycle. Early diagenetic models simulate the coupled transport and transformation processes that affect the chemical species of interest below the sediment-water interface (SWI) (Boudreau, 1996). While these reactive transport models have been frequently used to interpret multicomponent data sets collected in marine and lacustrine sediments, applications to riverbed sediments remain limited. Paraska et al. (2014), who reviewed 83 early diagenetic modeling studies published since 1996, only report four studies on river sediments (Devallois et al., 2008; Massoudieh et al., 2010; Trinh et al., 2012; Van Den Berg et al., 2000).

Moreover, existing early diagenetic models representing N transformations rarely account for reactive intermediates in general, and nitrite in particular. A limited number of studies have analyzed nitrite pore water profiles using modeling. Stief et al. (2002) and Meyer et al. (2008), for example, measured nitrite pore water profiles in a freshwater mesocosm experiment and an estuarine sediment, respectively. In both studies, an inverse reaction-transport model was used to extract the depth distributions of nitrite production and consumption rates. Inverse modeling, however, is unable to predict how the rate distributions change under varying boundary conditions and transport regimes, in contrast to the forward reactive transport modeling used here. Box modeling approaches have also been used to estimate nitrite exchanges between streambed sediments and the overlying river (e.g., Aissa-Grouz et al., 2015; Raimonet et al., 2015; Vilmin et al., 2014), or to simulate nitrite production and consumption in sediments incubation experiments (e.g., Babbin and Ward, 2013). However, because box models do not predict spatial distributions they are not appropriate to analyze pore water profiles. Closest to our modeling approach is that of Dale et al. (2011)

who developed a diagenetic model that includes nitrite as a reactive species and represents nitrification, denitrification, DNRA and anammox. This model was applied to a data set from a coastal marine site in the Baltic Sea.

In the present paper, we expand the reaction network for benthic N cycling in an existing early diagenetic computer code in order to explicitly include the reaction pathways producing and consuming nitrite. Reactive transport calculations are then used to interpret a data set comprising pore water profiles and benthic exchange fluxes of nitrate, nitrite and ammonium collected in the Seine River upstream and downstream of the SAV WWTP. Because of the highly dynamic and heterogeneous nature of streambed sediments, we primarily aim to capture the general trends of the measured pore water depth profiles and benthic fluxes. We then use the model as a sensitivity tool to delineate the main controls on benthic exchange fluxes of nitrite.

2.3 Field Sampling and Experimental Methods

2.3.1 Seine River

The Seine River is the second longest river in France (776 km). The climate is temperate, with oceanic and semi-continental influences. The mean annual discharge rate of the Seine River at Austerlitz Bridge in Paris is 310 m^3 s^{-1} (period 1979-2012, Raimonet et al., 2015). The summer river discharge is artificially maintained above 100 m^3 s^{-1} by water release from dam reservoirs upstream of Paris. Water temperature ranges from 5°C in winter to 25°C in summer. The drainage basin of the Seine River is characterized by intense urbanization and agriculture leading to nutrient enrichment, especially by nitrate.

The water quality of the middle reaches of the Seine River is significantly affected by effluents from the largest WWTP in Europe, known by its acronym SAV (> 5 million population equivalents) located 70 km downstream of Paris (**Figure 2.1**; Rocher et al., 2015; Vilmin et al., 2015). A recent hydro-ecological modelling study shows that the Seine River downstream of Paris is heterotrophic and that nutrient exchanges across the sediment-water interface (SWI) significantly impact the carbon, nitrogen and

phosphorus export fluxes to the Seine River estuary (Vilmin et al., 2015). Weekly measurements of 5-day Biological Oxygen Demand (BOD5) measured on water column samples collected in August 2012 upstream (Bougival) and downstream (Poissy) of SAV WWTP were on average 0.63 and 1.13 mg L^{-1}, respectively. In October 2013, the corresponding average BOD5 values were 1.25 and 1.36 mg L^{-1} (Data from "Vincent Rocher, SIAAP, pers.comm.").

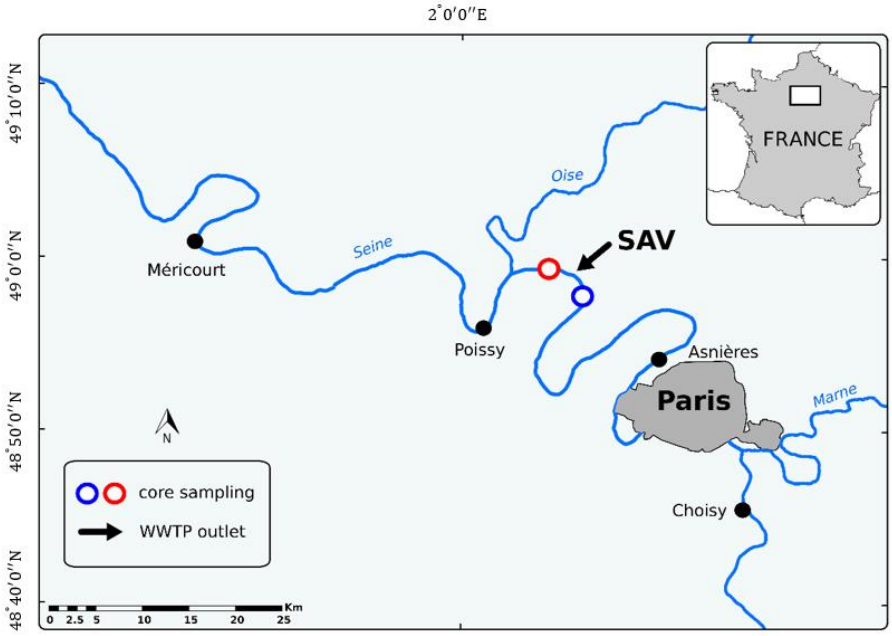

Figure 2.1. Locations of the SAV wastewater treatment plant (WWTP) and the upstream (blue circle) and downstream (red circle) core sampling sites.

2.3.2 Sediment coring and pore water extraction

Sediment cores were collected from two sites, one located upstream, the other downstream of the SAV WWTP (**Figure 2.1**), in August 2012 and October 2013 in order to measure vertical pore water concentration profiles of nitrate, nitrite and ammonium. Sampling stations were close to the shore, at water depths of 100-120 cm and 50-80 cm at the stations upstream and downstream of the WWTP, respectively. The Water temperatures at the sampling sites were higher in August (~23°C) than in October (~13°C). At each site, two pre-drilled (and taped) and seven undrilled Plexiglass cores (10-40 cm long; 8.4 cm diameter)

were obtained using the UWITEC© piston coring system (Mondsee, Austria). Pore waters were extracted by horizontally inserting Rhizon© samplers (MOM MicroRhizon™ samplers, Ejikelamp, Netherlands) into two replicate sediment cores through the small, pre-drilled holes along the sides of the tubes (1 cm depth intervals from +0.5 cm above to -9.5 cm depth below the SWI). Each Rhizon sampler collected about 2-4 ml filtered pore water directly into a vial. The pore waters were extracted within less than 5 hours after core retrieval. An aliquot of 0.3 ml of each pore water sample was immediately analyzed for NO_2^-, while the remaining sample was stored at -20 °C for later NH_4^+ and NO_3^- analyses.

2.3.3 Core incubations

Benthic fluxes of nitrate, nitrite and ammonium were measured in August 2012 and October 2013 on triplicate cores collected upstream and downstream of the WWTP. Note that benthic fluxes of nitrate and ammonium were not measured at the downstream site in August 2012. Sediment cores collected in Plexiglass tubes were transported to the laboratory and kept in the dark at 20 °C until the end of the incubations. Incubations started less than 5 hours after core collection. Overlying water was adjusted to 8 cm above the SWI. The bubbling of air at 3-4 cm above the SWI homogenized the overlying water and maintained oxygenated (air) conditions in order to mimic the fully oxic conditions at the SWI (Aissa-Grouz et al., 2015). The dissolved oxygen concentration above the SWI was monitored with an oxygen optode (Pyroscience©), calibrated in O_2 saturated water at the same temperature and salinity as the overlying water using the Firesting Logger software. Incubations ran for 15 hours in August 2012, and for one day in October 2013. Periodically, at time intervals ranging between 1 and 10 hours, 5 ml of overlying water were collected with a syringe and immediately filtered through a 0.2 μm pore size PVDF filter. A 0.3 ml aliquot of the filtrate was directly analyzed for NO_2^-; the remaining solution was stored at -20 °C for later NH_4^+ and NO_3^- analyses. The net benthic fluxes of NH_4^+, NO_2^- and NO_3^- were calculated from the linear changes in concentration and the known volumes of overlying water and the sediment surface area.

2.3.4 Analytical methods

Pore water oxygen profiles were measured with Clark-type polarographic microsensors equipped with a built-in reference and an internal guard cathode (Revsbech, 1989). The sensors have an outer tip diameter of 50 or 100 µm (Unisense, Århus, Denmark) and were operated with a motor-driven micromanipulator. The sensor current was measured with a picoamperometer connected to an A-D converter, which transferred the signals to a computer (Revsbech and Jørgensen, 1986). For each site, at least 5 oxygen profiles were recorded on the same core. The microelectrodes were calibrated in O_2 saturated overlying water at 20°C. The vertical resolution of the measurements was 50-100 µm. The position of the SWI was identified by the sharp break in the O_2 concentration gradient (Sweerts and de Beer, 1989). Oxygen pore water profiles were measured at the upstream and downstream sites in October 2013, but only at the downstream site in August 2012.

Nitrite concentrations were determined by the colorimetric method of Rodier (1984), using a UV/visible spectrophotometer. The method was adapted for microplate analysis to optimize the analysis time and pore water volume (0.3 ml; MDL: 0.1 µM). Ammonium and nitrate concentrations were measured by ionic chromatography (IC, Dionex; MDL: 0.1 µM). Organic carbon and total nitrogen concentrations were measured on air-dried sediment samples from the topmost 8 cm of the October cores at both locations: 2 g aliquots were decarbonated by adding 50 ml 1N HCL (normapur) and, after mixing, kept overnight at 50°C. The sediments were subsequently washed three times with 50 ml of MilliQ water (50 ml) and centrifuged. The decarbonated and washed sediment samples were then freeze dried and analyzed on an Elemental Analyzer**.**

2.4 Early Diagenetic Modeling

2.4.1 Conservation equations

An in-house developed, one-dimensional (1D) early diagenetic model was expanded by incorporating a more complete representation of N cycling in sediments. Here, we focus on the newly developed N reaction network; for a description of the original model and examples of applications, the

reader is referred to Couture et al. (2010) and Torres et al. (2015). The model is written in MATLAB® and solves the partial differential equations describing mass conservation of the selected pore water solutes and sediment-bound chemical species. The model considers three pools of organic carbon (one most reactive, one less reactive and one unreactive pool), and the following N species: particulate organic N (PON), nitrate (NO_3^-), nitrite (NO_2^-), ammonium (NH_4^+), dissolved nitrous oxide (N_2O) and dissolved nitrogen gas (N_2). Additional solute species included are molecular oxygen (O_2), sulfate (SO_4^{2-}), total sulfide (ΣH_2S), ferrous iron (Fe^{2+}) and methane (CH_4); additional solid species include reactive iron (hydr)oxides ($Fe(OH)_3$), iron monosulfide (FeS) and pyrite (FeS_2).

The reaction stoichiometries and rate expressions describing the N transformation processes included in the model are given in **Table 2.1.** Denitrification is a multi-step process associated with the production of multiple intermediates at each step. In the case of nitrite, denitrification produces and consumes nitrite during two steps; in the first step organic carbon reduces nitrate and produces nitrite, and in the second step, organic carbon consumes nitrite and produces nitrous oxide gas, schematically:

$$(CH_2O)_{org} + y(NH_3)_{org} + z(H_3PO_4)_{org} + \mathbf{2NO_3^-} \rightarrow$$
$$\mathbf{2NO_2^-} + \mathbf{yNH_4^+} + zHPO_4^{2-} + (y-2z)HCO_3^- + (1-y+2z)CO_2 + (1-y+2z)H_2O \quad 2.1$$

$$(CH_2O)_{org} + y(NH_3)_{org} + z(H_3PO_4)_{org} + \mathbf{2NO_2^-} \rightarrow$$
$$\mathbf{N_2O} + \mathbf{yNH_4^+} + zHPO_4^{2-} + (2+y-2z)HCO_3^- + (-1-y+2z)CO_2 + (-y+2z)H_2O \quad 2.2$$

Studies of the kinetics of the two steps of denitrification yield lower rates of nitrite reduction in comparison to nitrate reduction, hence leading to nitrite accumulation in pure cultures (Betlach and Tiedje, 1981). Here, nitrite production during denitrification and DNRA are calculated as adjustable fractions of the corresponding rates of nitrate consumption. These fractions represent the NO_2^- leakage into the environment from cells carrying out nitrate reduction (Richardson et al., 2009; Trimmer et al., 2005). Nitrification is represented as a two-step process with NO_2^- as the intermediate, consistent with the fact that the two steps are catalyzed by two distinct groups of microorganisms (Stein, 2015; Ward, 2013). Monod-

type dependencies on substrate concentrations are used to describe the rates of denitrification (organic matter and nitrate), nitrification step 1 (ammonium and oxygen), nitrification step 2 (nitrite and oxygen), anammox (nitrite, ammonium) and DNRA (organic matter and nitrate). Inhibition terms describe the reductions in the rates of denitrification, DNRA and anammox in the presence of dissolved molecular oxygen.

The model accounts for solute transport by molecular diffusion, sediment mixing, advective burial and pore water irrigation, and for solid-bound chemical constituents by advective burial and sediment mixing. The conservation equations describing the distributions of pore water (C_d) and solid-bound (C_s) concentrations are:

$$\frac{\partial(\emptyset C_d)}{\partial t} = D_B \frac{\partial^2(\emptyset C_d)}{\partial x^2} - \emptyset D_s \frac{\partial^2(C_d)}{\partial x^2} - \frac{\partial[\emptyset \omega C_d]}{\partial x} + \emptyset\alpha(C_{d0} - C_d) + \emptyset \sum R_d \quad 2.3$$

$$\frac{\partial[(1-\emptyset)\rho C_s]}{\partial t} = D_B \frac{\partial^2[(1-\emptyset)\rho C_s]}{\partial x^2} - \frac{\partial[(1-\emptyset)\omega\rho C_S]}{\partial x} + (1-\emptyset)\rho \sum R_s \quad 2.4$$

where $\emptyset$ is sediment porosity, α the pore water irrigation coefficient (yr^{-1}), ω the sediment burial velocity ($cm\ yr^{-1}$), D_s and D_B the molecular diffusion and sediment mixing coefficients, respectively ($cm^2\ yr^{-1}$), and ρ the sediment dry density ($g\ cm^{-3}$). In the absence of time series data, only steady state results are reported here, that is, the conservation **Equations 2.3** and **2.4** were solved with the LHS set equal to zero.

The rates R_d and R_s, for solutes and solids respectively, are positive when the corresponding chemical constituent is produced, and negative when consumed. For example, for nitrite, nitrate and ammonium the rate expressions are (see **Table 2.1** for the numbering of the rates):

$$\sum R(NO_2^-) = 0.8R_3 + 0.5R_6 + R_8 - R_7 - R_9 \quad 2.5$$

$$\sum R(NO_3^-) = R_9 - 0.8R_2 - 0.5R_5 \quad 2.6$$

$$\sum R(NH_4^+) = yR_1 + yR_2 + ((0.5 - \delta) + y)R_5 - R_7 - R_8 + R_{Rest} \quad 2.7$$

where R_{Rest} is the sum of the rates of ammonium release during the degradation of organic matter by dissimilatory iron(III) reduction, sulfate reduction and methanogenesis.

Table 2.1. Reaction formulas and rate expressions.

Process	Formula	Rate expression
Aerobic respiration[1]	$(CH_2O)_{org} + y(NH_3)_{org} + z(H_3PO_4)_{org} + O_2 + (2z\text{-}y)HCO_3^- \rightarrow \mathbf{yNH_4^+}$ $+zHPO_4^{2-} + (1\text{-}y+2z)CO_2 + (1\text{-}y+2z)H_2O$	$R1 = k1 \times [POC] \times \frac{[O_2]}{[O_2] + Ko}$
Denitrification	$(CH_2O)_{org} + y(NH_3)_{org} + z(H_3PO_4)_{org} + \mathbf{0.8NO_3 \rightarrow 0.4\ (1\text{-}\alpha\text{-}\beta)N_2} + \mathbf{yNH_4^+} +$ $\mathbf{0.8\alpha NO_2^-} + \mathbf{0.4\ \beta N_2O} + zHPO_4^{2-} + (0.8\text{-}\ 0.8\alpha + y\text{-}2z)\ HCO_3^- + (0.2\text{-}y+2z+$ $0.8\alpha)CO_2 + (0.6\text{-}y+2z\text{-}\ 0.8\alpha\text{-}0.4\ \beta)H_2O + (0.8\alpha\ \text{-}0.4\ \beta)H_2$	$R2 = k2 \times [POC] \times \frac{[NO_3^-]}{[NO_3^-] + kmno} \times \frac{kin}{[O_2] + Kin} \times \gamma$ Nitrite production : $R3 = 0.8\alpha \times R2$
DNRA	$(CH_2O)_{org} + y(NH_3)_{org} + z(H_3PO_4)_{org} + \mathbf{0.5NO_3^-} \rightarrow \mathbf{((0.5\text{-}\ \delta)\ + y)NH_4^+}$ $\mathbf{+0.5\ \delta NO_2^-} + zHPO_4^- + (y\text{-}2z)HCO_3^- + (1\text{-}y+2z)CO_2 + (0.33\text{-}y+2z)H_2O +$ δH_2	$R5 = k2 \times [POC] \times \frac{[NO_3^-]}{[NO_3^-] + kmno} \times \frac{kin}{[O_2] + Kin} \times (1-\gamma)$ Nitrite production : $R6 = 0.5\delta \times R5$
Anammox	$NH_4^+ + NO_2^- \rightarrow N_2 + 2H_2O$	$R7 = R7_{max} \times \frac{[NH_4^+]}{[NH_4^+] + Km1} \times \frac{[NO_2^-]}{[NO_2^-] + Km2} \times \frac{Kin}{[O_2] + Kin}$
Nitrification (step 1)	$NH_4^+ + 1.5O_2 \rightarrow NO_2^- + H_2O + 2H^+$	$R8 = R8_{max} \times \frac{[NH_4^+]}{[NH_4^+] + Km3} \times \frac{[O_2]}{[O_2] + Km4}$
Nitrification (step 2)	$NO_2^- + 0.5O_2 \rightarrow NO_3^-$	$R9 = R9_{max} \times \frac{[NO_2^-]}{[N0_2^-] + Km5} \times \frac{[O_2]}{[O_2] + Km6}$

[1]y and z are the molar N:C and P:C ratios of the degrading organic matter.

2.4.2 Parameter values and boundary conditions

The reaction and transport parameter values listed in **Tables 2.2, 2.3** and **2.4** were obtained following a procedure common in early diagenetic modeling (e.g., Wang and Van Cappellen, 1996; Dale et al., 2008, 2011; Couture et al., 2010; Krumins et al., 2013; Torres et al., 2015). Where possible, parameter values were retrieved directly from the literature (L parameters in **Table 2.2**) or else estimated a priori (E parameters in **Table 2.2**). An example of the latter is the sediment porosity, which was not measured and therefore assigned a typical value of 0.8. The remaining model parameters were then adjusted by trial and error to yield global fits of the model to the combined pore water geochemistry and benthic flux data sets. For the majority of these fitted parameters, the values were only allowed to vary within published ranges; these parameters are labeled CC (for constrained calibration).

Aqueous concentrations measured in the overlying water were assigned as upper boundary conditions for the pore water species. For all solid-bound species the deposition fluxes at the SWI were imposed (**Table 2.5**). Because the oxygen penetration depth depends primarily on the supply of the most reactive pool of sedimentary organic carbon (POC1), it was used to estimate the POC1 deposition flux. The deposition flux of the less reactive organic carbon pool (POC2) was then adjusted to best reproduce the pore water profiles of nitrate and ammonium. The resulting deposition fluxes of POC1 at the downstream site were higher than at the upstream site (**Table 2.5**), likely due to the deposition of organic matter released by the wastewater treatment plant. Given that the river was fully oxygenated, the deposition fluxes of FeS and FeS_2 were assumed equal to zero, while those of reactive ferric iron oxyhydroxides, represented as $Fe(OH)_3$, were adjusted to best fit the lower parts of the ammonium profiles. As lower boundaries, zero concentration gradients were imposed for all the chemical species.

Table 2.2. Model parameters.

Parameter	Description	Value	Source*
Ko	Half saturation constant of oxygen in aerobic respiration	8 μM	L[1]
Kmno	Half saturation constant of nitrate in denitrification	10 μM	L[1]
Km1	Half saturation constant of ammonium in anammox	5 μM	L[2]
Km2	Half saturation constant of nitrite in anammox	5 μM	L[2]
Km3	Half saturation constant of ammonium in nitrification (step 1)	10 μM	L[3]
Km4	Half saturation constant of oxygen in nitrification (step 1)	15.6 μM	L[3]
Km5	Half saturation constant of nitrite in nitrification (step 2)	10 μM	L[3]
Km6	Half saturation constant of oxygen in nitrification (step 2)	34 .4 μM	L[3]
Kin	Coefficient describing inhibition by O_2	8 μM	L[1]
Do2	Molecular diffusion coefficient for oxygen (@20°C)	651 $cm^{-2}\ y^{-1}$	L[1]
Dno3	Molecular diffusion coefficient for nitrate (@20°C)	540 $cm^{-2}\ y^{-1}$	L[1]
Dno2	Molecular diffusion coefficient for nitrite (@20°C)	534 $cm^{-2}\ y^{-1}$	L[4]
Dnh4	Molecular diffusion coefficient for ammonium (@20°C)	560 $cm^{-2}\ y^{-1}$	L[4]
γ	Fraction of total nitrate reduction occurring via denitrification	95 (%)	L[5]
∅	Porosity	0.8	E
ω	Burial velocity	0.88 cm y^{-1}	E
α	Nitrite leakage during denitrification	3-5 (%)	CC
β	Nitrous oxide leakage during denitrification	1 (%)	CC
δ	Nitrite leakage during DNRA	3-5 (%)	CC
k1	Degradation rate constant associated with POC1 for August and October	10 y^{-1}	CC
k2	Degradation rate constant associated with POC2 for August and October	1 y^{-1}	CC
C:N	Range of carbon to nitrogen ratio in different pools of organic matter	9.6 - 21.2	CC

*Values obtained from the literature = L; estimated = E; and using a constrained calibration = CC (see section 3.2)
[1]Van Cappellen and Wang, 1995
[2]Strous et al., 1999
[3]Raimonet et al., 2015
[4]Boudreau, 1997
[5]Canavan et al., 2007

Table 2.3. Reaction parameters based on model calibration for August 2012 and, in brackets, October 2013.

Process	**Upstream**	**Downstream**
	Maximum rate ($\mu mol\ cm^{-3}\ yr^{-1}$)	Maximum rate ($\mu mol\ cm^{-3}\ yr^{-1}$)
Anammox	$R6_{max}$= 3 (4)	$R6_{max}$= 14 (15)
Nitrification (step 1)	$R7_{max}$= 400 (800)	$R7_{max}$= 80 (225)
Nitrification (step 2)	$R8_{max}$= 1000 (2000)	$R8_{max}$= 170 (600)

Table 2.4. Parameters obtained by constrained model calibration. The ranges are based on the literature listed with the exception of the C:N ratio in different pools of organic matter

Parameter	**Value**	**Unit**	**Range**	**References**
k1	10	y^{-1}	$0 - 303$	Paraska et al., 2014
k2	1	y^{-1}	$0 - 1.1$	Paraska et al., 2014
$R6_{max}$	3-15	$\mu mol\ cm^{-3}\ yr^{-1}$	$0.7 - 263$	Crowe et al., 2017; Zhu et al., 2013; Yoshinaga et al., 2011
$R7_{max}$, $R8_{max}$	80-2000	$\mu mol\ cm^{-3}\ yr^{-1}$	$0 - 8833$	Altmann et al., 2003; Rysgaard et al., 1994; Cooper, 1984
α	3-5	%	0-8	Laverman et al., 2010*
β	1	%	0-0.08	Laverman et al., 2010
δ	3-5	%	0-8	Laverman et al., 2010*
C:N	9.6 - 21.2	-	10-31	This study (section 4.1)

*nitrite production as a percentage of the nitrate reduction rate.

Table 2.5. Upper boundary conditions at locations upstream and downstream of the SAV WWTP in August 2012 and October 2013.

Variables	Upstream		Downstream		Units	References
	August 2012	October 2013	August 2012	October 2013		
O_2	300	233	250	222	μM	Measurement
NO_2^-	5.4	3.5	15	6.6	μM	Measurement
NO_3^-	252	270	345	415	μM	Measurement
NH_4^+	5.3	25	6.7	70	μM	Measurement
SO_4^{2-}	513	585	513	585	μM	Model calibration
Fe^{2+}	0	0	0	0	μM	Assumed
POC1	1700	2700	2500	3800	μmol cm^{-2} y^{-1}	Model calibration
POC2	600	800	600	800	μmol cm^{-2} y^{-1}	Model calibration
POC3	500	500	500	500	μmol cm^{-2} y^{-1}	Model calibration
$Fe(OH)_3$	50	50	50	50	μmol cm^{-2} y^{-1}	Model calibration
H_2S	0	0	0	0	μmol cm^{-2} y^{-1}	Assumed
FeS	0	0	0	0	μmol cm^{-2} y^{-1}	Assumed
FeS_2	0	0	0	0	μmol cm^{-2} y^{-1}	Assumed

In the early diagenetic literature, infaunal activity is usually assumed to be the main cause of pore water irrigation and sediment mixing. Infaunal activity in the Seine river sediments is supported by the observation of shells and burrows in the upper 20 cm of sediment at both sites. However, fitting of the measured pore water profiles and benthic exchange fluxes yielded values of D_B at the SWI of up to 600 cm^2 yr^{-1} (**Table 2.6** and **2.7**), that is values exceeding those typically ascribed to bioturbation (Boudreau, 1997; Lecroart et al., 2007). Similarly, the inferred pore water irrigation coefficients, α, in the upper sediment layers tend to be on the high side of values reported for infaunal activity (Meile and Van Cappellen, 2003). The likely explanation is that in high-energy systems, such as estuaries and rivers, the top sediment layer is continuously mixed physically by the overlying water, which in the model formulation translates in high α and D_B values for the topmost, sub-millimeter sediment layer (Laverman et al., 2007). Below this surficial layer, α and D_B drop off very rapidly to values that are in line with values reported for infaunal bioirrigation and bioturbation.

2.5 Results and Discussion

2.5.1 Sediment respiration

The organic carbon concentrations measured in October 2013 in the upstream cores range from 3.8 to 6.9 wt. %. At the downstream site, the concentrations are markedly higher, varying between 6.6 and 11.4 wt. %. The sediment nitrogen concentrations are similarly higher at the downstream site (0.4-0.9 wt. %) than at the upstream site (0.1-0.3 wt. %). The organic matter in the downstream cores is also enriched in N (molar C:N = 10-15) compared to the upstream cores (molar C:N = 19-31). Higher organic C loadings at the downstream site are consistent with the reported BOD5 values (see *section 2.3.1 Seine River*), which imply higher rates of water column respiration downstream of the WWTP. The BOD5 values also suggest higher respiration rates in October compared to August. The shallow pore water oxygen penetration depths (2-3 mm) provide further evidence of high respiratory activity in the river sediments (**Figure A1**).

The model-derived POC1 deposition fluxes (**Table 2.5**), the depth-integrated rates of organic C oxidation, and the benthic O_2 consumption rates (**Table 2.8**) are in line with the above observations. They confirm that sediment respiration is higher downstream than upstream of the WWTP, and higher in October than in August. The total sediment O_2 consumption rates vary between 708 and 1665 µmol O_2 cm^{-2} yr^{-1}, which is consistent with sediment O_2 consumption rates typically reported for freshwater sediments (Rong, Shan, & Wang, 2016; Tomaszek & Czerwieniec, 2003). According to the model calculations, between 75 and 92 % of the total sediment O_2 consumption is due to oxygen respiration coupled to organic matter oxidation, with nitrification being the next most important pathway consuming O_2. The contribution of nitrification (step 1 plus step 2) to O_2 reduction, however, is significantly larger at the upstream (22-25%) site, compared to the downstream site (8-12 %). The inferred dominant roles of organic matter oxidation and nitrification in benthic O_2 uptake agrees with previous studies (Canavan et al., 2006; Clevinger et al., 2014; Hall and Jeffries, 1984).

2.5.2 Pore water N profiles

The impact of the WWTP is also seen in the water column chemistry: the bottom water concentrations of nitrate, nitrite and ammonium are all higher at the downstream site (**Table 2.5**). For example, the downstream bottom water nitrite concentrations are in the range of 10-15 µM, compared to 3-5 µM upstream concentrations. Depth profiles of the various pore water N species are shown in **Figure 2.2** for August and **Figure 2.3** for October. The profiles measured on the duplicate cores collected at the two sites exhibit significant variability, in particular for nitrite and ammonium. Given the high spatial heterogeneity, the model fits therefore only aim to capture the general trends of the concentration depth profiles. Irrespective of site and sampling time, the nitrate concentrations drop to zero within the upper 3-4 cm. Similar nitrate profiles have been observed in earlier work on estuarine and freshwater sediments (Meyer et al. 2005; Laverman et al. 2007). The steep nitrate pore water gradients reflect the very high rates of denitrification in the uppermost centimeters of sediments in these environments. The ammonium pore water profiles show increasing trends with depth, reaching concentrations of up to 2 mM in October.

According to the model results, most pore water ammonium is produced from the breakdown of organic matter (**Figures 2.2** and **2.3**).

Compared to nitrate, far fewer nitrite pore water profiles have been published, though nitrite has been shown to be present in sediment pore waters (Stief et al. 2002, Meyer et al. 2005) and in river water (Kelso et al. 1997, Von Der Wiesche & Wetzel 1998, Raimonet et al. 2015). The nitrite profiles measured in the sediments collected at the upstream site shows a subsurface peak at 3-4 cm depth. Similar subsurface peaks have previously been observed in estuarine and mangrove sediments using NOx microsensors (Meyer et al., 2008, 2005). At the downstream site, the highest nitrite concentrations are found right at the SWI. The nitrite profiles reflect the depth distributions of the processes that consume and produce nitrite, primarily nitrification, denitrification and anammox (see also Stief et al. 2002; Meyer et al. 2005). According to the model simulations, the absence of a pronounced nitrite peak at the downstream site is the result of the much higher rates of aerobic carbon oxidation right below the SWI and, in turn, the lower nitrification rates in the top centimeters of sediment. Also at the downstream site, higher rates of anammox in the presence of ammonium and nitrite affect the shape of nitrite profiles at the SWI. The generally low nitrite levels in the bottom portions of the cores are attributed to consumption by anammox.

2.5.3 Benthic N cycling: reaction rates

Depth-integrated rates estimated with the model are provided in **Table 2.9** and **Figures 2.4** and **2.5**. The figures schematically illustrate the mechanistic insights that can be gained by applying the reactive model to the pore water geochemistry and core incubation data. In particular, they show the close coupling between the various N transformation processes and benthic exchanges. As expected, denitrification is predicted to be the main N transformation pathway in the sediments, with most of the nitrate consumed by the denitrifiers supplied by influx from the overlying water, although nitrification also contributes 19-21% of the pore water nitrate supply at the upstream site. The depth-integrated rates of denitrification are much higher in October than in August. For nitrification, the largest differences in depth-integrated rates are observed between the upstream and downstream sites, because the lower deposition of highly reactive

organic matter (POC1, **Table 2.5**) at the upstream site leaves a greater fraction of pore water O_2 available for the aerobic oxidation of ammonium and nitrite.

The modeled rates of denitrification for the Seine River sediments fall in the range 497-1248 µmol cm^{-2} yr^{-1}. These rates are consistent with previous studies on Seine sediments (**Table 2.9**). Billen et al. (2007) report a range of benthic denitrification rates between 60 and 2500 µmol cm^{-2} yr^{-1} based on a large scale survey of direct measurements along the Seine drainage network, while Thouvenot-Korppoo et al. (2009) estimate mean rates in the range 125-625 µmol cm^{-2} yr^{-1} averaged over a stretch of the Seine River from 80 km upstream to 100 km downstream of Paris. The very high rates of denitrification observed in the Seine River sediments are characteristic of river systems receiving large anthropogenic inputs of nitrogen and organic carbon. For comparison, **Table A1** gives denitrification rates measured in sediments of other rivers and river impoundments.

The depth-integrated rates of DNRA are in the range of 16-41 µmol cm^{-2} yr^{-1}. Thus, DNRA accounts only for about 3% of the total rates of nitrate reduction in the sediments. As for denitrification, the rates of DNRA are higher in October than in August, due to the higher supply of reactive organic matter in October. The modeled depth-integrated rates of anammox in the Seine River sediments vary between 33 and 78 µmol cm^{-2} yr^{-1}, with higher values in the downstream than upstream sediments. The October pore water profiles also show measurable nitrite concentrations coexisting with high ammonium concentrations in the lower half of the cores, implying favorable chemical conditions for anammox at all depths except in the uppermost oxygenated sediment layers. The anammox rates estimated here are within the range reported for sediments in urban streams and wetlands (Shen et al. 2015; Wang et al., 2013; **Table A1**).

Table 2.6. Sediment mixing and pore water irrigation coefficients in August 2012.

	Downstream	
Depth (*x*)	**Sediment Mixing** $\mathbf{cm^2\ yr^{-1}}$	**Pore water irrigation** $\mathbf{yr^{-1}}$
$x < 0.1\ cm$	$D_B = 300$	$\alpha = 200$
$0.1 < x < 4\ cm$	$D_B = 100$	$\alpha = 50$
$4 < x < 20\ cm$	$D_B = 5$	$\alpha = 20$
	Upstream	
Depth (*x*)	**Sediment Mixing** $\mathbf{cm^2\ yr^{-1}}$	**Pore water irrigation** $\mathbf{yr^{-1}}$
$x < 0.1\ cm$	$D_B = 150$	$\alpha = 200$
$0.1 < x < 4\ cm$	$D_B = 150$	$\alpha = 50$
$4 < x < 20\ cm$	$D_B = 5$	$\alpha = 10$

Table 2.7. Sediment mixing and pore water irrigation coefficients in October 2013.

	Downstream	
Depth (*x*)	**Sediment Mixing** $\mathbf{cm^2\ yr^{-1}}$	**Pore water irrigation** $\mathbf{yr^{-1}}$
$x < 0.1\ cm$	$D_B = 600$	$\alpha = 300$
$0.1 < x < 2\ cm$	$D_B = 300$	$\alpha = 100$
$2 < x < 20\ cm$	$D_B = 10$	$\alpha = 15$
	Upstream	
Depth (*x*)	**Sediment Mixing** $\mathbf{cm^2\ yr^{-1}}$	**Pore water irrigation** $\mathbf{yr^{-1}}$
$x < 0.1\ cm$	$D_B = 500$	$\alpha = 300$
$0.1 < x < 3\ cm$	$D_B = 200$	$\alpha = 200$
$3 < x < 20\ cm$	$D_B = 10$	$\alpha = 10$

Table 2.8. Benthic O_2 consumption rates; values in brackets correspond to percentages of the total O_2 consumption rates.

Reaction rate	Upstream		Downstream	
(μmol O_2 cm^{-2} yr^{-1})	August 2012	October 2013	August 2012	October 2013
Organic matter oxidation with O_2	708 (75)	1230 (78)	1305 (88)	1665 (92)
Nitrification step 1	180 (19)	271 (17)	143 (10)	126 (7)
Nitrification step 2	60 (6)	82 (5)	23(2)	25 (1)
Fe oxidation by O_2	0.6 (<0.5)	0.002 (<0.5)	0.04 (<0.5)	0.007 (<0.5)
H_2S oxidation by O_2	0.4 (<0.5)	0.2 (<0.5)	4 (<0.5)	0.9 (<0.5)
Total	949 (100)	1583 (100)	1475 (100)	1817 (100)

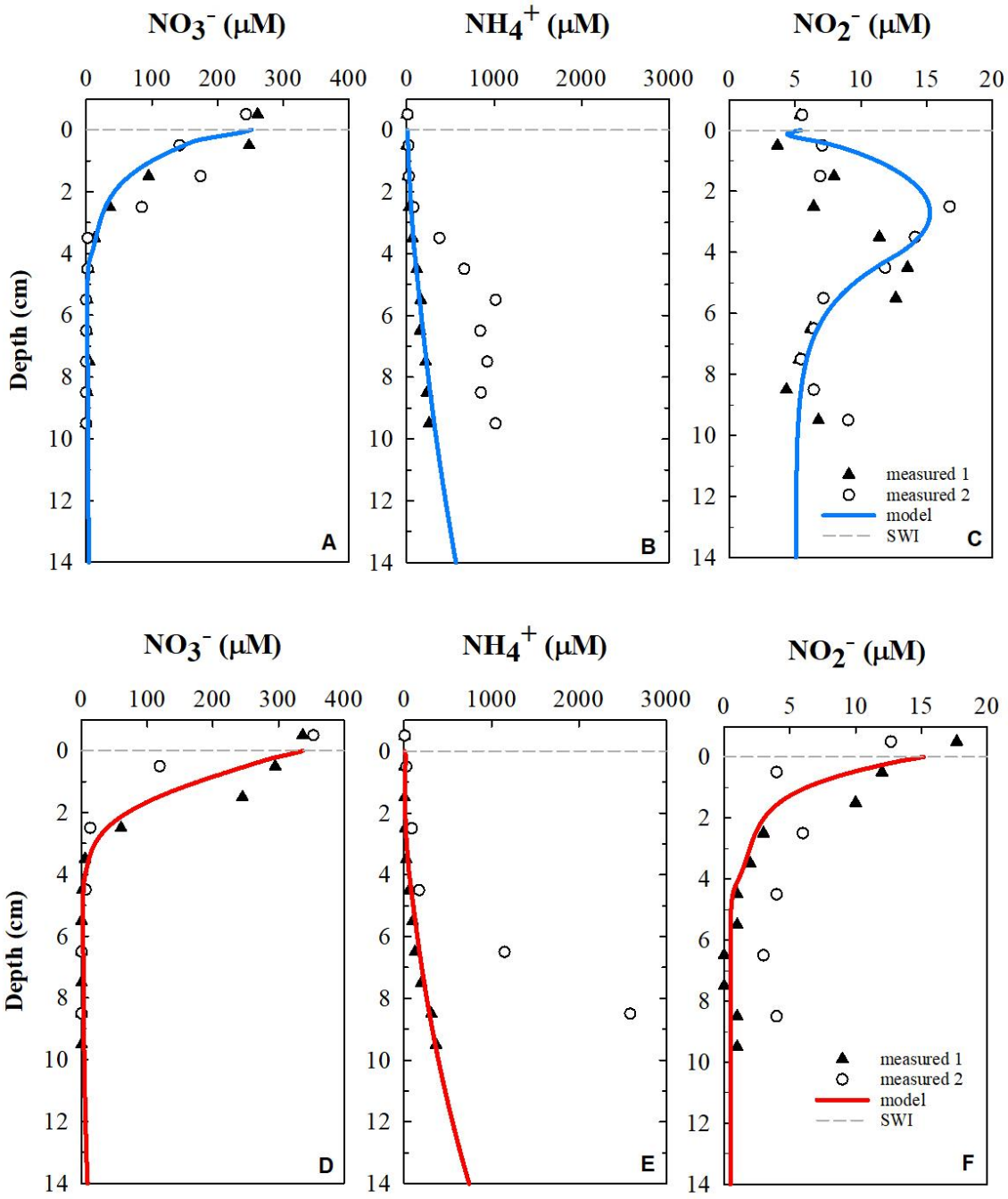

Figure 2.2 Measured and modeled pore water profiles of nitrogen species upstream (A, B, C) and downstream (D, E, F) of the SAV wastewater treatment plant in August 2012.

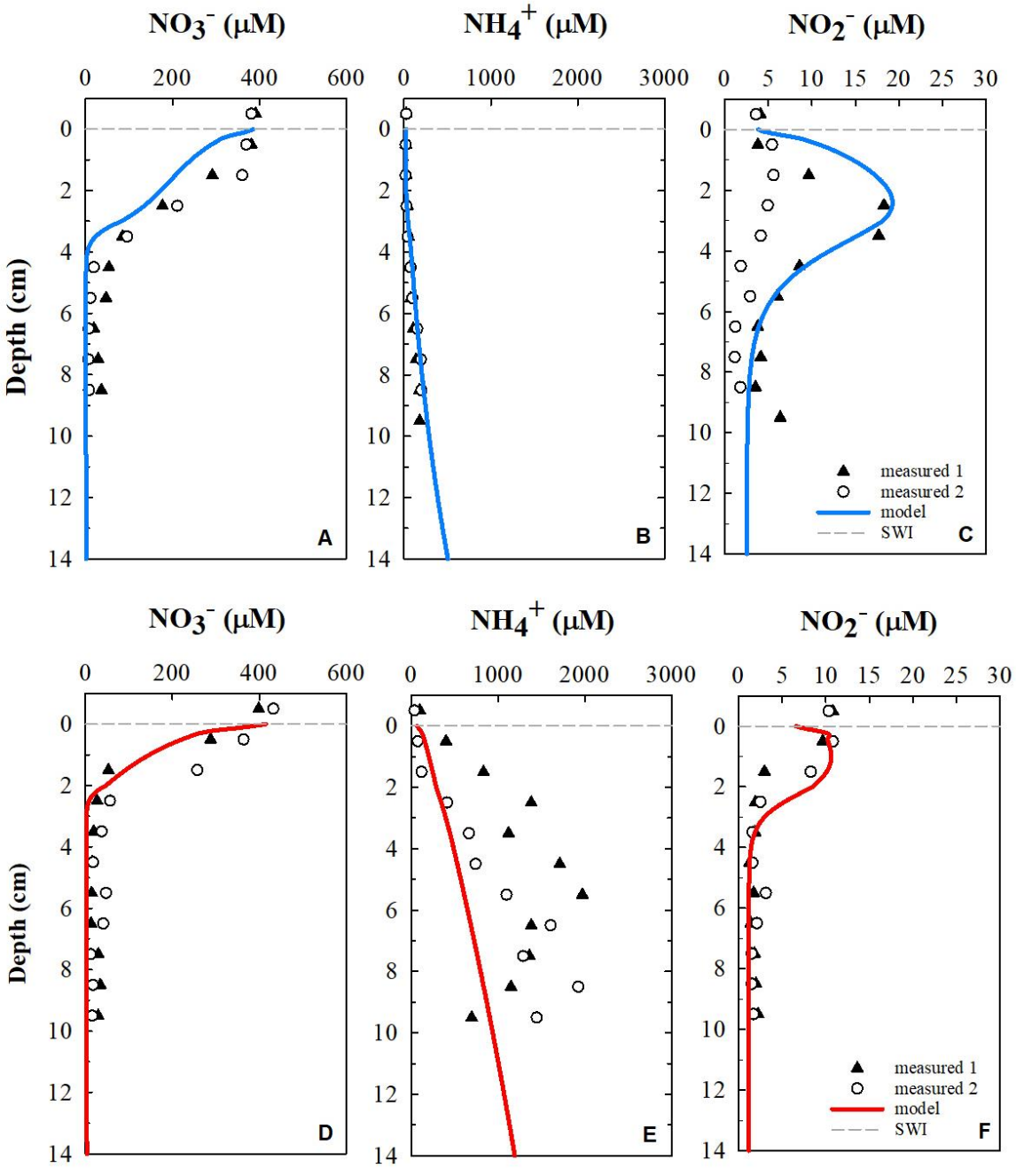

Figure 2.3. Measured and modeled pore water profiles of nitrogen species upstream (A, B, C) and downstream (D, E, F) of the SAV wastewater treatment plant in October 2013.

Table 2.9. Depth integrated rates (µmol N cm^{-2} yr^{-1}) for different processes upstream and downstream of the SAV WWTP in August 2012 and October 2013.

Reaction	Upstream		Downstream		Range in literature	References
	August 2012	October 2013	August 2012	October 2013		
Nitrification (step1)	120	191	95	84	< 5000	[1],[2],[3],[4],[5]
Denitrification	554	829	497	1248	< 13850	[5], [6],[7],[8],[9],[10],[11],[12]
DNRA	18	27	16	41	< 219	[13], [14],[15], [16]
Anammox	33	33	78	73	$0.1 - 720$	[17], [18], [19]

[1]: (Pauer, 2000), [2]: (Strauss et al., 2004), [3]: (Stief and de Beer, 2006), [4]:(Meyer et al., 2008), [5]: (Keffala et al., 2011), [6]:(Laursen and Seitzinger, 2002), [7]:(Canavan et al., 2006), [8]:(Tomaszek and Czerwieniec, 2000), [9]: (Seitzinger, 1988), [10]: (García-Ruiz et al., 1998), [11]: (Thouvenot-Korppoo et al., 2009), [12]: (Billen et al., 2007), [13]: (Gardner and McCarthy, 2009), [14]: (Dale et al., 2011), [15]; (McCarthy et al., 2007), [16]:(Gardner et al., 2006), [17]: (Zhao et al., 2013), [18]: (Shen et al., 2015), [19]: (Wang et al., 2013)

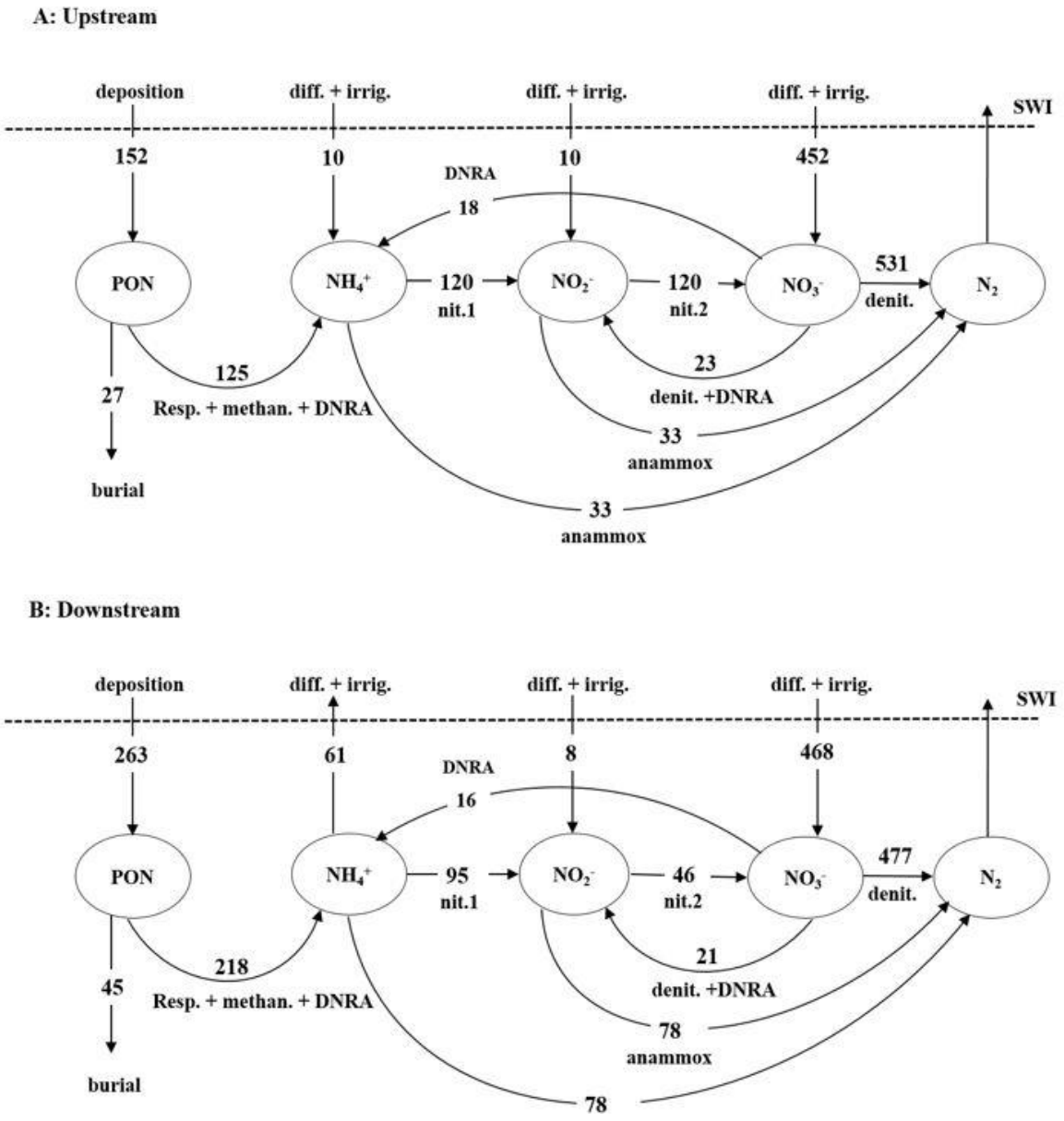

Figure 2.4. Sediment nitrogen budgets. The values refer to model-derived, depth integrated reaction rates and fluxes (µmol cm^{-2} yr^{-1}) for the sites upstream (A) and downstream (B) of the SAV WWTP in August 2012. (diff.: diffusion; irrig.: irrigation; nit.1: nitrification step1; nit2.: nitrification setp2, methan.: methanogenesis; resp.: respiration)

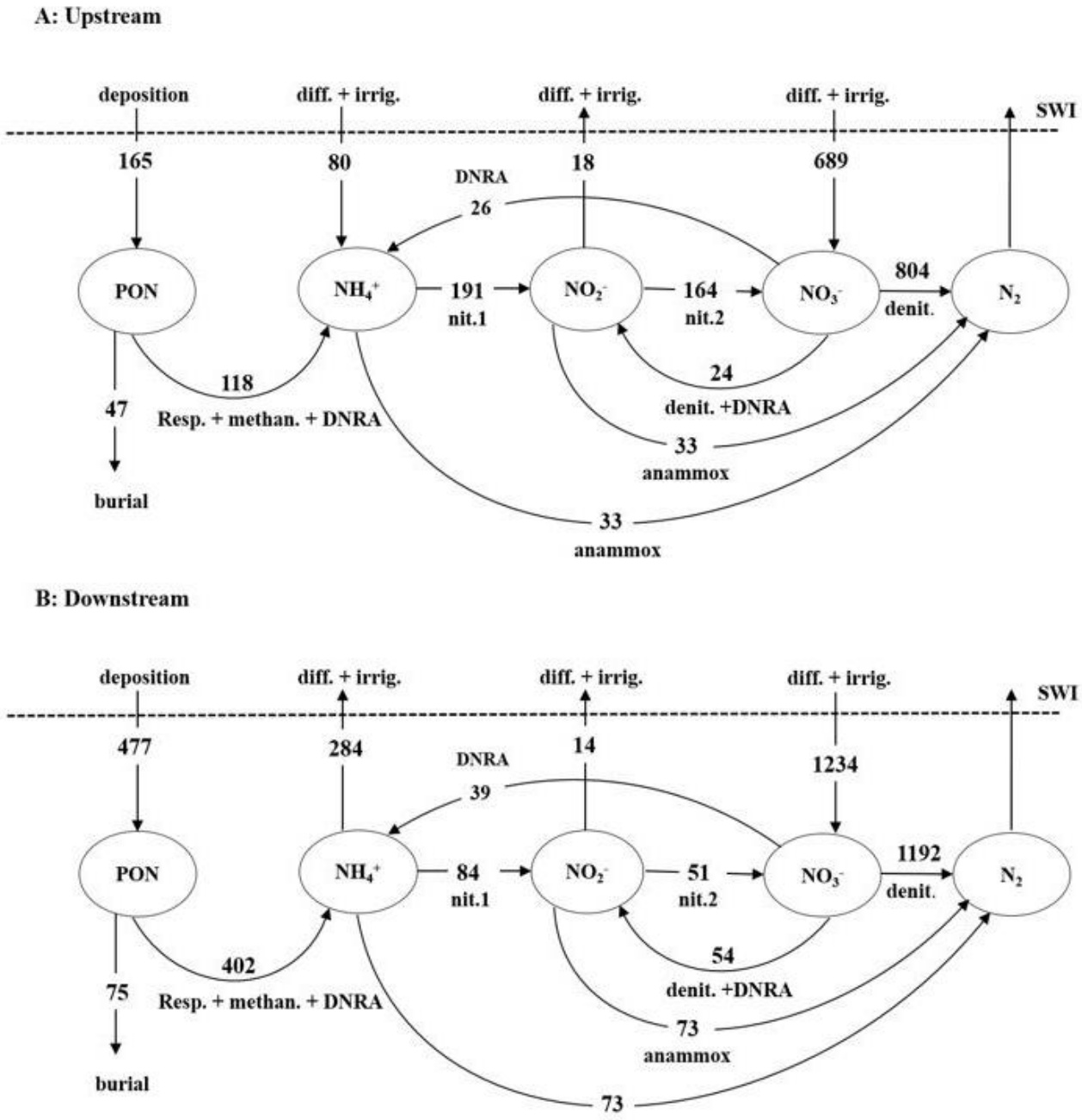

Figure 2.5. Sediment nitrogen budgets. The values refer to model derived-depth, integrated reaction rates and fluxes (µmol cm^{-2} yr^{-1}) for the sites upstream (A) and downstream (B) of the SAV WWTP in October 2013. (diff.: diffusion; irrig.: irrigation; nit.1: nitrification step1; nit2.: nitrification setp2, methan.: methanogenesis; resp.: respiration)

Table 2.10. Benthic nitrite fluxes reported in the literature; positive values indicate efflux to the water column, negative values indicate sediment uptake fluxes.

Location	Benthic nitrite fluxes at the SWI (μmol N cm^{-2} yr^{-1})	Explanation	References
Lake Sempach, Switzerland	+3.6 to +14.7	Deep, eutrophic and artificially oxygenated	(Höhener et al., 1994)
Lake Taihu, China	-27.1	Shallow and eutrophic	(McCarthy et al., 2007)
Guarapiranga reservoir, Brazil	+100.0	Eutrophic, located in a highly populated and industrialized area	(Mozeto et al., 2001)
Mangrove sediments, China	-15.0 to +32.4	Under light and dark condition in two seasons	(Kaiser et al., 2015)
Morlaix Bay, France	-9.5 to +8.1	Seasonal variations during a year	(Lerat, 1990)
Florida Bay, US	-1.5 to +1.9	Shallow subtropical	(Gardner and McCarthy, 2009)
Florida Bay, US	-1.3 to +45.5	After addition of nitrate in the overlying water	(Gardner and McCarthy, 2009)
Seine River, France	-8.3 to +17.5	Upstream and downstream of the SAV WWTP	(modeled, this study)

2.5.4 Benthic exchange fluxes

The benthic exchange fluxes of nitrate, ammonium and nitrite are summarized in **Figure 2.6**. As expected, the sediments act as sinks for nitrate. The benthic uptake fluxes of nitrate are higher at the downstream site, and much higher in October than August. Both the core incubations and model results imply that the upstream sediments are a relatively small sink for ammonium, while the downstream sediments are a source of ammonium to the overlying water, due to the much larger production of ammonium from sediment organic matter degradation. A key difference in sediment N cycling between the sites is that the ammonium generated by organic matter breakdown is completely oxidized by nitrification and anammox within the sediment at the upstream site, while a large fraction is exported to the water column at the downstream site.

At both sites, sediments remove nitrite from the overlying water in August, but become nitrite sources to the overlying water in October. As with the other benthic N exchange fluxes, the magnitudes of the nitrite fluxes are higher in October than in August, and higher at the downstream site than the upstream site. There are few published benthic nitrite fluxes to which the fluxes obtained here can be compared. However, as can be seen from the literature values summarized in **Table 2.10**, existing studies report both influxes and effluxes of nitrite for a variety of freshwater and nearshore marine sediments, in agreement with the bidirectional nitrite fluxes observed for the Seine River sediments. Previous studies also highlight the roles of the bottom water O_2 (Höhener et al., 1994) and nitrate concentrations (Gardner and McCarthy, 2009), the C:N ratio of the organic matter in the topmost layer of sediment (Lerat, 1990), and the time of the year (Gardner and McCarthy, 2009; Kaiser et al., 2015), in controlling whether sediments are a source or sink of nitrite (Kaiser et al., 2015).

It is important to stress that the pore water N distributions (**Figures 2.2** and **2.3**) and the benthic N fluxes (**Figure 2.6**) represent data acquired independently from one another on separate sediment cores. The ability of the model to simultaneously account for the key features of the pore water profiles and the core incubation fluxes, as well as the general consistency of the model-predicted reaction rates and

exchange fluxes with those reported for other freshwater depositional environments (**Tables 2.9** and **A1**), therefore supports the use of the model as a tool to predict nitrite benthic exchanges under variable environmental conditions. In particular, the directional switch of the nitrite fluxes can be attributed to the higher benthic oxygen demand in October compared to August, and the corresponding lower fractions of O_2 that are directed to nitrite oxidation (**Table 2.8**), hence resulting in excess nitrite production that is exported to the overlying water column.

The model also helps anticipate how benthic nitrite fluxes in the Seine River might respond to changes in WWTP discharges, bottom water chemistry or depositional fluxes. This is illustrated by the results of the sensitivity analyses in **Figure 2.7**, which show that the O_2 concentration in the overlying water and the deposition flux of reactive organic matter exert key controls on the benthic nitrite fluxes. For the August conditions, setting the bottom water O_2 concentration to zero causes the sediments at both locations to switch from being sinks to becoming sources of nitrite to the overlying river water (see also **Figure A2**). For the October conditions, the sediments at both locations are a source of nitrite whether O_2 is present in the overlying water or not, but the magnitude of the benthic efflux is much higher in the absence of O_2. The large increase in nitrite efflux under O_2 depleted bottom waters is due to the cessation of nitrification, which no longer prevents pore water nitrite from escaping to the overlying water column.

The deposition flux of reactive organic carbon (POC1) significantly impacts benthic nitrite exchanges (**Figures 2.7** and **2.8**), because it directly affects the production of pore water nitrite by denitrification. As shown in **Figure 2.8**, the nitrite benthic flux correlates positively with the supply of POC1 to the sediments, although the trends differ between the two locations and between the two sampling times. The POC1 deposition flux at which the sediments switch from sink to source of nitrite is two to three times lower under the October than August conditions, in part because of the more vigorous pore water irrigation in October compared to August (**Tables 2.6 and 2.7**), which promotes the export of nitrite to the overlying water. Under the October conditions, the POC1 deposition flux at the two sites would have to

drop below 1000 µmol cm^{-2} yr^{-1} in order for the sediments to become nitrite sinks. Not surprisingly, the deposition flux of the less reactive POC2 has much less of an effect on the benthic nitrite fluxes than POC1.

Bottom water ammonium concentrations affect the benthic nitrite fluxes by impacting nitrification (nitrite source) and anammox (nitrite sink). Sensitivity to changes in bottom water ammonium is relatively higher at the upstream site, because of the important role of nitrification in producing pore water nitrite (**Figures 2.4** and **2.5**). In the downstream sediments, where anammox is a major sink of nitrite, the effects of changes in bottom water ammonium on nitrification and anammox tend to balance each other out. In a similar vein, changes in bottom water nitrate concentrations result in opposing effects of denitrification (nitrite source) and anammox (nitrite sink). Hence, the benthic nitrite fluxes tend to be relatively insensitive to changing bottom water nitrate concentrations.

2.5.5 Nitrite budget

The experimental and modeling results show that the Seine sediments at the two locations can act as either a source or sink of nitrite. This raises the question of the role of benthic exchanges on the nitrite budget of the river. A full assessment of this role would require the systematic (seasonal) acquisition of benthic nitrite exchange data along the entire course of the river. Here, we provide rough estimations of the potential benthic nitrite supply and removal using a maximum nitrite efflux of around 30 µmol cm^{-2} yr^{-1}, as measured in October 2013 at the downstream site, and a maximum influx of around 10 µmol cm^{-2} yr^{-1}, as measured in the August incubations (**Figure 2.6**). Over a 300 km-long stretch of the Seine River, and for a representative width of 200 m plus an assumed 10% coverage by nitrite-exchanging streambed sediments, this results in an annual maximum benthic nitrite release of 6×10^5 mol yr^{-1} and a maximum uptake of 2×10^5 mol yr^{-1}. In comparison, the SAV WWTP discharged on average 6×10^7 mol yr^{-1} of nitrite between 2007 and 2013 (Aissa-Grouz et al., 2015), that is two orders of magnitude higher than the calculated benthic exchanges. Although our preliminary calculations need further corroboration, at this stage it appears that the benthic exchanges are a relatively small component of the Seine River nitrite budget downstream of the WWTP. If this is true, then the persistence of measurable nitrite concentrations as far as 300 km downstream

of Paris despite fully aerated conditions (Aissa-Grouz et al., 2015) may be due to the combination of high nitrite release from the SAV WWTP, high river discharge and low nitrification activity in the water column (Raimonet et al., 2017).

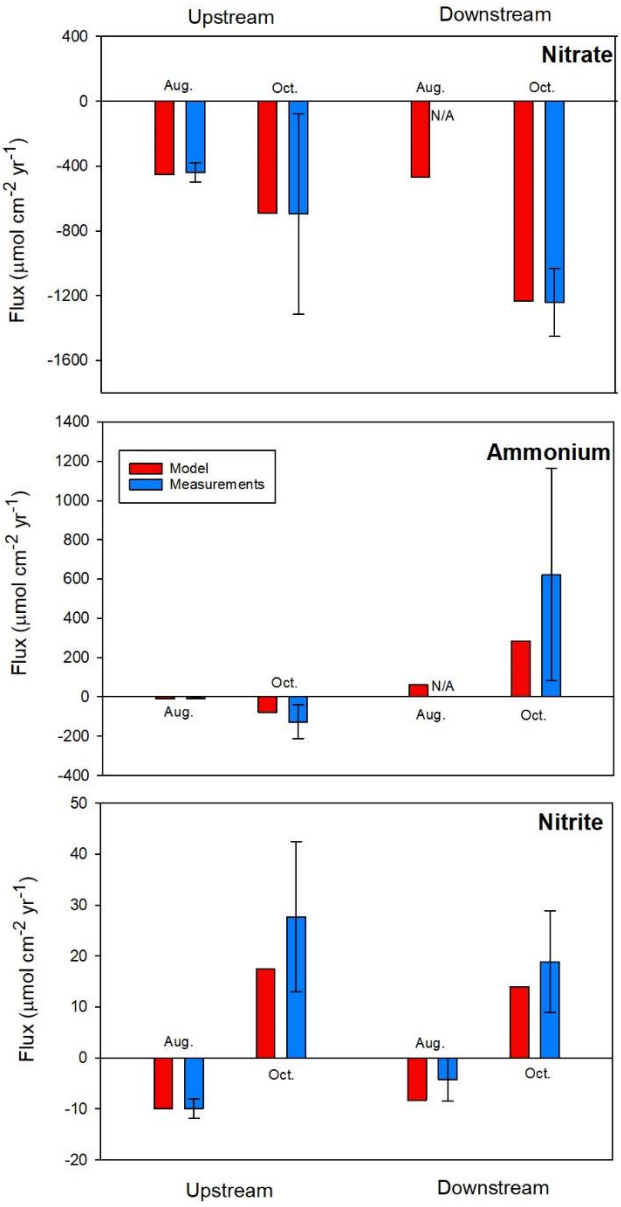

Figure 2.6. Measured and modeled nitrate (A), ammonium (B) and nitrite fluxes (C) across the sediment water interface (SWI) at the sampling sites upstream and downstream of the SAV WWTP in August 2012 and October 2013. Error bars represent standard deviations on triplicate cores.

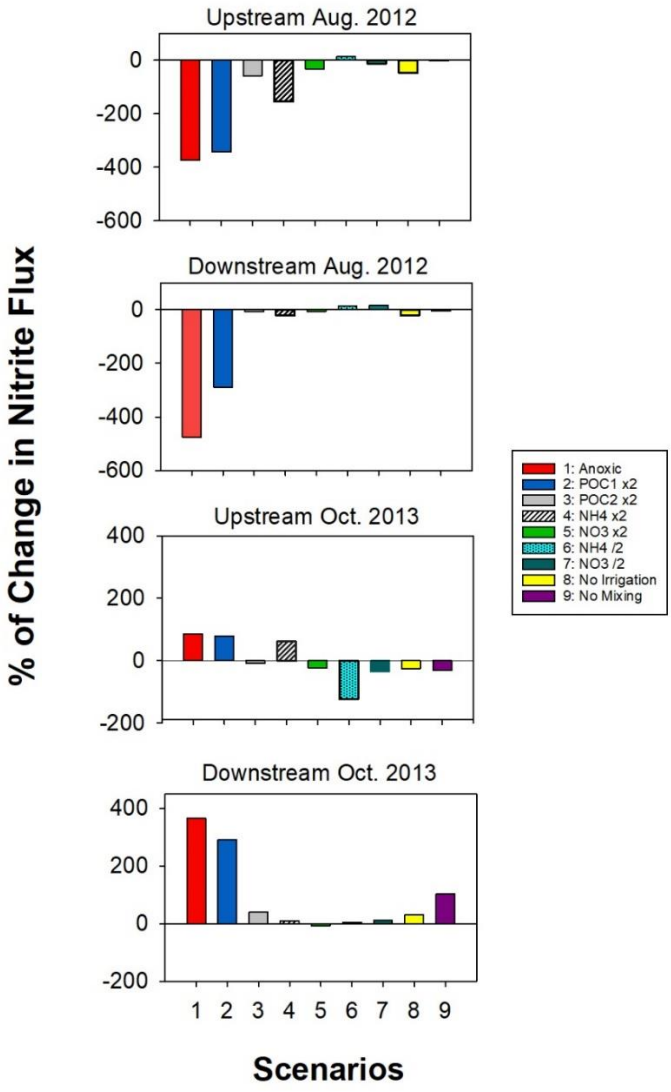

Figure 2.7. Sensitivity analyses of the nitrite flux at the SWI based on different scenarios. Scenarios include no bottom water O_2 (Anoxic), doubled deposition flux of POC1 at the SWI (POC1 x2), doubled deposition flux of POC2 at the SWI (POC2 x2), doubled concentrations of ammonium and nitrate in the overlying water (NH_4 x2, NO_3 x2, respectively), and halving concentrations of ammonium and nitrate in the overlying water (NH_4 /2, NO_3 /2, respectively). No irrigation corresponds to a simulation where a zero value was imposed to the pore water irrigation coefficient (α) and no mixing represents a simulation where a zero value was imposed to the sediment mixing coefficient (D_B). Negative changes imply a change in the direction of the benthic nitrite flux.

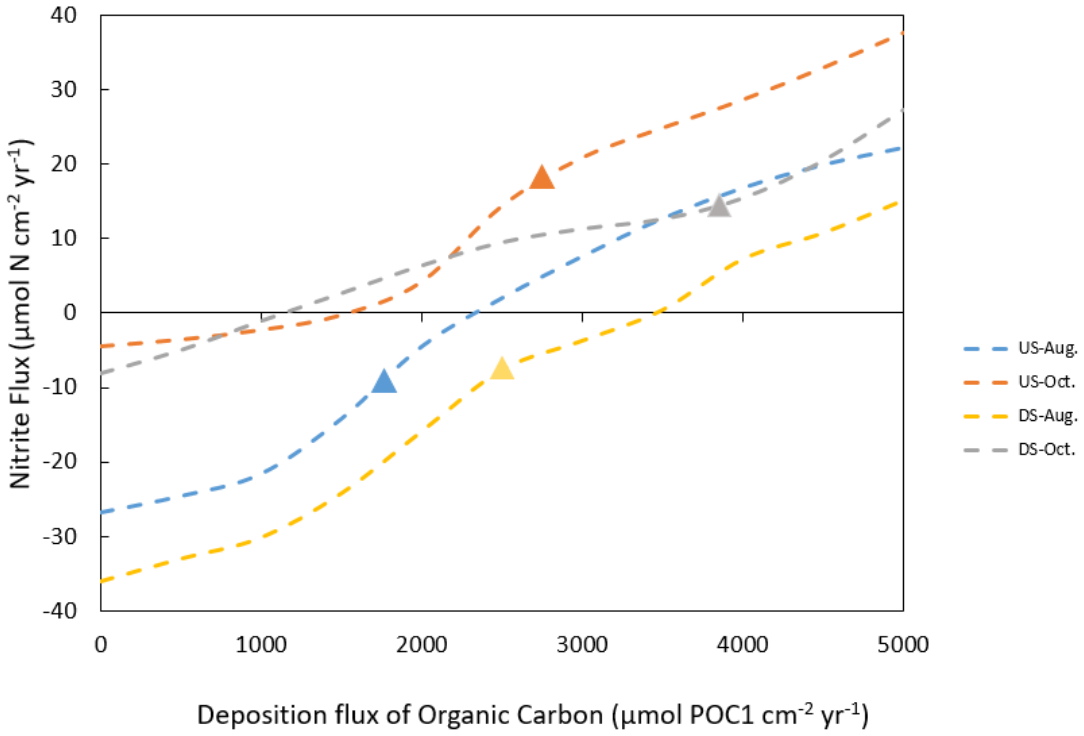

Figure 2.8. Nitrite fluxes across the SWI as a function of deposition flux of the most reactive organic carbon, POC1. Symbols correspond to fluxes simulated with the model-calibrated POC1 deposition fluxes at the two sites (US = upstream, DS = downstream) and two sampling times (August and October). Positive fluxes indicate nitrite efflux from sediment to water column, negative fluxes indicate uptake of nitrite by the sediments.

2.6 Concluding remarks

With the model presented in this paper we have analyzed how benthic nitrite exchanges in the Seine River are modulated by environmental conditions at, and early diagenetic processes below, the SWI. The model accounts for the key features of the observed pore water profiles of the different nitrogen species while at the same time reproducing the measured benthic fluxes of nitrate, nitrite and ammonium; it captures the differences between the sediments collected upstream and downstream of the SAV WWTP, and between the summer and fall sampling times. While the modeling results imply that denitrification dominates N cycling in the sediments, they also highlight the important roles of other transformation pathways, especially nitrification and anammox, and (bio)physical mixing processes in determining the distributions and benthic fluxes of the various N species. In particular, the model explains why, depending on the site location and sampling time, the sediments either release nitrite to the overlying water column or remove it. The simulation results further indicate that the SAV WWTP not only impacts downstream benthic nitrite fluxes through the discharge of N species contained in its effluents, but also by affecting the supply of labile organic matter and the dissolved oxygen concentration at the sediment-water interface.

As illustrated here for a comprehensive data set on N species, early diagenetic modeling can be a powerful tool for analyzing benthic transformations and fluxes in highly dynamic systems such as streambed sediments. Mechanistic modeling forces us to question our understanding of the processes and their interactions within sediments that give rise to the observed pore water geochemistry and benthic exchanges. As such, the modeling provides complementary information that cannot be deduced directly from the data alone. With the rapid improvement of analytical capabilities, including in situ microsensors, it is becoming increasingly routine to measure the relatively low concentrations of reactive intermediates in biogeochemical reaction networks. This creates an increasing demand for environmental reactive transport models that explicitly simulate the production, consumption and transport of reactive intermediates, as done here for nitrite. The model developed in this study should be broadly applicable to sediments in freshwater aquatic environments receiving high N and organic matter loads.

Chapter 3

Modeling dynamic changes in nitrogen isotopic compositions during freshwater sediment incubation experiments

Zahra Akbarzadeh, Anniet Laverman, Philippe Van Cappellen

3.1 Summary

The early diagenetic reactive transport model of nitrogen (N) presented in Chapter 2 is augmented by explicitly representing the N isotopic compositions of the various N species included in the model: nitrate, nitrite, ammonium and organic nitrogen. Changes in $\delta^{15}N$ values of these species are driven by isotopic fractionation during nitrification, denitrification, anammox and dissimilatory nitrate reduction to ammonium (DNRA), as well as differential diffusion rates due to isotope mass differences. As an application of the model, we simulate the temporal variations in isotopic composition of N species that would be measured in the overlying water during core incubation experiments of streambed sediments from the Seine River downstream of Paris, France. By considering different scenarios, we specifically aim to identify the controls on variations in $\delta^{15}N$ of nitrite exchanged across the sediment-water interface. The results highlight the key role of bottom water oxygenation on the isotopic variations of the aqueous N species. The sensitivity of the model results to the various N transformation processes will help design and interpret upcoming sediment incubation experiments with Seine River sediments that are planned by our French colleagues.

3.2 Introduction

In enzymatically catalysed reactions of the N cycle, molecules with light ^{14}N are usually slightly more reactive than those with heavy ^{15}N; therefore, reaction products are enriched (i.e., they have a higher proportion of the lighter isotope) and the remaining reactants are depleted (i.e., have a higher proportion of heavier isotopes) (Möbius, 2013). The isotopic fractionation factor is defined as $\alpha = {}^{14}k/{}^{15}k$, where ^{14}k and ^{15}k are the rate constants associated with the light and heavy isotopes in a one-step reaction, respectively. The isotopic enrichment factor for a given reaction pathway is reported as $\varepsilon = (\alpha - 1) \times 1000$.

Isotopic compositions of N species have been used extensively to identify the sources and track the transformations of N in aquatic environments. Isotopic compositions are conventionally reported in delta notations as $\delta(‰) = (\frac{R_{sample}}{R_{standard}} - 1) \times 1000$, where R is the isotopic ratio, that is, $R = {}^{15}N/{}^{14}N$. It is generally recognized that tracing isotopic compositions in environmental studies may unlock essential information (Sigman et al., 2009). For instance, in the case of nitrate, stable isotopes can help differentiate between the different biological processes producing nitrate, such as nitrification, denitrification and assimilation. Stable isotope signatures enable us to better constrain N budgets, which is particularly important when there are multiple sources of N to a given environment (Delconte et al., 2014), and to guide the development of predictive models of N cycling. The combination of isotopic data and quantitative modelling yields a robust tool for environmental assessment (Delconte et al., 2014). Extending mass balance calculations to include isotopes reduces the uncertainties of the model predictions.

Because nitrite is a reactive intermediate in the N cycle, interpreting its isotopic composition is less straightforward than those of nitrate and ammonium. Nitrite is produced and consumed in different reactions – denitrification, DNRA, nitrification steps 1 and 2, and anammox – each associated with their specific fractionation factors. Additionally, the evaluation of nitrite's isotopic signature in the presence of nitrification is complicated by the unusual fractionation factor of the second step of nitrification, which produces heavier N-nitrate (Casciotti, 2009). The isotopic composition of nitrite is strongly coupled to those of the other, usually more abundant N species. For instance, if ammonium available in the system is

enriched in ^{15}N, then nitrite produced from this ammonium will have a relatively high $\delta^{15}N$ (Jacob et al., 2016). Therefore, the measured isotopic signature of nitrite species may be the end result of the various N sources and N cycling processes. The final isotopic composition of nitrite in a given environment may be very different from that of nitrite entering the system.

Studies addressing fractionation factors affecting nitrite along with nitrate and ammonium in freshwater sediments under non-steady state conditions are scarce. The most common modeling approach in the literature for predicting isotopic compositions in unidirectional closed or open systems is the Rayleigh model (Casciotti, 2009). The Rayleigh model, however, is applicable only to individual isotope effects and unable to account for multiple processes that simultaneously influence both reactant and product pools. Some researchers (Casciotti and Buchwald, 2012; Granger and Wankel, 2016) have used time dependent box models to analyze dual isotope (N and O) measurements in the oceans. Rooze and Meile (2016) developed a reactive transport model to investigate N isotope effects of various N species including nitrite in marine environments, assuming steady state conditions.

In this chapter, we expand the existing early diagenetic model, presented in Chapter 2 of this thesis, by explicitly representing the two stable isotopes, ^{14}N and ^{15}N, in nitrate, nitrite, ammonium and organic N, and incorporating the isotopic fractionation effects of the N transformation processes. As an application, we then use the model to simulate the temporal variations in isotopic values of N species, including nitrate, nitrite, and ammonium, that would be observed under the non-steady state conditions of core incubation experiments with streambed sediments. The focus is on the temporal changes in the $\delta^{15}N$ of nitrite, which, as a reactive intermediate species, have received less attention in the literature. Multiple scenarios are simulated with the model to investigate the effects of different processes that fractionate N isotopes in sediments. A Monte Carlo analysis is used to estimate the uncertainties associated with the fractionation factors of the different processes. The model has been developed in anticipation of incubation experiments with Seine River sediments that will be carried out in France in October 2018 by our colleagues at the University of Rennes. The results of our work is helping them design the experiments. In particular, learning

from the results of the modeled scenarios, we propose to conduct two separate sets of core incubation experiments.

3.3 Methods

3.3.1 Temporal variations in bottom water (upper boundary conditions)

The upper boundary conditions of the model include the concentrations and isotopic compositions of aqueous N species at the sediment-water interface (SWI). In core incubation experiments where the overlying water column is kept well-mixed, the boundary concentrations are those measured during the experiment by sampling the free water above the sediment surface. Because of the benthic exchange fluxes and the finite volume of overlying water in the experiments, the boundary concentrations and isotopic compositions are continuously changing. To reproduce this in the model calculations, the elemental and isotopic compositions of the N species in the overlying water are updated every 60 minutes, based on the computed benthic fluxes across the SWI. We assume that no transformations occur between the different N species in the overlying water; therefore, the only sources or sinks for the overlying water are the benthic fluxes. All reactions are confined to the sediment below the SWI. For instance, a positive flux (from sediments to the overlying water) of nitrite will increase the nitrite concentration in the overlying water. If the benthic nitrite efflux from the sediment carries a different isotopic composition than the nitrite already present in the overlying water, the isotopic nitrite composition in the overlying water will change.

3.3.2 N isotopic fractionations

We introduce N isotopic fractionations to our early diagenetic model following the approach of Dale et al. (2009). For each species of N, two pools, one comprising the light the other and heavy N isotope, are considered in the model. The rate of each reaction consuming a given N species is then different for the light and heavy pools due to enzymatic discrimination in favor of light N. Therefore, for each fractionating reaction of the original reaction network, there are now two rate expressions when the reaction consumes one N species and four when two N species are consumed (see **Table 3.1**). For instance, the anammox reaction now has four rate expressions for the combinations light ammonium plus light nitrite, heavy

ammonium plus heavy nitrite, light ammonium polus heavy nitrite, and heavy ammonium plus light nitrite, with different fractionation factors for ammonium and for nitrite (**Table 3.2**).

If ${}_{A}N$ is N-containing substrate A that, through a one-step enzymatic process, produces ${}_{B}N$, then the rates of reaction are different for ${}^{14}_{A}N$ and ${}^{15}_{A}N$. In the case of first order decay, the representations of the reaction are as follows:

$${}^{14}_{A}N \xrightarrow{{}^{14}k} {}^{14}_{B}N \qquad 3.1$$

$${}^{15}_{A}N \xrightarrow{{}^{15}k} {}^{15}_{B}N \qquad 3.2$$

where ${}^{14}k$ and ${}^{15}k$ refer to the respective reaction rate constants of the light and heavy isotopes. For a given reaction *i*, the total rate of the reaction (r_i) is the sum of the rates for ${}^{14}N$ and ${}^{15}N$.

$$r_i = {}^{14}r_i + {}^{15}r_i \qquad 3.3$$

$${}^{14}r_i = {}^{14}k_i \times {}^{14}N \qquad 3.4$$

$${}^{15}r_i = {}^{15}k_i \times {}^{15}N \qquad 3.5$$

where the two rate constants are related to one another via the fractionation factor (see above).

The isotopic composition of an aqueous N species also affects its molecular diffusion rate. The ratio of the diffusion coefficients of two isotopologues in water is defined based on the square root of their reduced masses (LaBolle et al., 2008):

$$\frac{D_h}{D_l} = \sqrt{\frac{\mu_{lw}}{\mu_{hw}}} = \sqrt{\frac{m_l(m_h+m_w)}{m_h(m_l+m_w)}} \qquad 3.6$$

where m_l and m_h are the molecular weights of the molecules containing the light and heavy isotopes, respectively, and m_w is the molecular weight of water. The diffusion coefficients applied in the model calculations are reported in **Table 3.3**.

Table 3.1. Reaction formulae and rate expressions in the early diagenetic N model.

Process	Formula	Rate expression
Aerobic respiration[1]	$(CH_2O)_{org} + y(^*NH_3)_{org} + z(H_3PO_4)_{org} + O_2 + (2z-y)HCO_3^- \rightarrow y^*NH_4^+ + zHPO_4^{2-} + (1-y+2z)CO_2 + (1-y+2z)H_2O$	$R1 = k1 \times [POC] \times \frac{[O_2]}{[O_2] + Ko}$
Denitrification	$(CH_2O)_{org} + y(^*NH_3)_{org} + z(H_3PO_4)_{org} + 0.8^{14}NO_3 \rightarrow 0.4\,(1-\alpha-\beta)^{14}N_2 + y^*NH_4^+ + 0.8\alpha^{14}NO_2^- + 0.4\,\beta^{14}N_2O + zHPO_4^{2-} + (0.8-0.8\alpha+y-2z)\,HCO_3^- + (0.2-y+2z+0.8\alpha)CO_2 + (0.6-y+2z-0.8\alpha-0.4\,\beta)H_2O + (0.8\alpha-0.4\,\beta)H_2$	$R2l = k2 \times [POC] \times \frac{[^{14}NO_3^-] + [^{15}NO_3^-]}{[^{14}NO_3^-] + [^{15}NO_3^-] + Kmno} \times \frac{kin}{[O_2] + Kin} \times \frac{\alpha_{DNF}\,^{14}NO_3^-}{\alpha_{DNF}\,^{14}NO_3^- + {}^{15}NO_3^-} \times \gamma$ Nitrite production : $R3l = 0.8\alpha \times R2l$
Denitrification	$(CH_2O)_{org} + y(^*NH_3)_{org} + z(H_3PO_4)_{org} + 0.8^{15}NO_3 \rightarrow 0.4\,(1-\alpha-\beta)^{15}N_2 + y^*NH_4^+ + 0.8\alpha^{15}NO_2^- + 0.4\,\beta^{15}N_2O + zHPO_4^{2-} + (0.8-0.8\alpha+y-2z)\,HCO_3^- + (0.2-y+2z+0.8\alpha)CO_2 + (0.6-y+2z-0.8\alpha-0.4\,\beta)H_2O + (0.8\alpha-0.4\,\beta)H_2$	$R2h = k2 \times [POC] \times \frac{[^{14}NO_3^-] + [^{15}NO_3^-]}{[^{14}NO_3^-] + [^{15}NO_3^-] + Kmno} \times \frac{kin}{[O_2] + Kin} \times \frac{^{15}NO_3^-}{\alpha_{DNF}\,^{14}NO_3^- + {}^{15}NO_3^-} \times \gamma$ Nitrite production : $R3h = 0.8\alpha \times R2h$
DNRA	$(CH_2O)_{org} + y\,(^*NH_3)_{org} + z(H_3PO_4)_{org} + 0.5^{14}NO_3^- \rightarrow y^*NH_4^+ + (0.5-\delta)\,^{14}NH_4^+ + 0.5\delta^{14}NO_2^- + zHPO_4^- + (y-2z)HCO_3^- + (1-y+2z)CO_2 + (0.33-y+2z)H_2O + \delta H_2$	$R4l = k2 \times [POC] \times \frac{[^{14}NO_3^-] + [^{15}NO_3^-]}{[^{14}NO_3^-] + [^{15}NO_3^-] + Kmno} \times \frac{kin}{[O_2] + Kin} \times \frac{\alpha_{DNRA}\,^{15}NO_3^-}{\alpha_{DNRA}\,^{14}NO_3^- + {}^{15}NO_3^-} \times (1-\gamma)$ Nitrite production : $R5l = 0.5\delta \times R4l$
DNRA	$(CH_2O)_{org} + y(^*NH_3)_{org} + z(H_3PO_4)_{org} + 0.5^{15}NO_3^- \rightarrow y^*NH_4^+ + (0.5-\delta)\,^{15}NH_4^+ + 0.5\delta^{15}NO_2^- + zHPO_4^- + (y-2z)HCO_3^- + (1-y+2z)CO_2 + (0.33-y+2z)H_2O + \delta H_2$	$R4h = k2 \times [POC] \times \frac{[^{14}NO_3^-] + [^{15}NO_3^-]}{[^{14}NO_3^-] + [^{15}NO_3^-] + Kmno} \times \frac{kin}{[O_2] + Kin} \times \frac{^{15}NO_3^-}{\alpha_{DNRA}\,^{14}NO_3^- + {}^{15}NO_3^-} \times (1-\gamma)$ Nitrite production : $R5h = 0.5\delta \times R4h$

Anammox $^{14}NH_4^+ + {}^{14}NO_2^- \rightarrow {}^{14}N_2 + 2H_2O$

$$R6l = R6_{max} \times \frac{\left[{}^{14}NH_4^+\right] + \left[{}^{15}NH_4^+\right]}{\left[{}^{14}NH_4^+\right] + \left[{}^{15}NH_4^+\right] + Km1} \times \frac{\left[{}^{14}NO_2^-\right] + \left[{}^{15}NO_2^-\right]}{\left[{}^{14}NO_2^-\right] + \left[{}^{15}NO_2^-\right] + km2} \times \frac{Kin}{[O_2] + Kin} \times \frac{\alpha_{anx1}\left[{}^{14}NH_4^+\right]}{\alpha_{anx1}\left[{}^{14}NH_4^+\right] + \left[{}^{15}NH_4^+\right]} \times \frac{\alpha_{anx2}\left[{}^{14}NO_2^-\right]}{\alpha_{anx2}\left[{}^{14}NO_2^-\right] + \left[{}^{15}NO_2^-\right]}$$

Anammox $^{14}NH_4^+ + {}^{14}NO_2^- \rightarrow {}^{14}N^{15}N + 2H_2O$

$$R6lh = R6_{max} \times \frac{\left[{}^{14}NH_4^+\right] + \left[{}^{15}NH_4^+\right]}{\left[{}^{14}NH_4^+\right] + \left[{}^{15}NH_4^+\right] + Km1} \times \frac{\left[{}^{14}NO_2^-\right] + \left[{}^{15}NO_2^-\right]}{\left[{}^{14}NO_2^-\right] + \left[{}^{15}NO_2^-\right] + Km2} \times \frac{Kin}{[O_2] + Kin} \times \frac{\alpha_{anx1}\left[{}^{14}NH_4^+\right]}{\alpha_{anx1}\left[{}^{14}NH_4^+\right] + \left[{}^{15}NH_4^+\right]} \times \frac{\left[{}^{15}NO_2^-\right]}{\alpha_{anx2}\left[{}^{14}NO_2^-\right] + \left[{}^{15}NO_2^-\right]}$$

Anammox $^{15}NH_4^+ + {}^{14}NO_2^- \rightarrow {}^{14}N^{15}N + 2H_2O$

$$R6hl = R6_{max} \times \frac{\left[{}^{14}NH_4^+\right] + \left[{}^{15}NH_4^+\right]}{\left[{}^{14}NH_4^+\right] + \left[{}^{15}NH_4^+\right] + Km1} \times \frac{\left[{}^{14}NO_2^-\right] + \left[{}^{15}NO_2^-\right]}{\left[{}^{14}NO_2^-\right] + \left[{}^{15}NO_2^-\right] + Km2} \times \frac{Kin}{[O_2] + Kin} \times \frac{\left[{}^{15}NH_4^+\right]}{\alpha_{anx1}\left[{}^{14}NH_4^+\right] + \left[{}^{15}NH_4^+\right]} \times \frac{\alpha_{anx2}\left[{}^{14}NO_2^-\right]}{\alpha_{anx2}\left[{}^{14}NO_2^-\right] + \left[{}^{15}NO_2^-\right]}$$

Anammox $^{15}NH_4^+ + {}^{15}NO_2^- \rightarrow {}^{15}N_2 + 2H_2O$

$$R6h = R6_{max} \times \frac{\left[{}^{14}NH_4^+\right] + \left[{}^{15}NH_4^+\right]}{\left[{}^{14}NH_4^+\right] + \left[{}^{15}NH_4^+\right] + Km1} \times \frac{\left[{}^{14}NO_2^-\right] + \left[{}^{15}NO_2^-\right]}{\left[{}^{14}NO_2^-\right] + \left[{}^{15}NO_2^-\right] + Km2} \times \frac{Kin}{[O_2] + Kin} \times \frac{\left[{}^{15}NH_4^+\right]}{\alpha_{anx1}\left[{}^{14}NH_4^+\right] + \left[{}^{15}NH_4^+\right]} \times \frac{\left[{}^{15}NO_2^-\right]}{\alpha_{anx2}\left[{}^{14}NO_2^-\right] + \left[{}^{15}NO_2^-\right]}$$

Nitrification (step 1) $^{14}NH_4^+ + 1.5O_2 \rightarrow {}^{14}NO_2^- + H_2O + 2H^+$

$$R7l = R7_{max} \times \frac{\left[{}^{14}NH_4^+\right] + \left[{}^{15}NH_4^+\right]}{\left[{}^{14}NH_4^+\right] + \left[{}^{15}NH_4^+\right] + Km3} \times \frac{[O_2]}{[O_2] + Km4} \times \frac{\alpha_{nit1}\left[{}^{14}NH_4^+\right]}{\alpha_{nit1}\left[{}^{14}NH_4^+\right] + \left[{}^{15}NH_4^+\right]}$$

Nitrification (step 1)	$^{15}NH_4^+ + 1.5O_2 \rightarrow {}^{15}NO_2^- + H_2O + 2H^+$	$R7h = R7_{max} \times \frac{[^{14}NH_4^+] + [^{15}NH_4^+]}{[^{14}NH_4^+] + [^{15}NH_4^+] + Km3} \times \frac{[O_2]}{[O_2] + Km4} \times \frac{[^{15}NH_4^+]}{\alpha_{nit1}[^{14}NH_4^+] + [^{15}NH_4^+]}$
Nitrification (step 2)	$^{14}NO_2^- + 0.5O_2 \rightarrow {}^{14}NO_3^-$	$R8l = R8_{max} \times \frac{[^{14}NO_2^-] + [^{15}NO_2^-]}{[^{14}NO_2^-] + [^{15}NO_2^-] + Km5} \times \frac{[O_2]}{[O_2] + Km6} \times \frac{\alpha_{nit2}[^{14}NO_2^-]}{\alpha_{nit2}[^{14}NO_2^-] + [^{15}NO_2^-]}$
Nitrification (step 2)	$^{15}NO_2^- + 0.5O_2 \rightarrow {}^{15}NO_3^-$	$R8h = R8_{max} \times \frac{[^{14}NO_2^-] + [^{15}NO_2^-]}{[^{14}NO_2^-] + [^{15}NO_2^-] + Km5} \times \frac{[O_2]}{[O_2] + Km6} \times \frac{[^{15}NO_2^-]}{\alpha_{nit2}[^{14}NO_2^-] + [^{15}NO_2^-]}$

Table 3.2. Fractionation factors associated with the N reactions included in the model.

Process	symbol	range	Source	Value used in the scenarios
Denitrification	α_{DNF}	1.013–1.030	(Casciotti, 2009), (Rooze and Meile, 2016) (Quan and Falkowski, 2009)	1.02
DNRA	α_{DNRA}	1.013–1.030	assumed similar to denitrification	1.02
Nitrification1	α_{nit1}	1.014–1.038	(Casciotti, 2009), (Rooze and Meile, 2016) (Quan and Falkowski, 2009)	1.016
Nitrification2	α_{nit2}	0.9872	(Casciotti, 2009), (Rooze and Meile, 2016)	0.9872
Anammox (nitrite)	α_{anx1}	1.018	(Rooze and Meile, 2016)	1.018
Anammox (ammonium)	α_{anx2}	1.016	(Rooze and Meile, 2016)	1.016
Mineralization (Ammonium)	α_{min}	1.001	(Quan and Falkowski, 2009)	1.001

Table 3.3. Diffusion coefficients (@20°C) based on Equation 3.6.

Species	Diffusion coefficient ($cm^2\ yr^{-1}$)
$^{14}NO_3^-$	540
$^{15}NO_3^-$	536.8
$^{14}NO_2^-$	534
$^{15}NO_2^-$	530.0
$^{14}NH_4^+$	560
$^{15}NH_4^+$	552.6

Table 3.4. Upper boundary conditions used in the model simulations.

Specie	Concentration	δN	References of δN
NO_3^-	300 µmol L^{-1}	+7.6 ‰	(Rooze and Meile, 2016)
NO_2^-	15 µmol L^{-1}	-10 ‰	(Jacob et al., 2016)
NH_4^+	6 µmol L^{-1}	+5 ‰	(Granger and Wankel, 2016)
PON1	56.6 µmol $cm^{-2}\ y^{-1}$	+7 ‰	(Rooze and Meile, 2016)
PON2	28.3 µmol $cm^{-2}\ y^{-1}$	+7 ‰	(Rooze and Meile, 2016)

3.3.3 Incubation experiments

The model is applied to several scenarios pertaining to core incubation experiments that are anticipated to take place in October 2018 with sediments of the Seine River in France (see Chapter 2 for details on the sediments). The model output focuses on the temporal variations in N species concentrations and isotopic compositions of ammonium, nitrate, and nitrite in the overlying water of the incubations. The modeling scenarios assume that incubations will start in the lab by the instantaneous addition of fresh overlying water up to 10 cm above the sediment water interface (SWI). Samples of the overlying water will be collected periodically. The overlying water will be replenished to maintain a constant water volume (or height) above SWI. Pore water profiles of nitrate, nitrite, and ammonium will be measured in additional cores obtained at the same time as those used in the incubations. The pore water profiles will assist us in confirming the modeled reaction rates under steady state conditions.

3.3.4 Scenarios

General information about applied scenarios

The baseline scenario uses the variables and boundary conditions provided in **Tables 3.2** and **3.4.** The simulation continues its run until steady-state. The steady state conditions are then used as the initial conditions for the transient simulation of the core incubations. The transient simulation assumes that, once the collected core is in the lab, the deposition flux of organic matter stops and the concentrations of aqueous species in the overlying water start changing with time due to the (calculated) exchange fluxes between the sediments and the overlying water. In the baseline scenario the overlying water is successively sparged with air (oxic bottom water) and nitrogen gas (anoxic bottom waters). The simulation experiment lasts 200 hours, during which five successive oxic and anoxic cycles are imposed. Under oxic conditions, the oxygen concentration in the overlying water is maintained at 300 μmol L^{-1}.

Scenarios 1 to 3 reproduce the baseline scenario, except that one of the N transformation reactions is blocked (i.e., the corresponding rate constants are set equal to zero) at the start of the non-steady state phase. The blocked reactions include nitrification (both steps), denitrification and DNRA, and anammox,

respectively. Scenario 4 explores the isotopic effect of DNRA on the isotopic composition of ammonium, and finally, in the scenario 5, we look into the effect of the mass-related differences in diffusion coefficients of isotopically light and heavy N species on the isotopic values of nitrite in the overlying water (**Table 3.5**)

3.4 Results and Discussion

Baseline Scenario

In the simulation of the baseline scenario, the nitrate concentration decrease during both the oxic and anoxic cycles, but the decrease is steeper during the anoxic periods (**Figure 3.1**). During oxic periods, the overlying water nitrite concentrations decrease as the sediments take up nitrite from the overlying water (**Figure 3.2**). In contrast, during the anoxic periods, the sediments release nitrite to the overlying water, leading to nitrite accumulation. The $\delta^{15}N$ values of nitrite in the overlying water decrease under oxic conditions and increase under anoxic conditions (**Figure 3.3**). Similarly, ammonium concentrations decrease during oxic periods and increase during anoxic periods (except for the first oxic cycle). Concurrently, the $\delta^{15}N$ values of ammonium under oxic (anoxic) conditions increase (decrease).

Nitrate isotopic composition

Nitrate concentrations in the overlying water are affected by the transformation processes of nitrate in the sediments, including denitrification and DNRA and the second step of nitrification, with the latter being the only process that produces nitrate. During the anoxic periods, denitrification and DNRA rates in the sediments increase sharply (**Fig 3.4**), therefore, the nitrate $\delta^{15}N$ increases faster than when oxygen is present in the overlying water. In the presence of bottom water oxygen, however, due to lower nitrate reduction rates and more production of nitrate by nitrification, the nitrate fluxes from the overlying water to sediments are smaller and the increase in nitrate $\delta^{15}N$ in the overlying water is slower.

Nitrite isotopic composition

The sediments act as a sink of nitrite under oxic conditions and a source of nitrite under anoxic conditions. When oxygen is present, the second step of nitrification is active. This step is accompanied by a rare, inverse isotope fractionation. Thus, the first step of nitrification, where nitrite is produced from

ammonium, favors the use of light ammonium and thus produces light nitrite. In contrast, during the second step, heavy nitrite is preferentially used, leaving lighter nitrite behind and producing heavier nitrate (Casciotti, 2009). Therefore, under oxic conditions, when sediments take up nitrite from the overlying water for use in the second step of nitrification, the residual nitrite remaining in the overlying water reservoir becomes isotopically lighter. As oxygen drops to zero in the next cycle, the production of nitrite via nitrate reduction dominates in the sediments, the direction of the nitrite flux switches and sediments release nitrite to the overlying water, leading to the accumulation of nitrite in the overlying water. This nitrite efflux to the water column originates from denitrification and DNRA in the sediments, which over time produce increasingly heavier nitrite.

Ammonium isotopic composition

Similar to nitrite, sediments are a source of ammonium during the anoxic periods and a sink under oxic conditions. The latter reflects the impact of nitrification (step1). Oxic respiration and denitrification have a minor effect on the ammonium isotopic composition, because of the small isotopic fractionation associated with the mineralization of organic N (**Table 3.2**). However, when mineralization and the first step of nitrification happen simultaneously during the oxic periods, light ammonium is preferentially oxidized, and heavy ammonium builds up in the overlying water.

Table 3.5. Simulation scenarios.

Scenarios (#)	Description
Baseline scenario	Variables and boundary condition are explained in Table 3.4. The scenario includes a steady state simulation and a non-steady-state, which is assumed to describe the incubation experiment in the lab. We successively imposed oxic and anoxic conditions in the overlying water during incubation.
1	Baseline scenario for steady state condition + blocking nitrification (step 1 & step 2) in the sediments during incubation.
2	Baseline scenario for steady state condition + blocking anammox in the sediments during incubation.
3	Baseline scenario for steady state condition + blocking denitrification and DNRA in the sediments during incubation.
4	Baseline scenario for steady state condition + the DNRA contribution to the total nitrate reduction promoted during incubation.
5	Assuming equal diffusion coefficient for heavy and light isotopes of nitrate, nitrite, and ammonium in the sediments during the incubation.

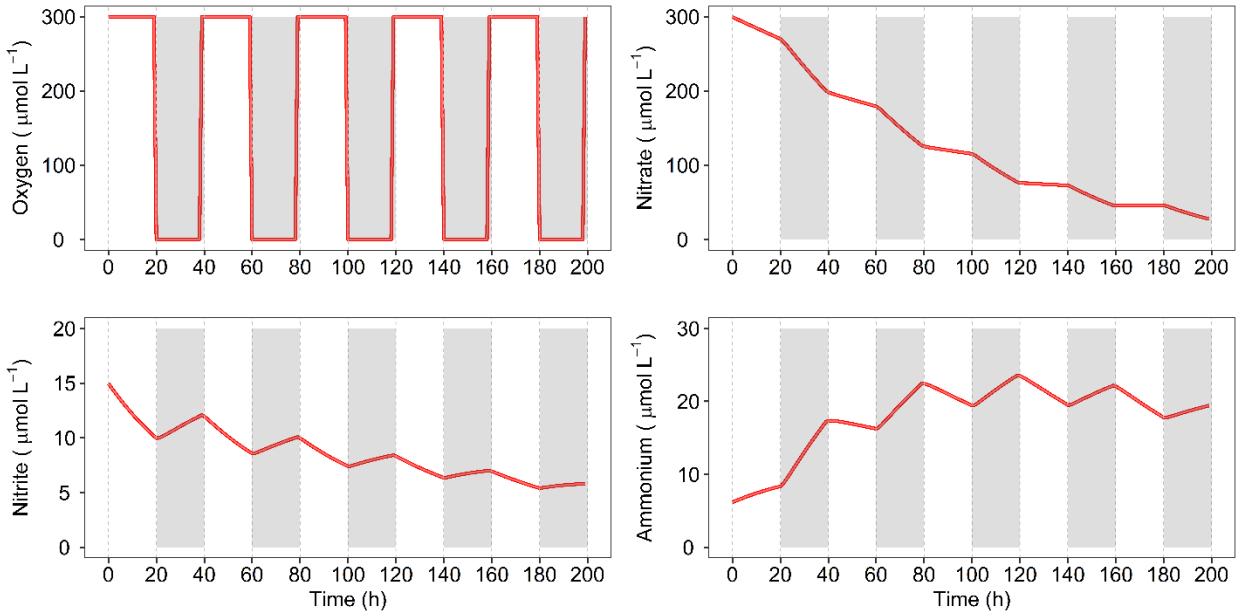

Figure 3.1. Concentrations of dissolved oxygen and N species in the overlying water as a function of time in the baseline scenario. For the N species, the aqueous concentrations are the sum of the isotopically light and heavy forms. The white and gray bands represent the oxic and anoxic periods, respectively.

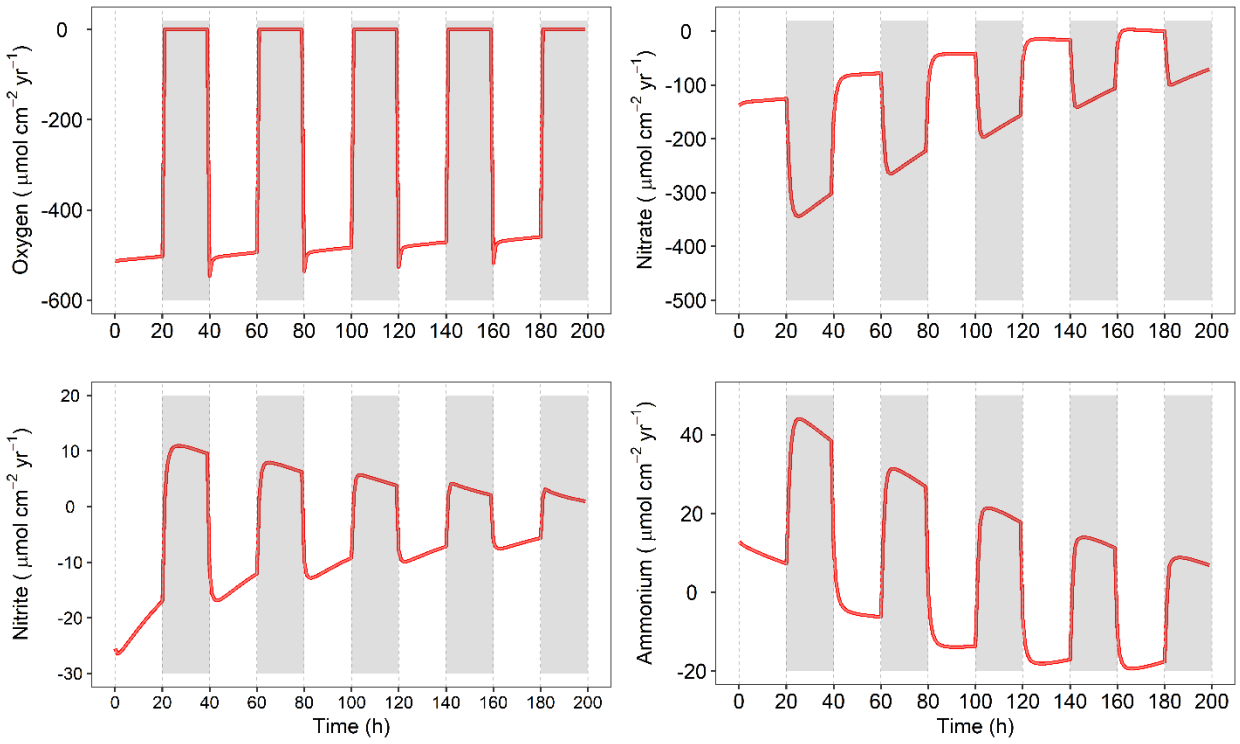

Figure 3.2. Variations in the benthic fluxes of dissolved oxygen and N species as a function of time in the baseline scenario. Positive fluxes indicate the direction of the fluxes from the sediments to the overlying water and vice versa.

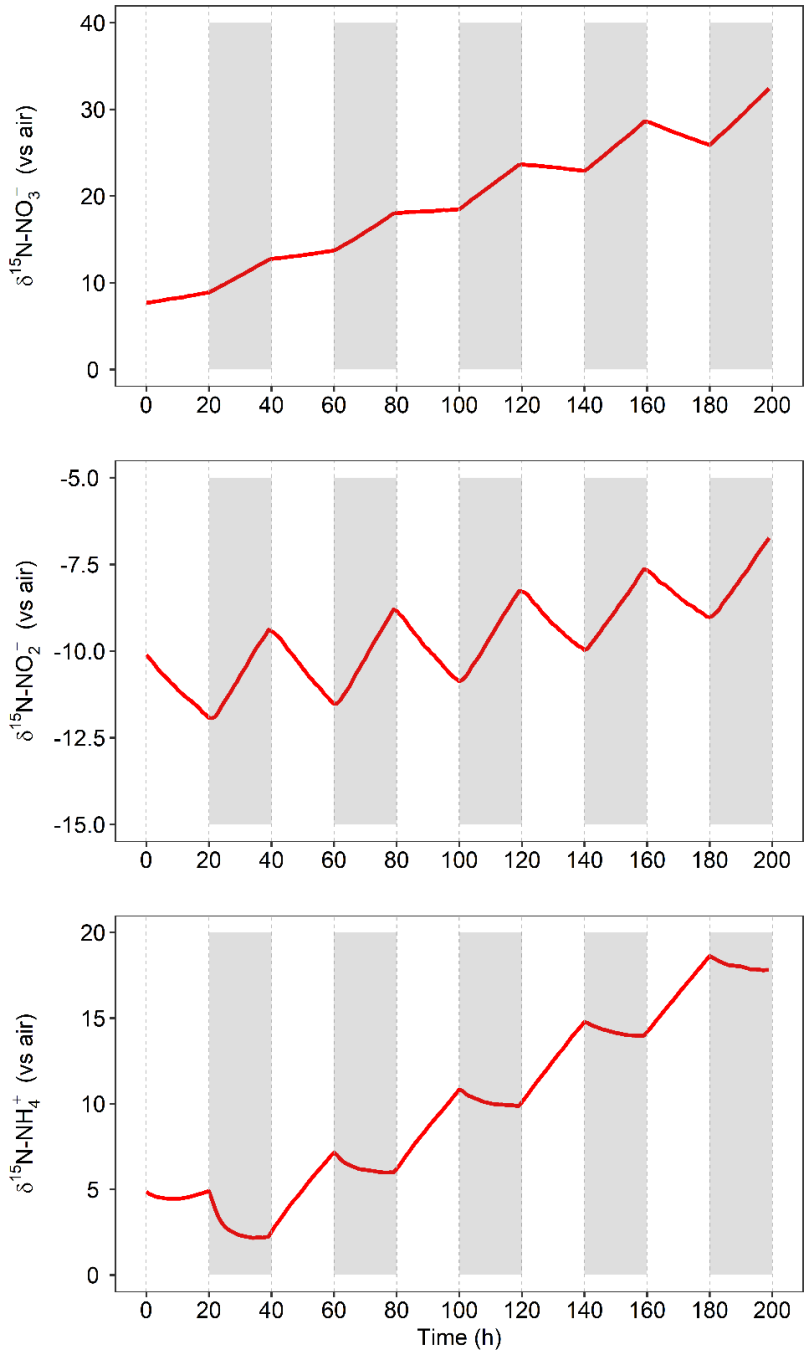

Figure 3.3. Temporal variations of the isotopic compositions of N species in the overlying water in the baseline scenario.

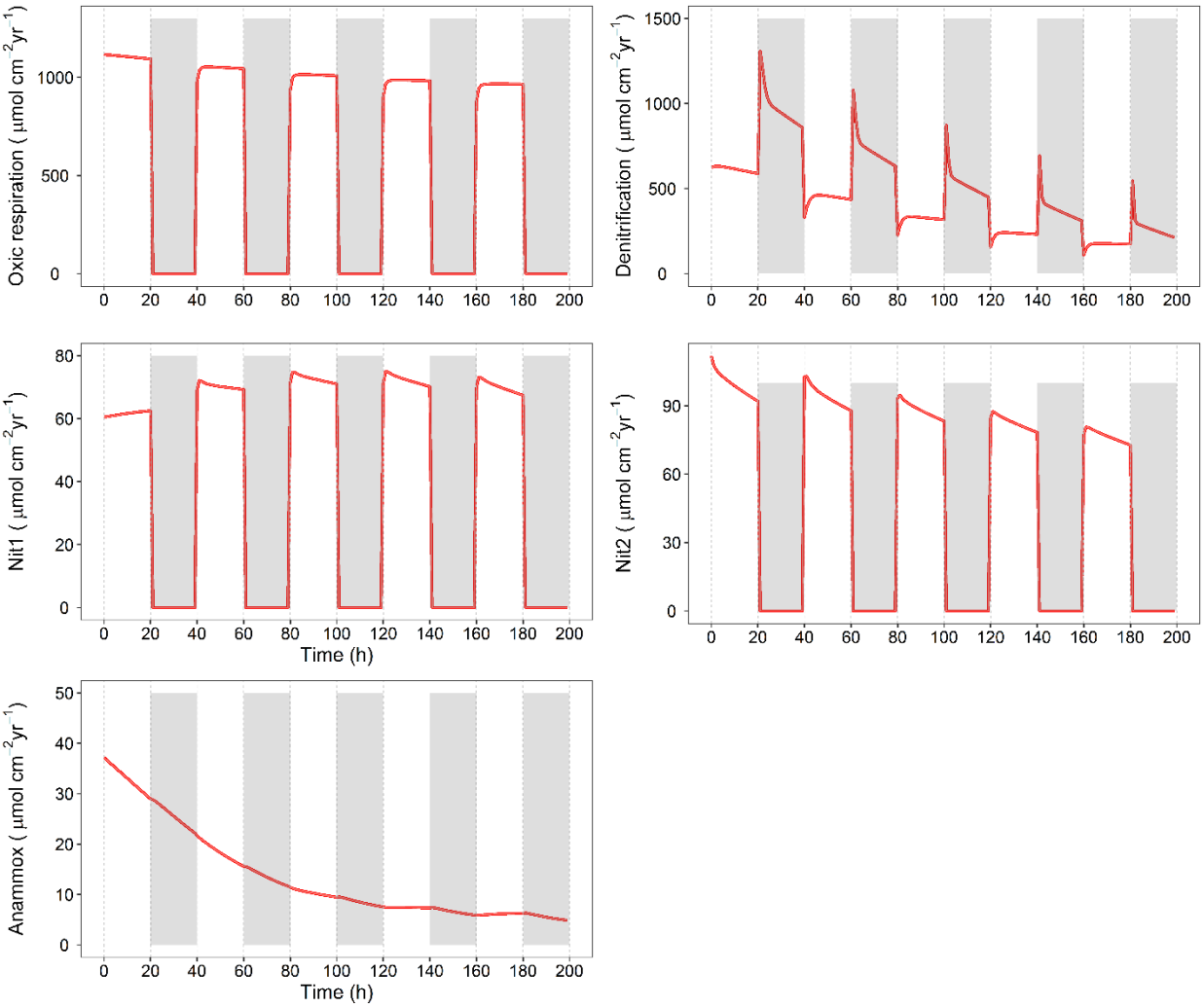

Figure 3.4. Temporal changes of the integrated rates of N reaction processes in the sediments in the baseline scenario. Nit1and nit2 stand for step 1 and step 2 of nitrification.

Sensitivity analysis

A Monte Carlo analysis is used to estimate the uncertainties associated with the fractionation factors of the different N processes. The fractionation factor of each process in **Table 3.1** is assigned a uniform probability density function (PDF) based on the range reported in the literature (**Table 3.2**). Non-steady-state simulations were run 100 times, each time randomly selecting values of the fractionation factors from the corresponding PDFs. At each time step (every 1 hour), the isotopic composition of nitrite in the overlying water is computed, with the results shown in **Figure 3.5**. While the trends of changes in nitrite $\delta^{15}N$ values during alternating oxic and anoxic cycles remain the same, the wide range of $\delta^{15}N$ values of nitrite implies that a unique interpretation of the temporal evolution of the nitrite isotopic composition during a core incubation experiment may be difficult to achieve. It is therefore essential to have complementary data, including changes in the $\delta^{15}N$ of other N species and pore water profiles.

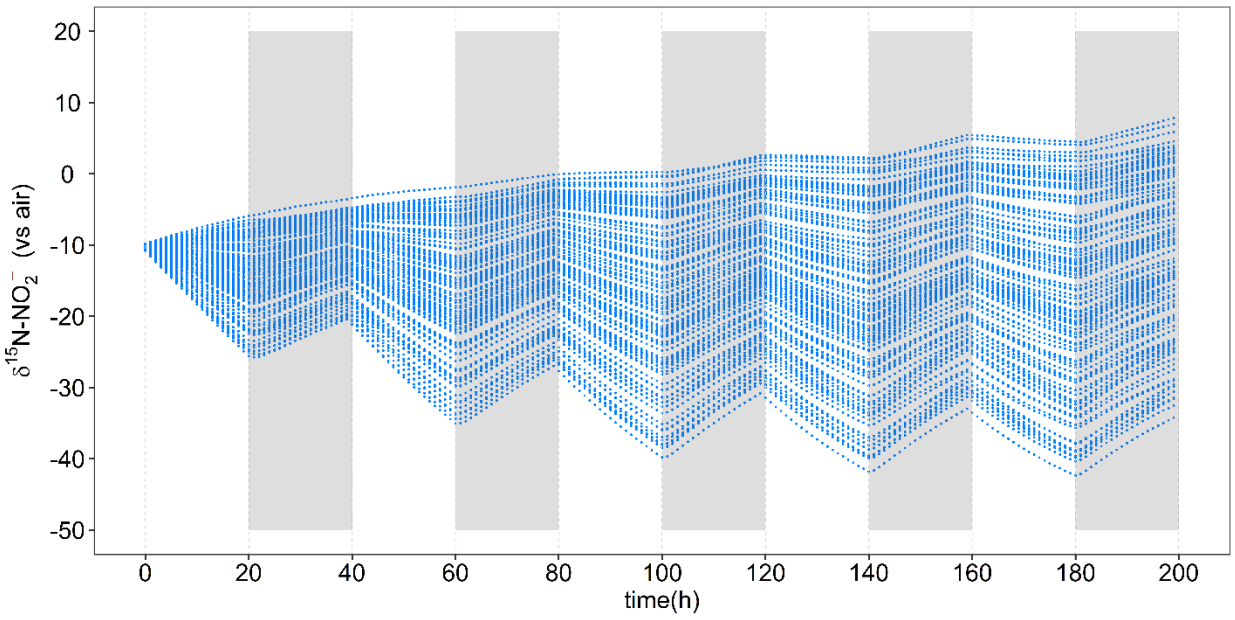

Figure 3.5. Monte Carlo simulations: results of 100 simulations of the baseline scenario are shown. In each simulation the model randomly selects fractionation factors for the N transformation processes from the PDFs listed in Table 3.2.

Scenarios 1 to 3

Blocking of nitrification in the baseline scenario lowers the consumption of nitrite in the sediments by the second step of nitrification, which leads to less uptake of heavy nitrite from the overlying water during oxic conditions and therefore a rise in the nitrite $\delta^{15}N$ value (**Figure 3.6**). Blocking of anammox also lowers the consumption of nitrite but, because this process favors the light nitrite (as opposed to step 2 of nitrification), the opposite effect occurs and the $\delta^{15}N$ of nitrite in the overlying water decreases. Blocking nitrate reduction processes (denitrification and DNRA) in the sediments is associated with a slight rise in the $\delta^{15}N$ of nitrite in the overlying water, because nitrate reduction processes are a source of light nitrite to the overlying water.

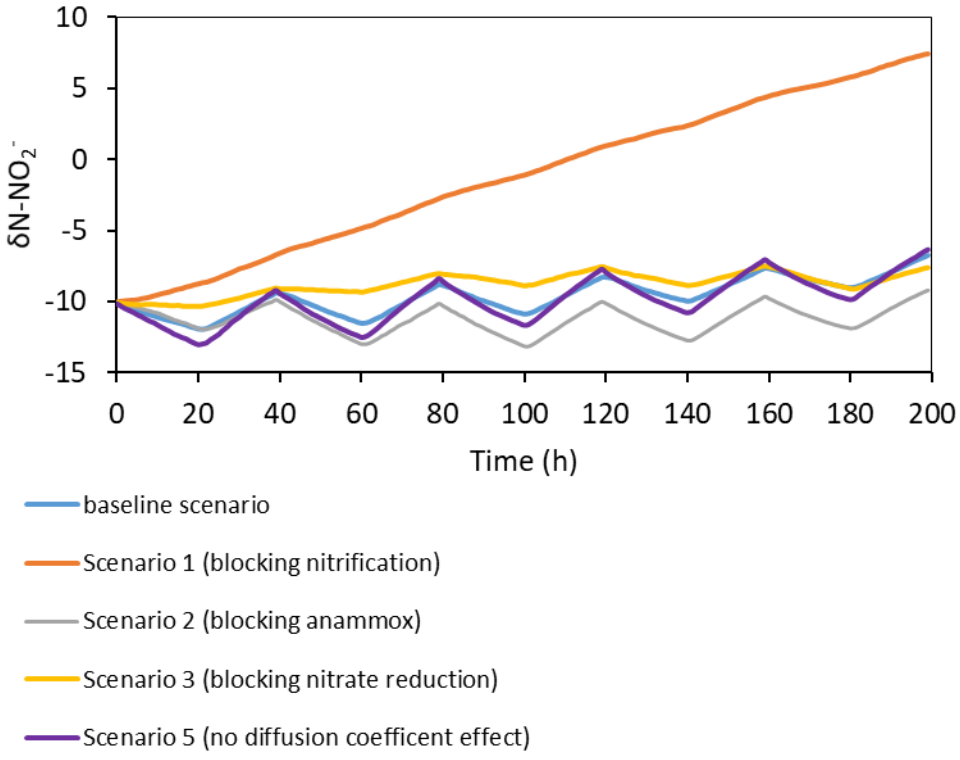

Figure 3.6. Variations in $\delta^{15}N$ of nitrite in the overlying water as a function of time under different scenarios. See text for details.

Scenario 4 and DNRA effect on the isotopic composition of ammonium

Denitrification and DNRA differ in the effect they have on the ammonium $\delta^{15}N$. In denitrification, all the released ammonium is generated from organic N, However, in DNRA, part of the produced ammonium originates from nitrate and, therefore, will have an isotopic composition closer to that of nitrate (light nitrate is preferred in DNRA). **Figure 3.7** shows how the $\delta^{15}N$ values of ammonium decrease in the overlying water when the contribution of DNRA to total nitrate reduction increases.

Scenario 5 and the diffusion effect

In this scenario, the diffusion coefficients of the isotopically light and heavy N-species are assigned the same isotope values. The results demonstrate that the mass-induced differences between diffusion coefficients can cause slight changes in the isotopic compositions of nitrite in the overlying water (**Figure 3.6**).

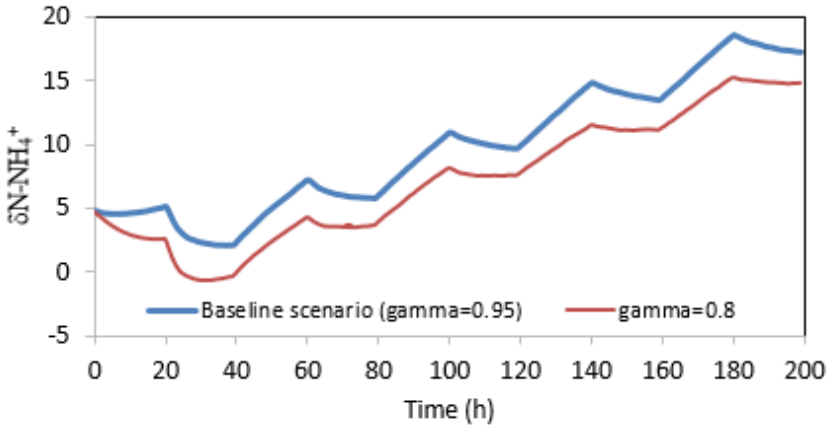

Figure 3.7. Variations in the isotopic composition of ammonium as a function of time for different contributions of DNRA to total nitrate reduction. The fraction of nitrate reduction due to DNRA is equal to (1-gamma).

3.5 Proposed core incubation experiments

The modeling results of the baseline scenario highlight the role of the presence of O_2 on the isotopic composition of nitrite in the overlying water. Therefore, bottom water O_2 can be used to identify the isotopic

fractionation effects of the reactive processes under oxic conditions versus those influencing the nitrite concentrations under anoxic conditions. Hence, incubation experiments are designed to occur under two different conditions of the overlying water; with and without O_2. In oxic incubation, the oxygen concentrations in the overlying water will be maintained at 250 μM with constant air sparging. In a separate incubation, anoxic conditions will be provided by bubbling nitrogen gas during the incubation period. Temperature will be set at 20°C, and fractionation factors of the different processes, diffusion coefficients, and upper boundary conditions of different N species remain as in the baseline scenario (explained in **Tables 3.2**, **3.3** and **3.4**, respectively, except for the O_2 concentrations, which are kept at 250 μM during the oxic incubation). Both incubations will last 72 hours and during this period the isotopic compositions of the ammonium, nitrate and nitrite will be measured every six hours. Pore water profiles of nitrate, nitrite, and ammonium will be measured at the beginning and end of the experiments. Model-predicted porewater profiles and delta values of N species at the beginning of the experiments are shown in **Fig. 3.8**.

Figures 3.9 and **3.10** illustrate the modeling results for the oxic and anoxic core incubations, respectively. The trends of the changes in concentrations and isotopic values of N species in the oxic and anoxic incubations are similar to the baseline scenario during the oxic and anoxic cycles, respectively (see section 3.4). In general, nitrate concentrations decrease in the overlying water over time, and overlying water becomes enriched in heavy nitrate, with a steeper enrichment under anoxic conditions. Ammonium and nitrite concentrations increase under both oxic and anoxic conditions, however, the increases during anoxic conditions are noticeably larger (from 6 μM at the beginning to 48 μM at the end of the incubation for ammonium, and from 15.2 μM to 27 μM for nitrite under anoxic conditions). Nitrite isotopic values change from -10.0 to -10.8‰ under oxic conditions, and from -10.0 to -1.8‰ during anoxic conditions. Therefore, the difference between the isotopic values of nitrite at the end of the oxic and anoxic incubations will be around 9‰ (**Table 3.11**). This difference is due to the isotopic fractionation effects of nitrification, which is dominant under oxic conditions, versus those of denitrification, DNRA, and anammox that are promoted during anoxic conditions.

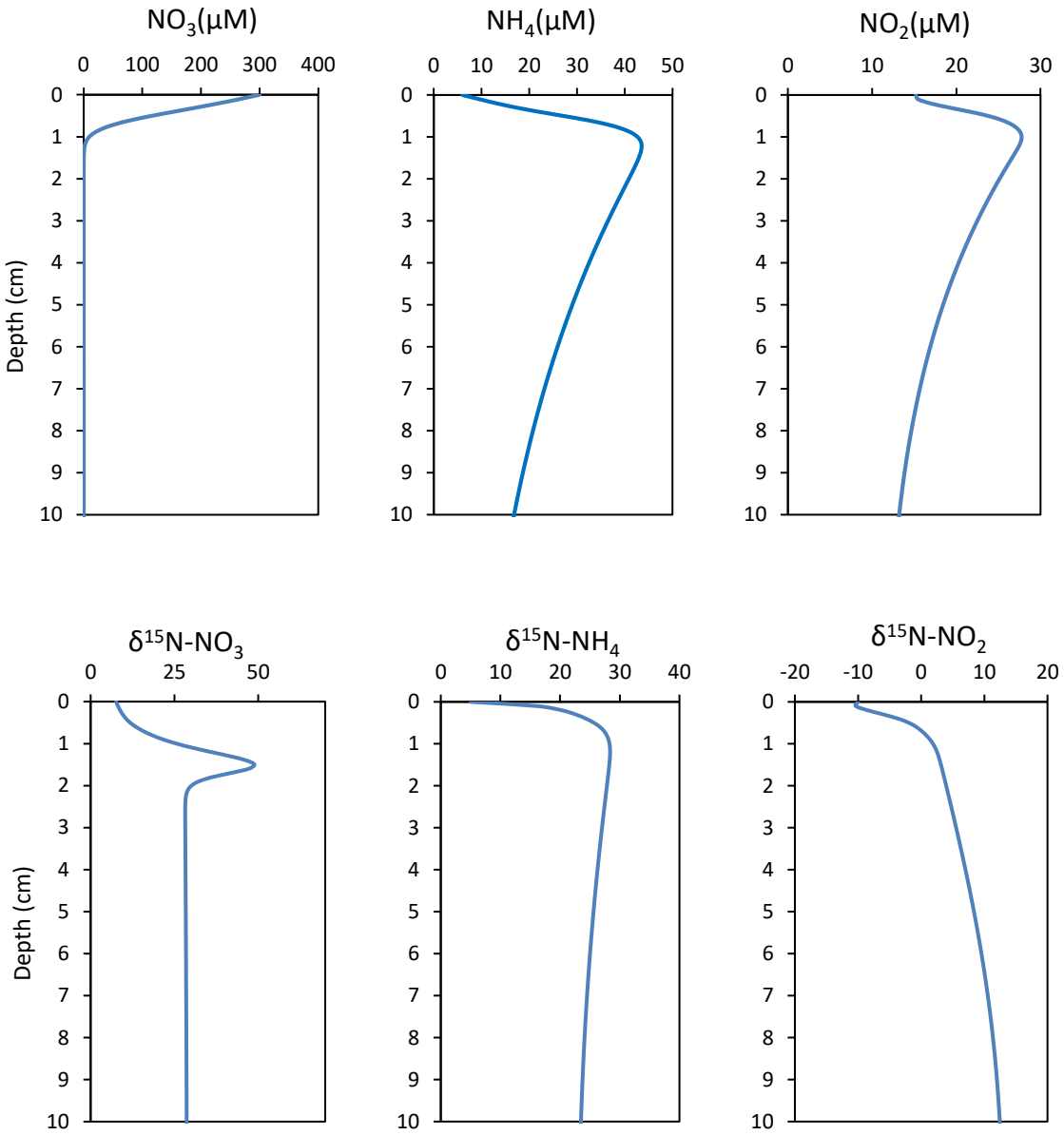

Figure 3.8. Steady state pore water profiles of concentrations and isotopic compositions of nitrate, ammonium and nitrite at the beginning of the core incubation experiments.

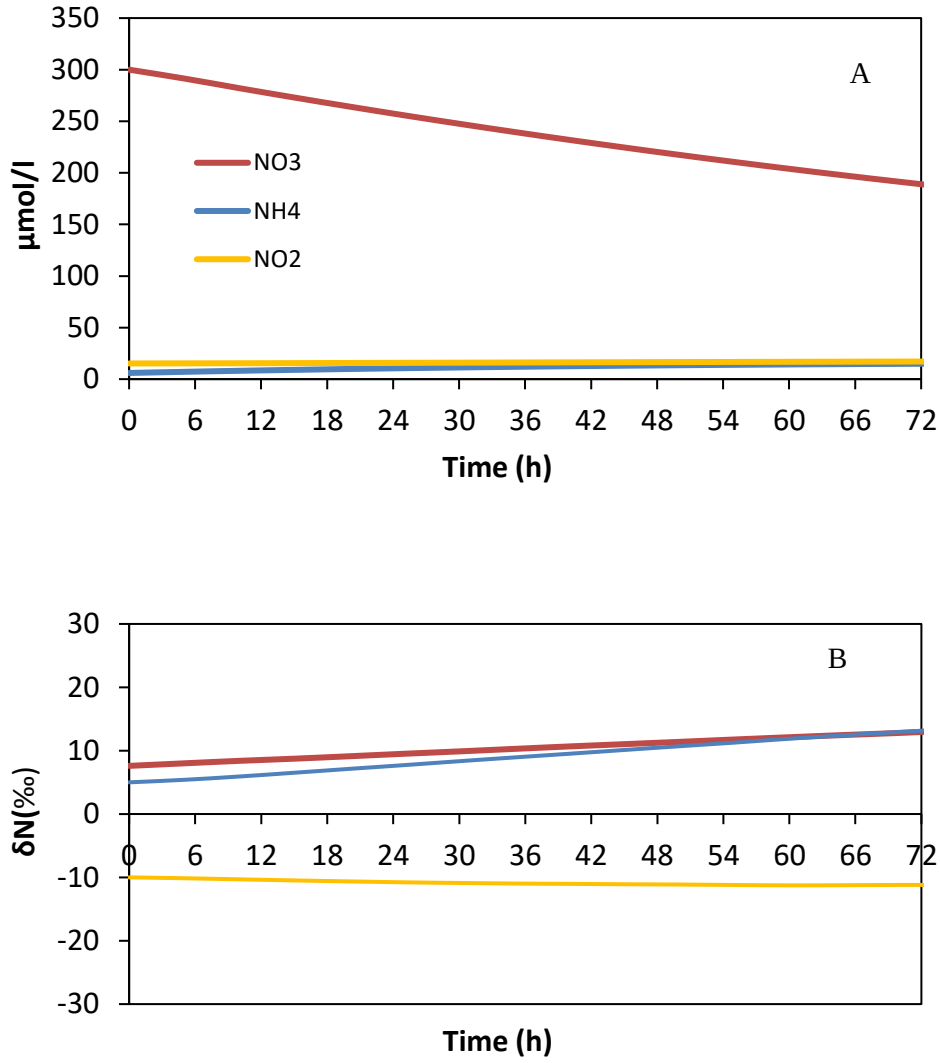

Figure 3.9. Modeling results of the temporal variations in nitrate, ammonium and nitrite concentrations (A) and isotopic compositions (B) in the overlying water during 72 hours of core incubation experiments under **oxic** bottom water conditions with constant bubbling of air (aqueous O_2 concentration in the overlying water is maintained at 250 µM).

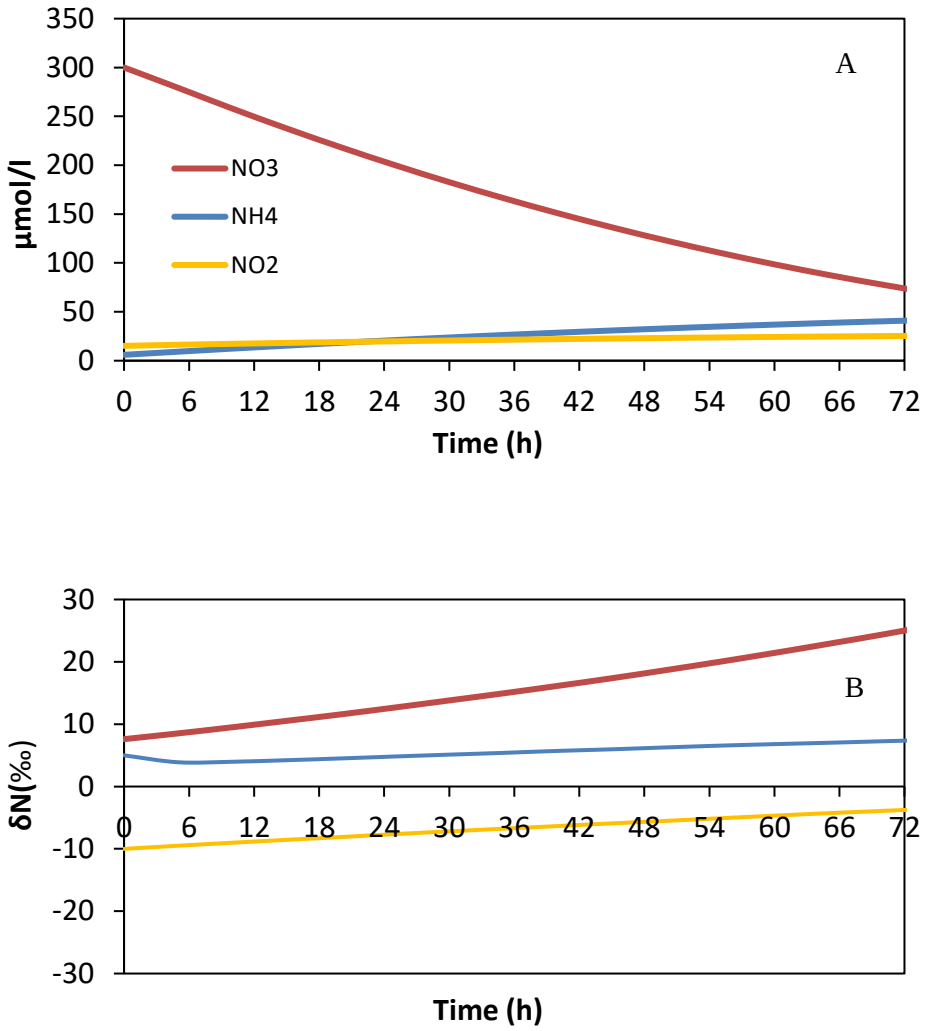

Figure 3.10. Modeling results of the temporal variations in nitrate, ammonium and nitrite concentrations (A) and isotopic compositions (B) in the overlying water during 72 hours of core incubation experiments under **anoxic** conditions when the overlying water is continuously sparged with nitrogen gas.

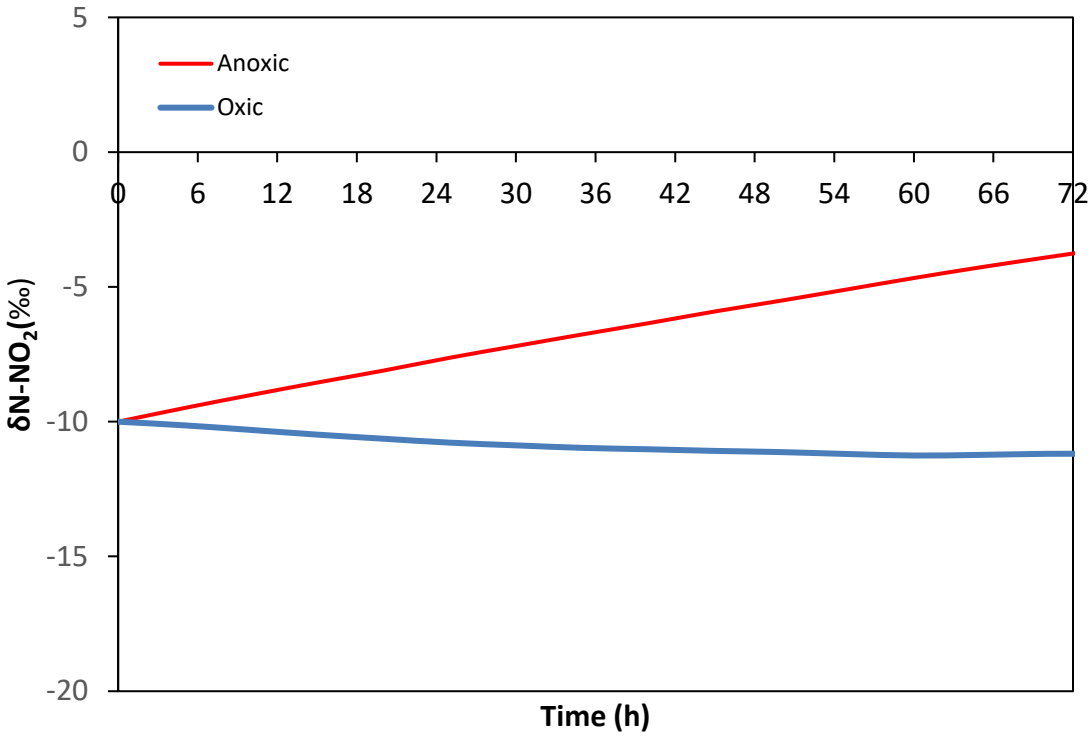

Figure 3.11. Temporal variations in nitrite isotopic compositions under oxic and anoxic conditions in the overlying water of the core incubation experiments. The difference between $^{15}\delta$ values of nitrite under oxic conditions vs anoxic conditions will be around 9‰ by the end of the planned 72 hours.

3.6 Conclusions

We expanded the existing early diagenetic model presented in Chapter 2 of this thesis, by accounting for the isotopic compositions of nitrate, nitrite, ammonium, and organic N. We use the model through several scenarios to look into temporal variations in δ^{15}N values of different N species under non-steady state conditions inspired from core incubation experiments. The modeling results agree with our understanding of the isotopic fractionation effects in the biogeochemical cycling of N in sediments. The model will therefore provide a useful framework for interpreting the isotopic signatures associated with benthic N exchanges.

Chapter 4

Effects of damming on river nitrogen fluxes: a global analysis

Zahra Akbarzadeh, Taylor Maavara, Stephanie Slowinski, Philippe Van Cappellen

This Chapter has been submitted as a research paper for publication in *PNAS.*

4.1 Summary

We quantify the impact of damming on global riverine nitrogen (N) fluxes using a reservoir N mass balance model. In-reservoir processes represented in the model include primary production and mineralization of organic N, plus denitrification and sedimentary burial. In addition, N fixation is explicitly accounted for as a source of N, assuming that the N to phosphorus (P) ratio of riverine inflow regulates the magnitude of N fixation in reservoirs. The model is scaled up via a Monte Carlo analysis that yields global relationships between N elimination in reservoirs, either by denitrification or burial, and the hydraulic residence time. These relationships are then combined with N loads to rivers generated by the Global-NEWS model and the estimated N fixation fluxes. According to the results, in year 2000 worldwide N fixation in reservoirs was on the order of 70 Gmol y^{-1} or about 10% of the riverine N influx to reservoirs, while denitrification and burial in reservoirs eliminated approximately 7% of N loading to the global river network. The latter is predicted to double to 14% by 2030, mainly as a result of the current boom in dam building. The results further imply that, largely due to N fixation in reservoirs, damming causes a global upward shift in riverine N:P ratios, thus lessening N limitation in receiving water bodies.

4.2 Introduction

Humans have altered the flow of nitrogen (N) transported by rivers from land to sea, not only by increasing N loading to rivers from non-point sources and wastewater discharges (Wollheim et al., 2008), but also by building dams (Van Cappellen and Maavara, 2016). We are currently in the midst of the second-largest boom in dam construction since the 1950s. The number of large hydroelectric dams, which currently represent about 20% of dams worldwide, is expected to double following the completion of dams currently under construction or planned to be completed by 2030 (Zarfl et al., 2015). When a dam is built the water residence time increases in the section of river that is transformed into the reservoir, while turbulence decreases. These conditions promote the in-reservoir biogeochemical cycling of N, with removal of particulate N by burial in sediments accumulating in the reservoir and by gaseous emissions to the atmosphere. Thus, the growing fragmentation of river networks by dams is expected to increasingly affect the magnitude and speciation of N fluxes in river basins (Harrison et al., 2009; Tomaszek and Koszelnik, 2003).

Because of burial and denitrification, dams are generally assumed to decrease riverine fluxes of total N (Harrison et al., 2009). However, N fixation can also act as a source of N to reservoirs (Cook et al., 2010; Horváth et al., 2013; Howarth et al., 1988; Jankowski et al., 2012). Hence, N fixation can be a confounding factor when assessing the overall role of reservoirs on riverine N fluxes along the land to ocean aquatic continuum. Multiple factors regulate N fixation in freshwater systems (Forbes et al., 2008). Among these, it is widely accepted that a low external input of N, relative to that of phosphorus (P), stimulates N fixation in lakes and reservoirs (Levine and Schindler, 1999; Nõges et al., 2008; Pinto and Litchman, 2010; Schindler et al., 2008; Vrede et al., 2009). However, there are relatively few data available to quantify the global contribution of N fixation to reservoir N budgets.

The elimination of N in a reservoir is usually estimated as the difference between the annual flux of N carried with the river inflow and the flux of N flowing out through the dam (Tomaszek and Koszelnik, 2003). Using this approach, Harrison et al. (2009) propose that in the mid-1990s, lakes and reservoirs eliminated 1407 Gmol N yr^{-1} globally, with reservoirs responsible for 33% of this value (464 Gmol N yr^{-1}).

These authors calculated elimination as a fraction of the N input, based on the apparent settling velocity in the lake or reservoir and the hydraulic load. Their model was calibrated using a dataset of 80 lakes and 35 reservoirs, and the resulting empirical relationship was then extrapolated worldwide. More recently, (Beusen et al., 2015) estimated that, at the end of the 20th century, 1929 Gmol N yr^{-1} were being eliminated in river systems, with 24% taking place in reservoirs (463 Gmol N yr^{-1}). The latter authors used the IMAGE-GNM model, which calculates N elimination as a function of the nutrient N uptake velocity, temperature and N concentration in the aquatic system. Both these model studies report total removal of N in reservoirs, but do not distinguish between denitrification and burial. Moreover, neither studies account for N fixation in dam reservoirs.

In the present study, we expand on the earlier work by 1) estimating global N fixation in reservoirs and global elimination of N due to river damming, 2) differentiating between the two main reservoir sinks of N, sediment burial and denitrification, and 3) providing these results in a spatially explicit format. In addition, we perform our analyses for four time points: the years 1970, 2000, 2030 and 2050. We further distinguish gross and net elimination of N by reservoirs. Gross elimination is defined here as the sum of the denitrification and burial fluxes in a reservoir. Net N elimination is defined as gross N elimination minus N fixation.

In this work, we follow the approach developed by Maavara *et al.*, (2014, 2015, 2017) and used previously to estimate the modifications of the global riverine fluxes of nutrient silicon (Si), phosphorus (P) and organic carbon (C_{org}) by damming. A process-based model represents the in-reservoir biogeochemical N transformations. Probability density functions are assigned to the parameters describing the physical and biogeochemical properties of and processes in reservoirs in order to account for their worldwide variability. Next, Monte Carlo simulations are used to generate a virtual reservoir database from which globally representative equations for N burial and denitrification are derived. These equations are applied to databases of existing and future reservoirs, combined with nutrient loads obtained from the Global-NEWS model (Mayorga et al., 2010) and N fixation fluxes calculated from the degree of N limitation in the river inflow. Spatially explicit estimates of N fixation, denitrification and N burial in

reservoirs are then presented for the world's river basins at the different time points. The estimates for 2030 and 2050 are based on the Millennium Ecosystem Assessment (MEA) scenarios (Alcamo et al., 2005), implemented in Global-NEWS.

4.3 Methods

4.3.1 Model concept

The model includes three pools of reactive N: dissolved inorganic nitrogen (DIN), dissolved organic nitrogen (DON) and particulate organic nitrogen (PON) (**Figure 4.1**). Total N (TN) refers to the sum of DIN, DON and PON. The pools include both the water column and the upper, active portion of the reservoir sediments. The model computes annually averaged pool sizes and fluxes. At a yearly time scale, the reservoirs are assumed to be well mixed. Each N pool is supplied by riverine input and discharges downstream of the dam. The river discharge, reservoir volume, TN concentration of the river inflow, and the relative proportions of DIN, DON and PON in the inflow TN, are assigned probability distribution functions (PDFs). The PDFs account for the ranges and global variability of the input variables; they are based on published observational data for lentic environments. The PDFs used here, and the references from which they were generated, are listed in **Table B1**. Note that the inputs of N by atmospheric deposition and groundwater discharge are assumed to be negligible, relative to the riverine supply.

Reservoir processes represented are N fixation, denitrification, primary production, mineralization and hydrolysis (**Figure 4.1**). Denitrification and burial of PON below the active upper sediment layer permanently remove N from the aquatic system, while N fixation acts as an additional source of N to the reservoir. The mathematical formulations used to compute the fluxes associated with the in-reservoir N processes are presented below. As for the riverine N inputs, PDFs are assigned to the parameters in these formulations.

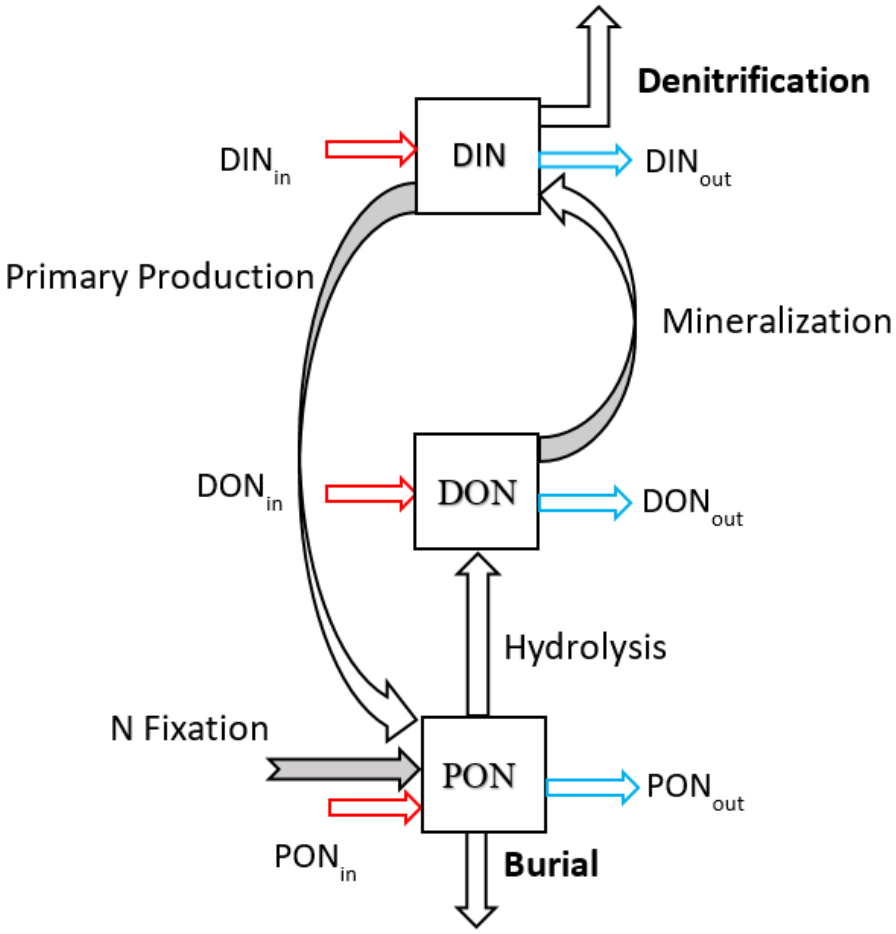

Figure 4.1. Reservoir nitrogen mass balance model with three pools (DIN = dissolved inorganic N, DON = dissolved organic N, PON = particulate organic N). Red arrows and blue arrows represent inflow into and outflow from the reservoir, respectively.

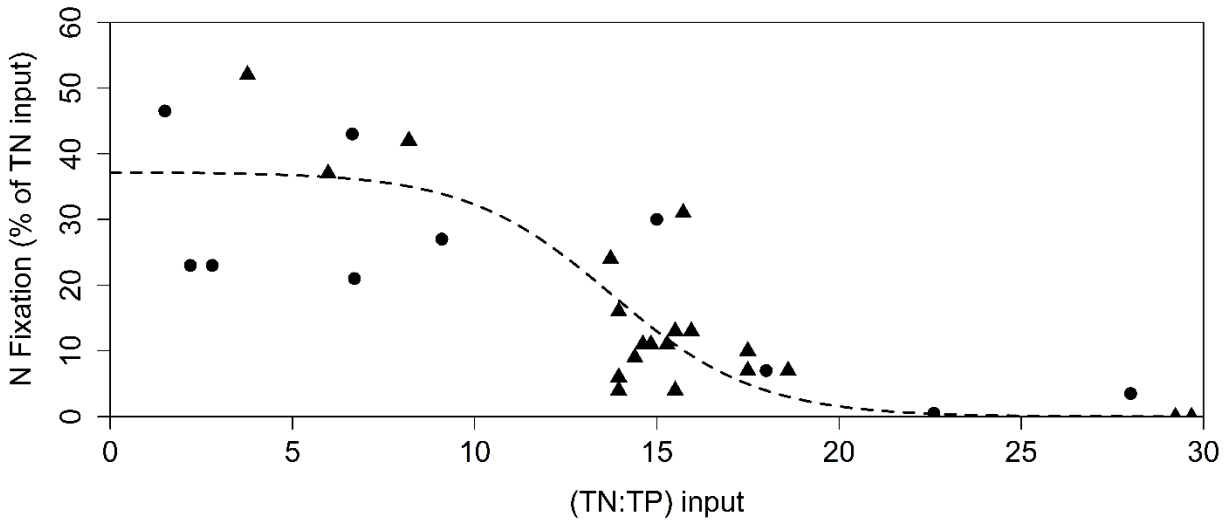

Figure 4.2. Relationship between the TN:TP ratio of riverine input to lakes and reservoirs and the corresponding N fixation as a percentage of the TN input (riverine input plus N fixation). TP stands for total phosphorus, which consists of total dissolved P (TDP), particulate organic P (POP), exchangeable P (EP), and unreactive particulate P (UPP) obtained from our P mass balance model for reservoirs (Maavara et al., 2015). Symbols represent data collected from the literature for individual reservoirs or lakes (see Table B2). Triangles show data for Experimental Lake 227; circles represent other lakes and reservoirs. The curve is the sigmoidal curve fit used in the model (Equation 4.2, R^2=0.66).

4.3.2 In-reservoir processes

Mineralization, hydrolysis and burial fluxes are modeled with first-order kinetics:

$$F = k \bullet M \qquad 4.1$$

where F is the flux in mol N yr^{-1}, k is an apparent first order rate coefficient in yr^{-1}, and M is the mass of N (in mol) in the pool from which the flux originates. The probability distribution functions (PDFs) for the first order rate coefficients describing in-reservoir mineralization, hydrolysis and burial are given in **Table B1**. For N elimination by burial, a uniform distribution is assigned to the first order rate constant, k_{bur}. The range of k_{bur} is adjusted by trial and error, until the average molar TN:TP ratio of buried material in the virtual reservoir data set generated by the Monte Carlo simulations (**Figure B1**) matches that of sedimentary material of lentic systems reported in the literature (17 data points, median TN:TP = 7.3). The computed total P (TP) concentrations of buried material are those obtained with our previous P mass balance model for reservoirs (Maavara et al., 2015). Note that TP is defined here as the sum of particulate organic P (POP), exchangeable P (EP) and unreactive particulate P (UPP). The outflow fluxes through a dam of the different N species are also calculated using **Equation 4.1**, where *M* stands for the corresponding reservoir pool masses and the rate coefficient is set equal to the inverse of the water residence time (τ_r), that is, the flushing rate of the reservoir (Maavara et al., 2015). The inflow fluxes to reservoirs in the Monte Carlo analysis are based on PDFs describing river discharge, TN concentrations and the proportions of the different species that make up the inflow TN concentration (**Table B1**). The flux of N added to the reservoir by N fixation is calculated using an empirical relationship that links the relative contribution of N fixation (N_{fix}) to the relative abundances of N and phosphorus (P) in the riverine inflow. The relationship, shown in **Figure 4.2**, builds on 30 data points from reservoirs and lakes for which the annual mean TN:TP ratio of the river inflow and the corresponding fraction of N fixation are either directly reported or can be calculated from the data provided (**Table B2**). As expected, the highest N_{fix} values are observed for the lower TN:TP input ratios, that is, when primary production in the reservoir tends to be N limited. The data fit shown in **Figure 4.2** is given by:

$$N_{fix}(\%) = \frac{\alpha}{(1+\exp(0.5\times TN{:}TP+\beta))} \quad 4.2$$

where the values of the parameters α and β are 37.2 and -6.877, respectively. **Equation 4.2** is modified to account for the effect of the hydraulic residence time in the reservoir on N fixation.

Natural algal communities require time to establish themselves and, therefore, the water residence time needs to be long enough to avoid the algae from being flushed out (Paerl and Tucker, 1995; Søballe and Kimmel, 1987; Straškraba et al., 1993). This is particularly true for N fixing bacteria, due to their relatively slow growth rates (Maberly et al., 2002). That is, at short water residence times, the doubling time can become a more important limiting factor than nutrient availability (Straškraba et al., 1993). This is represented by introducing a unitless rate multiplier (μ):

$$N_{fix}(\%) = \frac{\alpha}{(1+\exp(0.5\times TN{:}TP+\beta))} \bullet \mu \quad 4.3$$

For N fixing algae, the minimum water residence time is estimated to be on the order of 10 days, while the organisms function at their maximum capacity when the residence time exceeds 60 days (Straškraba et al., 1993). The relationship between μ and the water residence time (τ_r) is therefore expressed as follows (**Figure B2**):

$$\mu = \mathrm{erf}(\frac{\tau_r - 0.028}{0.04}) \quad 4.4$$

where τ_r is expressed in years. To account for uncertainties in the N_{fix} estimates, we assume a normal distribution with a standard deviation of ±10% around the N_{fix} values predicted by **Equation 4.2**. For consistency, the N demand of primary productivity in a given reservoir, that is the N uptake flux associated with photosynthesis, is imposed as the upper limit for the N fixation flux.

Estimations of the N fluxes associated with primary production and denitrification are derived from the corresponding carbon (C) fluxes obtained with the previously developed organic C (C_{org}) mass balance model for reservoirs (Maavara et al., 2017). Thus, the N uptake flux by primary production ($\mathrm{mol\ N\ yr^{-1}}$) is given by:

$$F_{up} = R_{up} \bullet \frac{TDP}{TDP+K_{sp}} \bullet \frac{16}{106} \quad 4.5$$

where R_{up} is the maximum photosynthesis rate in $\mathrm{mol\ C\ yr^{-1}}$, TDP is the total dissolved P concentration in the reservoir, K_{sp} is the half-saturation TDP concentration, and the fraction 16:106 is the Redfield ratio for algal biomass production that converts C moles into N moles. Values of R_{up} are from Maavara et al. (2017): they are computed as the product of the annual chlorophyll concentration in the reservoir and the maximum chlorophyll-specific carbon fixation rate. The chlorophyll concentration in turn depends to the photosynthetically active radiation (PAR) and the attenuation of PAR by biotic and abiotic processes. Correction factors further account for the effects of water temperature and the yearly fraction of ice-free days. The second term on the RHS of **Equation 4.5** assumes that the availability of P is the ultimate limiting nutrient for annual primary production. In other words, we assume that, on an annual basis, N fixation balances any N deficit of the riverine nutrient supply. The values of TDP and K_{sp} are those calculated with the reservoir P mass balance model of Maavara et al. (2015).

Denitrification fluxes (F_{den} in $\mathrm{mol\ N\ yr^{-1}}$) are calculated as fractions of the corresponding C_{org} mineralization fluxes (F_{minC} in $\mathrm{mol\ C\ yr^{-1}}$) in Maavara et al. (2017). Assuming the idealized stoichiometry of denitrification, where 4 nitrate ions are consumed per 5 C_{org} mineralized (Akbarzadeh et al., 2018), the denitrification fluxes are given by:

$$\mathrm{F_{den}} = 0.8 \bullet \mathrm{F_{minC}} \bullet \frac{[\mathrm{DIN}]}{[\mathrm{DIN}]+\mathrm{K_{DEN}}} \qquad 4.6$$

where DIN is the concentration of DIN in mol N L^{-1} and K_{DEN} is an empirical coefficient. The last term on the RHS corresponds to the fraction of the C_{org} mineralization flux that is coupled to nitrate reduction. **Equation 4.6** is applied to the in-reservoir decomposition of allochthonous (i.e., supplied from the upstream catchment) and autochthonous C_{org} (i.e., produced in the reservoir), as well as the C_{org} of the soil organic matter and biomass flooded upon closure of the dam (see Maavara et al., 2017, for details). Because of slightly improved fits to the Monte Carlo output, the calculated reservoir DIN concentration is used in **Equation 4.6** in the case of the allochthonous and autochthonous C_{org} pools, while the river inflow DIN concentration is used in the case of flooded C_{org}.

The value of K_{DEN} in **Equation 4.6** is an independently constrained fitting parameter calibrated using literature data for sediments for which both the depth-integrated C_{org} decomposition rate and the depth-integrated denitrification rate are reported (**Figure B3**, **Table B3**). In a number of instances, the sediment oxygen demand serves as a measure of the depth-integrated rate of C_{org} decomposition (Canfield et al., 1993; Van Cappellen and Gaillard, 1996). The resulting value of K_{DEN} is fairly large (115 μmol L^{-1}), implying that in most reservoirs, except those receiving very high nitrate loadings, denitrification is responsible for a relatively small fraction of the total C_{org} oxidation. The same value of K_{DEN} is applied to all three C_{org} pools.

4.3.3 Scaling up

The N mass balance model is run 6000 times, each time randomly selecting parameter values from the predefined PDFs in **Table B1**. The ensemble of Monte Carlo simulations yields a database of hypothetical N cycling in reservoirs. The key assumption is that the N dynamics in this virtual set of reservoirs are representative of those of real reservoirs. From the virtual data set, we then extract global relationships that express the relative importance of N burial and denitrification as a function of a reservoir's water residence time, τ_r (**Figure B4**). Following Maavara et al. (2015, 2017) we fit the Monte Carlo data to:

$$f_i = a_i - \frac{b_i}{1 + c_i \times \tau_r} \qquad 4.7$$

where f_i is the fraction of the total TN input (that is, river input plus N fixation) to the reservoir that is eliminated either by sediment burial or denitrification, and a_i, b_i and c_i are the parameters fitted to the mean values of f_i in the virtual database. Separate parameter sets apply to burial and denitrification (**Table B4**). The parameter values also differ for the different MEA scenarios for the years 2030 and 2050, because of the effect of variable air temperatures associated with the MEA scenarios (Fekete et al., 2010).

For the year 1970 and 2000 simulations, the global relationships (i.e. **Equation 4.7**) are applied to the reservoirs built before 1970 and 2000, respectively, that are compiled in the Global Reservoirs and Dams (GRanD) database (Lehner et al., 2011). The database accounts for at least 76% of the actual global volume

of reservoirs at the end of the 20th century (Lehner et al., 2011). For the 2030 and 2050 scenarios, the year 2000 GRanD reservoirs are augmented with the database of Zarfl et al. (2015), which contains hydroelectric dams that are currently under construction or planned to be in operation by 2030. For the 2050 model simulations, no new dams are assumed to be built after 2030. The river inputs of N and P to the reservoirs are those generated using the catchment-specific yields predicted by the Global-NEWS model. For a full description of the methodological approach, the reader is referred to Maavara et al. (2015, 2017). It is important to note that, at each of the selected time points (years 1970, 2000, 2030 and 2050), the existing dam databases only cover a fraction of the total number of reservoirs worldwide. Therefore, the flux calculations presented here should be viewed as minimum estimates of the global impacts of dams on riverine N fluxes.

4.3.4 Sensitivity

A bootstrapping method is used to evaluate the sensitivity of the model output to the model parameters. First, we generate 6000 runs for year 2000, referred as the virtual dam dataset, from which 5000 samples with replacement are selected randomly. The observed N fixation fluxes ($\hat{y}_i$) of the 30 data points from reservoirs and lakes used to generate **Figure 4.2** are then compared to those model simulated fluxes (y_i) that have the same corresponding TN:TP ratios in the river inflow. The average sum of squared prediction errors (SSPE) is computed as:

$$\mathrm{SSPE} = \frac{1}{n}\sum_{i=1}^{n}(y_i - \hat{y}_i)^2 \qquad 4.8$$

where n is the number of observations (here 30). The entire process is repeated 5000 times and, each time, the new virtual dataset is fitted to **Equation 4.2** and a new SSPE is calculated. The resulting 5000 SSPE values (**Figure B5**) are symmetrically distributed around the value of SSPE for the virtual dataset of dams (dashed line in **Figure B5**), hence, showing low sensitivity of the model results to the random sampling process. The standard deviations of the parameters α and β in **Equation 4.2** are 0.007 and 0.162, respectively, which translate in a ±11% standard deviation for the estimated global N fixation in reservoirs in year 2000.

The same procedure is repeated for N burial and denitrification: values for the parameters a, b and c in **Equation 4.7** are estimated based on 5000 iterations for N burial and denitrification separately. Standard deviations of the parameter values are presented in **Table B5**. For the global flux estimates, this translates into standard deviations of ±11% and ±8% for N burial and denitrification in reservoirs in the 2000.

4.4 Results

4.4.1 Hindcasting: 1970 and 2000

For 1970, the model predicts a global TN gross elimination in dam reservoirs of 170 Gmol yr^{-1}, 69 and 101 Gmol yr^{-1} via N burial and denitrification, respectively (**Figure 4.3**; **Table 4.1**). This gross elimination (denitrification plus burial) represents 34% of the global input of TN (river inflow plus N fixation) into reservoirs in 1970, and 5.7% of the total N loading to river systems (which includes N that does not pass through a dam). Note that denitrification associated with the oxidation of C_{org} of the soil organic matter and biomass flooded upon closure of the dam are reported separately in **Table 4.1** and are not considered in the gross and net elimination calculations. In 1970, global N fixation in reservoirs is 38 Gmol yr^{-1} or 7.6% of the estimated TN input to reservoirs. The five top river basins in 1970 with the highest gross elimination of TN in reservoirs are, in order of decreasing importance: Mississippi, Zambezi, Volga, Niger, and Saint Lawrence (**Table 4.2**; **Figure 4.4**). The five top river basins for N fixation are: Volga, Mississippi, Saint Lawrence, Columbia (North America) and Ganges-Brahmaputra (**Table 4.3**).

For year 2000, the model-estimated TN elimination fluxes via N burial and denitrification are 110 and 159 Gmol yr^{-1}, respectively, or a total gross elimination of 269 Gmol yr^{-1}, which represents a 58% increase relative to 1970. In 2000, 36% of the TN input to reservoirs is eliminated, equivalent to 7.4% of total N loading to the world's rivers. Global N fixation in reservoirs increases to 70 Gmol yr^{-1}, nearly a doubling compared to 1970. Similar to 1970, the basins of the Mississippi and Zambezi Rivers remain the top two watersheds eliminating most TN behind dams in 2000. However, major contributions are now also seen for the basins of the Parana River (70 dams), the Chang Jiang (353 dams), and the Tocantins River in

South America (4 dams). The shifts in the geographical distributions of TN elimination and N fixation in reservoirs between 1970 and 2000 are illustrated in **Figures 4.4** and **4.5**.

4.4.2 Forecasting: 2030 and 2050

The presentation of the results focus on the year 2030; the 2050 results are very similar to those of 2030 because the simulations assume no new dams are constructed after 2030 (**Table 4.1** and **Figure 4.3**). Global gross N elimination by dams rises from 270 Gmol yr^{-1} in 2000 to 573 Gmol yr^{-1} in the 2030 GO (Global Orchestration) scenario. Even in the environmentally most favorable scenario (AM, Adapting Mozaic), gross N elimination increases by 74% from 2000 to 2030. Based on these projections, in 2030 dam reservoirs eliminate between 31% (GO scenario) and 32% (AM scenario) of the TN influx to reservoirs by denitrification plus N burial. Relative to 2000, global N fixation in 2030 is projected to grow by at least 154% (178 Gmol yr^{-1}, AM scenario) and up to 268% (258 Gmol yr^{-1}, technogarden or TG scenario).

The 2030 and 2050 results highlight the major role of ongoing dam construction in Southeast Asia and to a lesser extent South America (**Figures 4.4**, **4.5** and **4.6**). From 2000 to 2030, the largest changes in in-reservoir N fixation, N burial and denitrification fluxes are predicted to happen in Asia, where both the number of dams and TN loading to rivers will experience large increases (Seitzinger et al., 2010; Zarfl et al., 2015). In the 2030 simulations one single watershed, that of the Chang Jiang River, accounts for 15% of the total global gross elimination of N in reservoirs. In this watershed, the TN loading to reservoirs is estimated to increase by 41% between 2000 and 2030 (from 105.7 Gmol yr^{-1} to 148.7 Gmol yr^{-1} under the GO scenario), while at the same time the number of dams will increase from 353 to 495. Additionally, in 2030, 32% of the total global N fixation in reservoirs will occur in three river basins in Southeast Asia: Chang Jiang, Ganges, and Mekong.

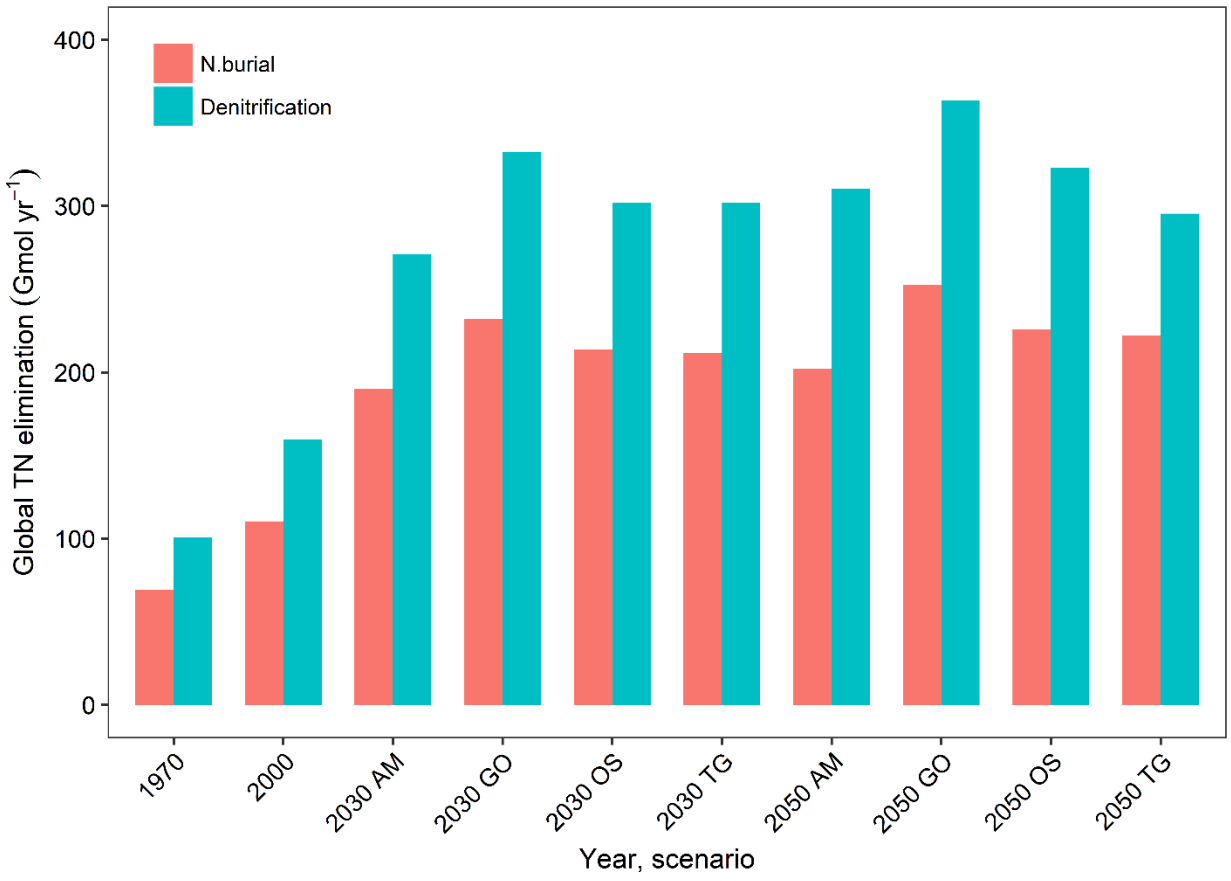

Figure 4.3. Global TN elimination via denitrification and N burial for years 1970, 2000, 2030 and 2050. The Millennium Ecosystem Assessment (MEA) scenarios are identified in the caption of Table 4.1.

Table 4.1. Global effects of dams on riverine N fluxes in years 1970, 2000, 2030 and 2050. The 2030 and 2050 projections are based on the four Millennium Ecosystem Assessment (MEA) scenarios: AM = adaptive mosaic, GO = global orchestration, OS = order from strength, TG = technogarden. Denitrification coupled to mineralization of organic carbon flooded upon closure of dams is not considered in the calculations of global N elimination in reservoirs.

Global estimations	**1970**	**2000**	**2030 AM**	**2030 GO**	**2030 OS**	**2030 TG**	**2050 AM**	**2050 GO**	**2050 OS**	**2050 TG**
River N loading, Gmol yr^1	2973	3631	3411	3778	3632	3512	3500	3999	3790	3554
N fixation in reservoirs, Gmol yr^1	38	70	178	248	219	258	240	284	236	266
TN input to reservoirs (Including N fixation), Gmol yr^1	500	757	1458	1848	1744	1617	1657	2137	1809	1720
TN buried, Gmol yr^1	69	110	193	235	217	215	206	257	229	227
TN denitrified , Gmol yr^1	101	159	275	338	307	308	317	371	328	302
TN gross elimination, Gmol yr^1	170	269	468	573	524	523	523.5	627	557	529
TN denitrified by flooded Corg, Gmol yr^1	996	544	480	520	509	492	0	0	0	0
N uptake by primary production, Gmol yr^1	84.5	149.2	403.7	616.3	556.2	590.6	577.9	662.4	598	635.2
Fraction of global TN riverine load eliminated (gross elimination), %	5.7	7.4	13.7	15.2	14.4	14.9	15.0	15.7	14.7	14.9
N Fixation as a fraction of global TN riverine load, %	1.3	1.9	5.2	6.6	6.0	7.3	6.9	7.1	6.2	7.5
Fraction of global TN riverine load eliminated (net elimination), %	4.4	5.5	8.5	8.6	8.4	7.5	8.1	8.6	8.5	7.4
Fraction of global TN input to reservoirs eliminated (gross elimination), %	34.0	35.6	31.8	30.7	29.7	31.9	31.2	29.1	30.5	30.4
N fixation as a fraction of global TN input to reservoirs, %	7.6	9.3	12.1	13.3	12.4	15.7	14.3	13.1	12.9	15.3

Table 4.2. Top 10 watersheds ranked according to annual mass of N eliminated by denitrification plus burial in dam reservoirs, for years 1970, 2000, and 2030 (GO scenario). All units are Gmol N yr^1.

Rank	Watershed	TN gross elimination	Riverine TN load into watershed*	N fixation in reservoirs of watershed	No. of reservoirs	TN Gross elimination as % of TN input **
1970						
1	Mississippi	28.5	79.7	2.9	552	35
2	Zambezi	12.2	34.5	0.5	25	35
3	Volga	11.8	21.4	3.3	17	48
4	Niger	9.8	28.9	0.4	27	33
5	Saint Lawrence	8.0	42.1	1.6	162	18
6	Ganges	7.6	155.2	1.4	59	5
7	Yenisei	7.0	23.3	0.4	3	30
8	Nile	5.7	7.1	0.8	11	72
9	Dnper	4.4	7.9	1.0	5	49
10	Columbia	4.1	18.8	1.6	114	20
2000						
1	Mississippi	26.1	70.8	1.5	703	36
2	Zambezi	19.8	38.5	3.4	49	47
3	Niger	13.3	32.4	0.8	52	40
4	Parana	11.4	65.0	3.4	70	17
5	Volga	10.2	50.3	3.1	17	19
6	Chang Jiang	9.0	105.7	3.8	353	8
7	Ganges	8.7	226.0	2.4	86	4
8	Yenisei	8.2	25.0	0.9	7	32
9	Saint Lawrence	8.0	44.1	0.8	182	18
10	Tocantins	5.3	31.8	1.2	4	16
2030 (GO scenario)						
1	Chang Jiang	84.4	148.7	44.2	495	44
2	Ganges	44.6	239.4	19.4	486	17
3	Mekong	28.1	56.8	16.1	138	39
4	Mississippi	28.1	71.9	3.8	703	37
5	Amazon	25.5	275.7	11.0	191	9
6	Zambezi	22.2	40.0	4.3	64	50
7	Parana	18.2	65.4	12.0	418	24
8	Niger	15.9	34.5	1.7	74	44
9	Salween	12.9	18.9	4.7	26	54
10	Volga	12.7	24.4	5.7	17	42

* Not all the riverine TN load into a watershed necessarily passes through a dam.

** Riverine TN load into a watershed plus N fixation in the reservoirs of that watershed.

Table 4.3. Top 10 watersheds ranked according to annual mass of N fixed in dam reservoirs, for 1970, 2000, and 2030 (GO scenario).

Rank	Watershed	N Fixation in reservoirs of watershed	Riverine TN load into Watershed	No. of reservoirs	Fixation as % of TN input
1970					
1	Volga	3.3	21.4	17	13
2	Mississippi	2.9	79.7	552	4
3	Saint Lawrence	1.6	42.1	162	4
4	Columbia	1.6	18.8	114	8
5	Ganges	1.4	155.2	59	1
6	Dnper	1.0	7.9	5	11
7	Chang Jiang	0.8	58.5	225	1
8	Nelson	0.7	9.8	76	7
9	Balsas	0.6	3.1	9	16
10	Trinity	0.5	2.0	18	20
2000					
1	Chang Jiang	3.8	105.7	353	3.5
2	Parana	3.3	65.0	70	4.8
3	Volga	3.1	50.3	17	5.8
4	Ganges	2.4	226.0	86	1.1
5	Columbia	1.7	18.5	130	8.4
6	Balsas	1.5	5.5	12	21
7	Mississippi	1.5	70.8	703	2.1
8	Dnper	1.3	12.8	6	9.2
9	Zhujiang	1.2	32.7	50	3.5
10	Tocantins	1.2	31.8	4	3.5
2030 (GO scenario)					
1	Chang Jiang	44.2	148.7	495	23
2	Ganges	19.4	239.4	486	7
3	Mekong	16.1	56.8	138	22
4	Parana	12.0	65.4	418	16
5	Amazon	11.0	275.7	191	4
6	Volga	5.7	24.4	17	19
7	Salween	4.7	18.9	26	20
8	Zambezi	4.3	40.0	64	10
9	Tocantins	3.9	32.6	88	11
10	Mississippi	3.8	71.9	703	5

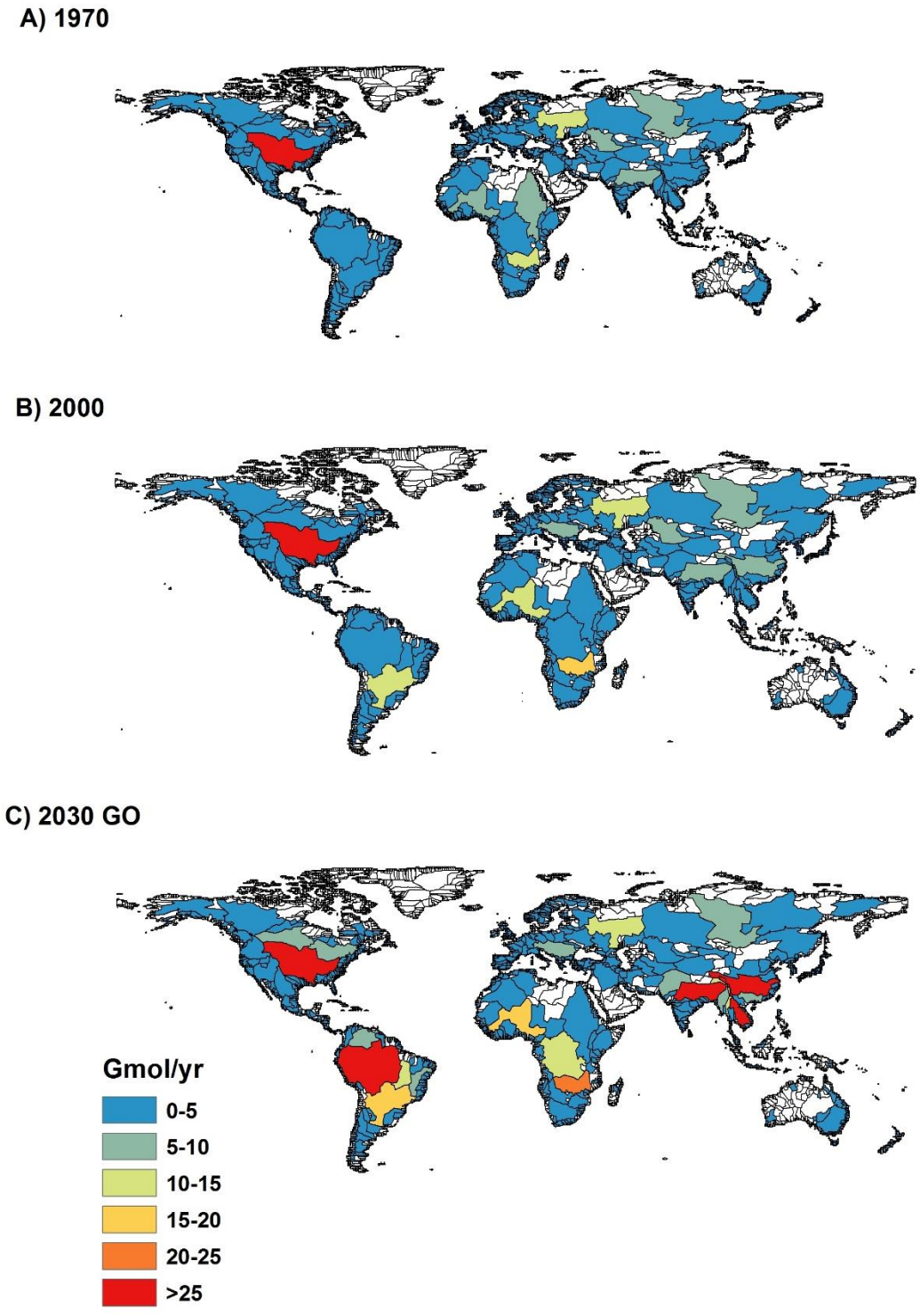

Figure 4.4. Total gross N elimination (denitrification plus burial) in individual watersheds in 1970 (A), 2000 (B), and 2030 under GO scenario (C).

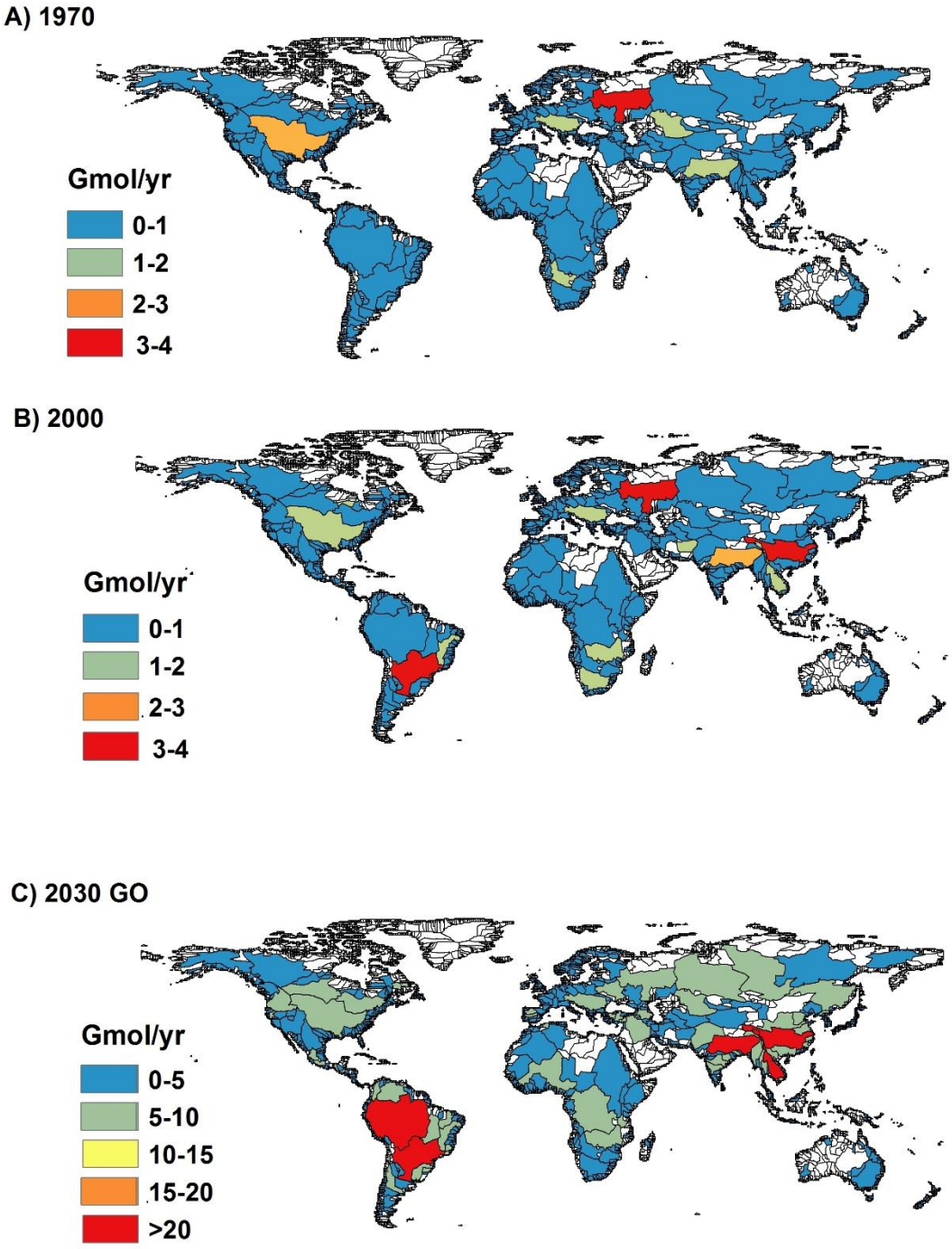

Figure 4.5. N fixation in individual watersheds in 1970 (A), 2000 (B), and 2030 under GO scenario (C).

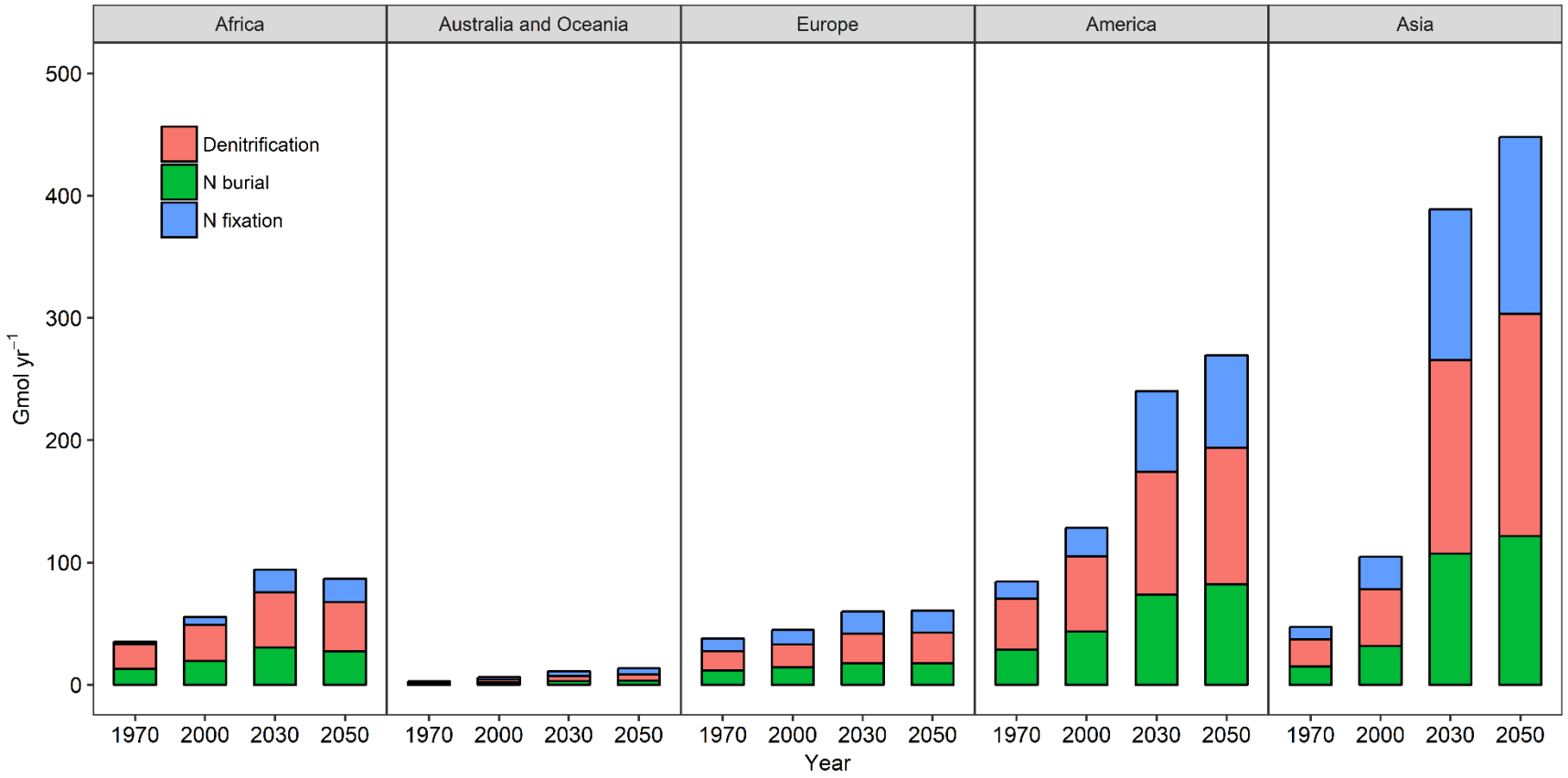

Figure 4.6. Denitrification, N burial and N fixation per continent for years 1970, 2000, 2030 (GO scenario) and 2050 (GO scenario).

4.5 Discussion

4.5.1 Nutrient elimination by dams

The damming of rivers creates new biogeochemical reactors along the aquatic continuum. The cycling of bioactive elements in dam reservoirs changes their fluxes and chemical speciation (Van Cappellen and Maavara, 2016). It is generally assumed that the presence of dams reduces the net fluxes of nutrients in river systems. This is the case for P and silicon (Si), which are retained by burial of particle-associated P and Si in sediments accumulating in reservoirs (Maavara et al., 2015, 2014). The key difference between N and the nutrient elements P and Si, however, is that the latter two nutrient elements have no natural gas-phase forms. Elimination (or retention) of P and Si by a given dam can therefore be obtained directly from the difference between the inflow into the reservoir of the dissolved and particulate species of the elements and their outflow through the dam, typically integrated at an annual time-scale.

The same mass balance inflow-outflow method has been used to quantify N elimination in reservoirs. That is, the difference between the TN load to a reservoir and the TN outflow through the dam is attributed to TN elimination by burial and denitrification in the reservoir (Némery et al., 2016; Tomaszek and Koszelnik, 2003). In some cases, the inflow-outflow mass balance calculations are combined with measurements of denitrification rates (David et al., 2006; Garnier et al., 1999; Koszelnik et al., 2007b) or N sedimentation rates (Vanni et al., 2011). The role of N fixation is usually neglected in existing N budgets of reservoirs. However, because N fixation is a source of new N to reservoirs, ignoring N fixation can underestimate the efficiency of N elimination, particularly in N-limited reservoirs.

4.5.2 N fixation

The balance of N fixation versus N burial plus denitrification (i.e., versus gross elimination) controls whether the presence of a dam increases or decreases the riverine N flux. Till now, only a few studies have included N fixation in mass balance calculations of N elimination in reservoirs (Kunz et al., 2011b, 2011a; Ramírez-Zierold et al., 2010). Based on our results, in year 2000, N fixation added 70 Gmol N to reservoirs worldwide (**Table 4.1**). At the same time, gross elimination by dams equaled 270 Gmol N,

which represents 36% of the total TN input to reservoirs (river inflow plus N fixation). When neglecting N fixation as a source of N to reservoirs, the inflow-outflow method predicts that elimination in year 2000 amounts to only 200 Gmol N yr^{-1}, or 29% of the TN river inflow (687 Gmol yr^{-1}). As these calculations illustrate, accounting for N fixation or not has a non-negligible impact on the assessment of the N elimination efficiency of dam reservoirs.

The changes in global N fixation in reservoirs with time are driven by changes in the number, geographical location and hydraulic residence time distribution of dams, as well as changes in the absolute and relative supplies of N and P to the reservoirs. Between 1970 and 2050, global in-reservoir N fixation is predicted to increase more than fivefold (**Table 4.1**). This large increase is caused primarily by the rising number of dams, but also by the increase in the relative loading of reactive P to reservoirs, which in turn increases the demand for N fixation in N limited reservoirs. For instance, N fixation is estimated to be highest for the Technogarden (TG) scenario although the global TDP inflow to reservoirs is lower for the TG than GO scenario. The latter, however, also has a higher TN inflow that leads to a lower N fixation demand. As a result of the combination of the various drivers, the model calculations predict that the contribution of N fixation to the global TN input to reservoirs increases from around 8% in 1970 to 12-16% in 2030-2050.

A significant number of studies have highlighted the role of N fixation in sustaining primary production in lakes (Howarth et al., 1988). However, the fraction of the N input to lentic systems supplied by N fixation varies greatly, from 0 to 99.5% (Horne & Galat, 1985; Mugidde *et al.*, 2003; Schindler, 2012; Horváth *et al.*, 2013). According to our results, the global contribution of N fixation to the annual N demand of primary production in reservoirs ranges between 39 and 47% for the different time points and future scenarios considered. This relatively small range implies that the large increase in absolute N fixation in reservoirs in the period 1970-2050 mostly reflects the increasing amount of in-reservoir primary productivity, which in terms of N demand grows from 84 Gmol yr^{-1} in 1970 to 662 Gmol yr^{-1} in 2050 (GO scenario).

4.5.3 Denitrification and burial

Together, global reservoir denitrification plus N burial exceed N fixation under all conditions considered (**Table 4.1**). Thus, globally, dams reduce the flow of TN carried by rivers. At the start of the 21st century, 7.4% of the riverine N load was eliminated via N burial and denitrification behind dams. Taking into account N fixation in reservoirs, net elimination in year 2000 amounted to 5.5% of the riverine N load. With the world's growing number of dams, reservoirs are expected to become an even larger sink of N: by 2050, denitrification and burial could be eliminating as much as 16% of the riverine N load.

Most published studies that report estimates of global N elimination in lakes and reservoirs do not distinguish between denitrification and sedimentary burial (Beusen et al., 2015; Harrison et al., 2009; Wollheim et al., 2008) . Here, we explicitly separate the two elimination mechanisms (**Figure 4.3**). For instance, our results for year 2000 imply that denitrification eliminated 21% (159 Gmol yr^{-1}) of the TN input to reservoirs (river inflow plus N fixation), while burial accounted for 14% (110 Gmol yr^{-1}). The model calculations thus point to denitrification as the main N elimination mechanism in reservoirs; its contribution to gross elimination varies between 57% and 61% in the model calculations. This finding is consistent with other studies that conclude on a dominant role for denitrification in TN elimination in lakes and reservoirs (Cook et al., 2010; Grantz et al., 2014; Kunz et al., 2011a).

The global efficiency of N elimination in reservoirs by denitrification and burial decreases from 36% in 2000 to 30±2% in 2030-2050. This drop is due the fact that our 2030 and 2050 projections account for the construction of the 3700 new hydrolelectric dams with capacity ≥1 MW that are reported by Zarfl et al. (2015) to be under construction or planned to be operational by 2030. Hydroelectric dams have relatively short water residence times, which lowers their elimination efficiencies. As shown in **Figure 4.7**, the average water residence time of reservoirs decreases from year 2000 to 2030 across all continents (except Antarctica where there are no dams). The most significant reduction in water residence time occurs in South America, where a more than fivefold increase in the number of large hydroelectric dams is expected (from 300 dams in 2000 to 1598 dams in 2030). Consequently, in 2030, fifty percent of the reservoirs in South America will have a residence time lower than 0.1 yr^{-1}.

The results of the 2030 and 2050 model calculations only represent the effects of dams included in the published survey of large hydroelectric dams by Zarfl et al. (2015). Anecdotal evidence suggests that many more dams, in particular smaller ones, are being or will be built in the coming decades. These unreported dams will likely cause departures from the results presented here, including the water residence time distributions shown in **Figure 4.7**. Thus, to more reliably assess the effects of damming on the continental cycles of N and other nutrient elements will require further, internationally coordinated, efforts to generate a comprehensive inventory of all existing and future dams.

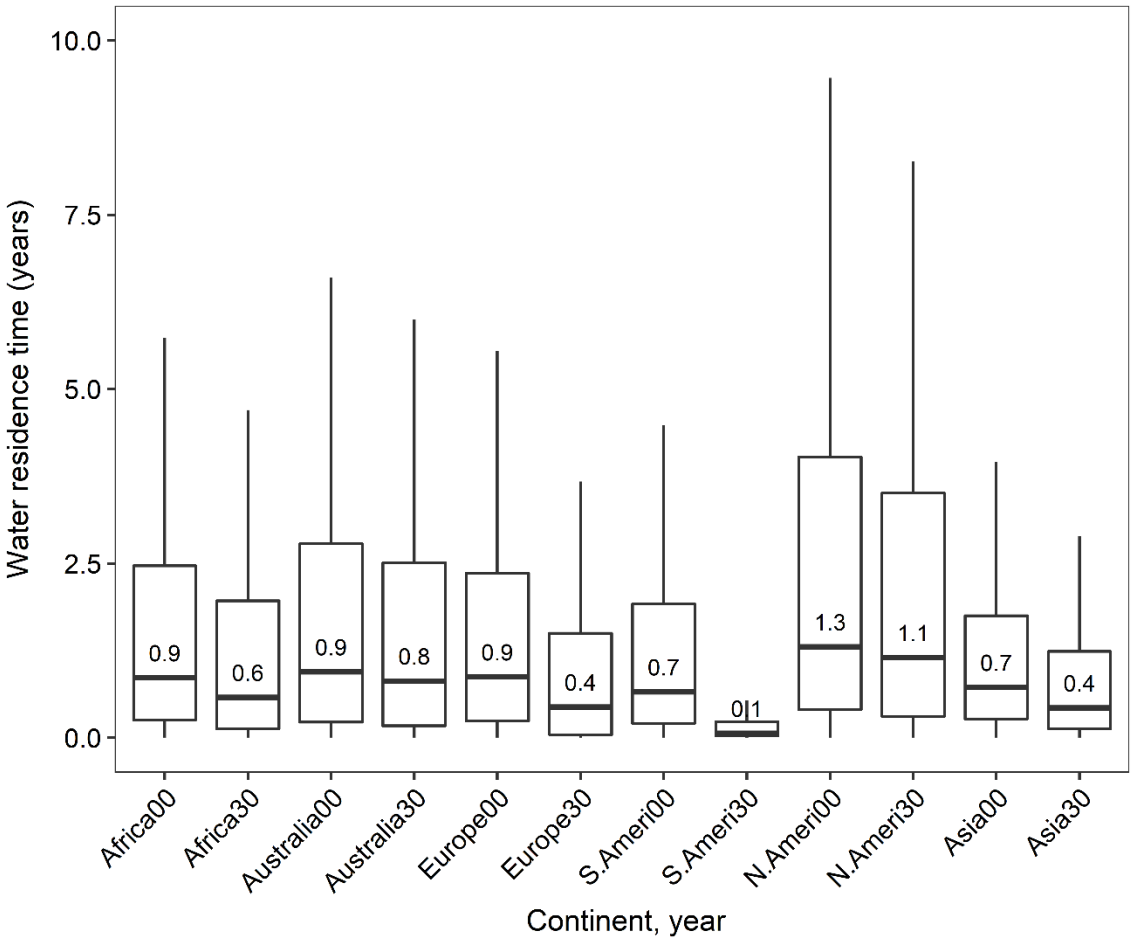

Figure 4.7. Box plots of the distributions of water residence times of reservoirs in different continents, for years 2000 and 2030, with 00 corresponding to 2000 and 30 to 2030. The solid line within boxes indicates the median; edges of boxes indicate first and third quartiles; and whiskers indicate variability outside the upper and lower quartiles. Outliers are not shown. The values of the medians are indicated in the boxes.

4.5.4 N:P ratios

The model-based, average global molar TN:TP ratios delivered to reservoirs are on the order of 12-13 (**Figure 4.8**). That is, on average, reservoirs are N limited, which in turn drives in-reservoir N fixation. The input TN:TP values are a function of the nutrient loadings in watersheds predicted by the Global-NEWS model and, in the case of dam cascades, also the effects of upstream dams. The relatively small temporal changes in the average input TN:TP ratios to reservoirs are driven by multiple factors, including changes in land use, agricultural practices, water treatment and atmospheric N inputs. For example, the increase in median values of the input TN:TP ratio from 12.4 to 13.2 between 1970 and 2000 likely reflects more restrictive policies on P use in fertilizers and detergents, and increased wastewater treatment (Bouwman et al., 2009; Mackenzie et al., 2002).

The differences between inflow and outflow TN:TP ratios in **Figure 4.8** are the result of the in-reservoir processes affecting both nutrient elements. As can be seen in the figure, the median TN:TP ratios of dam outflows are predicted to be systematically higher than those of reservoir inflows across all four time points considered. The upward shift in TN:TP ratios is primarily the result of N fixation in N limited reservoirs, along with a relatively more efficient P removal by burial in reservoir sediments (Maavara et al., 2015). Because of in-reservoir processes the outflow from reservoirs approaches the theoretical Redfield ratio of 16:1 for phytoplankton production. Such a shift in the TN:TP ratio of reservoir outflow has been noted in other studies (Ashton, 1981; Cook et al., 2010; Grantz et al., 2014; Vanni et al., 2011). The decrease in median TN:TP ratios between inflow and outflow is less pronounced in the 2030 and 2050 projections than in earlier years. Again, this reflects the ongoing boom in hydroelectric dam construction, which leads to a downward shift in the reservoir water residence time distributions (**Figure 4.7**) and therefore a lower extent of in-reservoir processing of the nutrient elements. Overall, however, damming of rivers should reduce the degree of N limitation of primary production in receiving freshwater and coastal marine ecosystems.

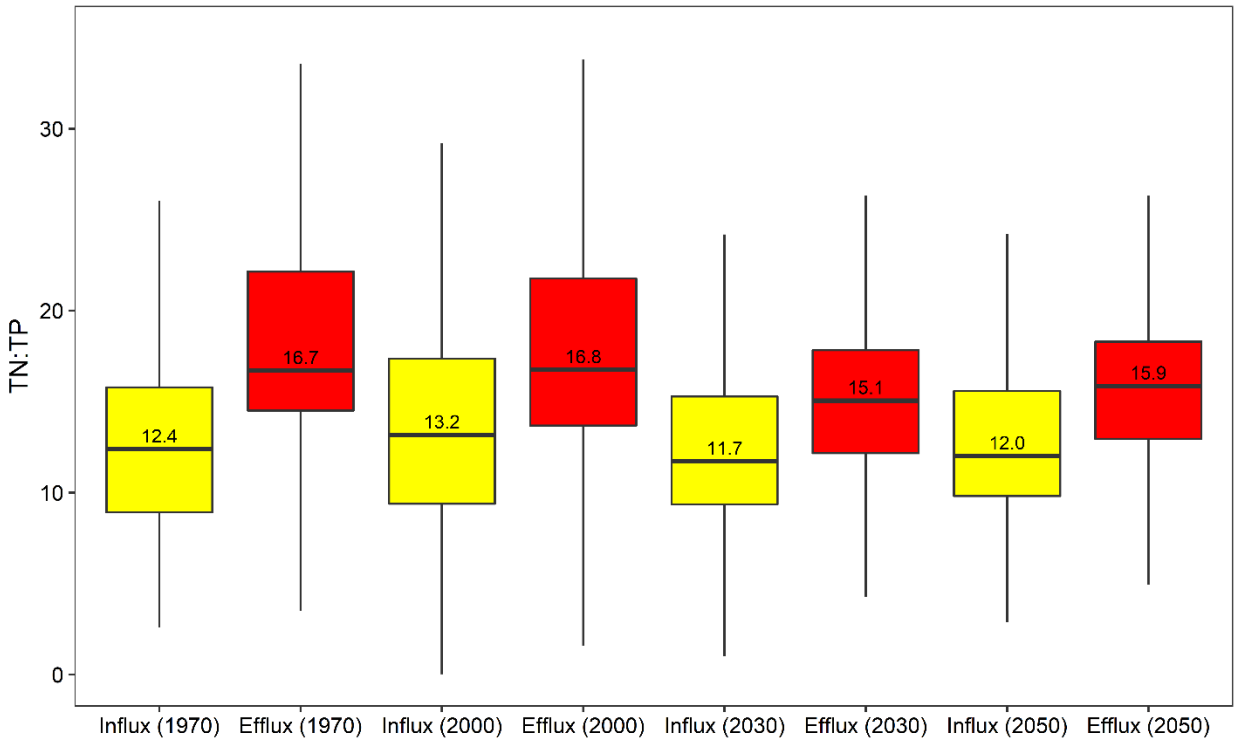

Figure 4.8. Global TN:TP ratios of river inflow (in yellow) and dam outflow (in red) of reservoirs in 1970, 2000, 2030 (GO scenario), and 2050 (GO scenario). In each box plot, the central mark is the median; the edges of the box are the 25th and 75th percentiles; and the whiskers extend to the most extreme data points not considered outliers. The values of the medians are indicated in the boxes. Note that the numbers of reservoirs included in the analysis differ for years 1970 (4393 dams), 2000 (6847 dams), 2030 (10547 dams), and 2050 (10547 dams).

4.6 Conclusion

Damming creates hotspots of biogeochemical activity in river networks. In-reservoir N fixation, denitrification and sediment burial modify the flows of dissolved and particulate forms of N carried by rivers. Globally, dam reservoirs act as a sink of N, because denitrification and burial (i.e., gross elimination) exceed N fixation. According to our results, at the start of this century, dams globally eliminated 7.4% of N loading to river networks, but this could rise to 15% by mid-century as a result of the rapid building of new dams, particularly in South America and Southeast Asia. The findings of our study further suggest that dams increase the N:P ratio of riverine discharge, principally due to in-reservoir N fixation, thereby reducing N limitation of primary production in receiving lentic and coastal marine environments. Damming therefore has important implications for managing the impacts of cultural eutrophication.

Chapter 5
Conclusions

5.1 Summary of major findings

The general aim of my thesis was to quantify nitrogen (N) cycling along the river continuum across different scales. From the regional scale, with the analysis of the sediments of a N polluted river in Chapter 2, to the global scale, with a global analysis of past, present and future changes in the riverine fluxes of N due to river damming in Chapter 4.

In Chapter 2, I present a comprehensive reaction-transport model to describe the fate of reactive N in streambed sediments. Special attention is given to nitrite as a highly toxic reactive intermediate in the N cycle that is rarely represented in early diagenetic models. The model explicitly accounts for the production and consumption of nitrite via nitrification, denitrification, dissimilatory nitrate reduction to ammonium (DNRA) and anammox. I use the model to analyze a pore water and sediment incubation dataset collected in Seine River sediments downstream of Paris, France. The Seine River is a strongly human-impacted river through urbanization and agricultural activities with elevated concentrations of nitrite beyond environmental guidelines in some locations and seasons.

Four sets of data were collected during two sampling times (summer and fall) from two sites, one upstream and one downstream of the largest wastewater treatment plant (WWTP) that serves the Paris conurbation. The model successfully captures the key features and general trends of the porewater profiles of N species, while simultaneously estimating the benthic fluxes of those species across the sediment-water interface (SWI). The model is used to explain why sediments can act as either a source or sink of nitrite for the overlying water at the different site locations and sampling times. The model results indicate that while denitrification dominates the N transformation processes within sediments of the Seine River, nitrification and anammox and bio(physical) processes play important roles in modulating the benthic exchange fluxes of the different N species. The model results also highlight that the WWTP impacts the benthic fluxes of nitrite at the downstream site, not only by releasing nitrite to the river system through effluent discharges, but also by providing high loads of labile organic carbon (C) that drive the biogeochemical activity in the sediments.

Early diagenetic models are a powerful tool for analyzing the biogeochemical role of sediments in highly dynamic systems such as rivers. Such models provide insights into the main environmental factors at the SWI, and processes below the SWI, that impact the benthic exchanges fluxes of reactive compounds, including N species. With the growing number of studies that use advanced techniques, for example in situ microsensors, to measure the low concentrations of intermediate reactive species such as nitrite, reactive transport models become essential for the interpretation and analysis of the results. The model developed in this study can be widely applied to N polluted streambed sediments with high loads of labile organic C. For example, my model is currently used by our French collaborators in the study of a eutrophic coastal system in France. The Villan Bay ecosystem is strongly influenced by high loads of nitrate released by agricultural activities. My model is used specifically to estimate the capacity of sediments in removing nitrate from the water column (Ratmaya et al., in preparation).

In Chapter 3, I expand the early diagenetic model of Chapter 2 by representing the isotopic compositions of the N species nitrate, nitrite, ammonium and organic nitrogen, and incorporating the isotopic fractionations associated with the N transformation processes. I use the model to investigate the variations in N isotopic compositions across the SWI under dynamic conditions representative of sediment core incubations. The model results demonstrate that N isotopic compositions of the N species are strongly influenced by the presence of dissolved oxygen in the overlying water. That is, the isotopic signatures record switches between oxic and anoxic conditions. Additionally, the results highlight the effects of the fractionation factors on N isotopic values, such as the impact of the inverse isotopic effect of the second step of nitrification on the nitrite isotopic composition and the effect of DNRA on the isotopic composition of ammonium. The N isotope model will be applied in sediment incubation experiments planned by our French colleagues (see below).

Finally, in Chapter 4, I quantify the effect of damming on the global riverine N fluxes. Damming of rivers has increased significantly over the last 60 years and the number of dams is going to continue to rise. By creating a hot spot for biogeochemical activity, closing of a dam promotes the in-reservoir biogeochemical cycling of N, which results in N elimination by burial in sediments accumulating in the

reservoir and gaseous emissions to the atmosphere through denitrification. I use a process-based reservoir N mass balance model, which I scale up to all the river basins in the world. The flows of dissolved and particulate forms of N carried by rivers are modified by in-reservoir N fixation, denitrification and sediment burial. As denitrification and burial (i.e., gross elimination) globally exceed N fixation, dam reservoirs act as a net sink for riverine N. The results indicate that in year 2000, 7.4% of N loading to river networks were eliminated in dam reservoirs. This percentage may grow to 15% by 2050 due to the rapid construction of new dams, particularly in Southeast Asia and South America. By coupling my results to those of the earlier work on phosphorous (P), I further show that dams lead to a global increase in the N:P ratio of riverine discharge, hence reducing the magnitude of N limitation of primary production in receiving lentic and coastal marine environments. This finding has important implications for the development of nutrient abatement strategies intended to mitigate the impacts of cultural eutrophication.

5.2 Future work

The immediate next step of this thesis lies in the continuation of the work presented in Chapter 3. The addition of N isotopes to the early diagenetic model will be coupled to core incubation experiments that are planned to be carried out by our colleagues at the University of Rennes. The experiments will involve Seine River sediments. Pore water profiles of nitrate, nitrite and ammonium will be measured in the cores and the temporal variations of nitrite isotopic compositions in the overlying water will be monitored during incubations. The scenarios investigated in Chapter 3 by the early diagenetic model are being used in the design of the experiments, for example by informing the time scales over which changes in isotopic compositions will be measurable, and the expected magnitudes of these changes. In terms of the isotopic simulation capabilities, the next step would be the incorporation of oxygen isotopes to the N early diagenetic model. Dual isotopes of N and oxygen together will make a powerful tool in identifying the sources of N in the sediments and assisting in the recognition of the N transformation processes below the sediment-water interface. In particular, dual isotopes will help in analyzing nitrite

data as it is potentially influenced by many processes. Dual isotopes signatures are a powerful tool in constraining the N budget in sediments (Casciotti, 2016).

The next step for the improvement of the diagenetic model will be its coupling to a stream N model, therefore representing the dynamic fate and transport along the entire stream system. Stand-alone early diagenetic models usually ignore the dynamic interactions and feedbacks between the stream water and the stream sediments by a priori imposing boundary conditions (Peña et al., 2010; Soetaert et al., 2000)

The reservoir N mass balance model of Chapter 4, coupled with those of P and C (Maavara et al, 2015, 2017) is being used in another study to predict the N_2O emissions form dam reservoirs, rivers and estuaries (Maavara et al., submitted). Additionally, the reservoir N mass balance model of this study together with similar models for Si (silicon), P and C models (Maavara et al, 2014, 2015, 2017) is being used to identify the changes in nutrient ratios in the coastal waters due to dam constructions, and hence to predict the changes in coastal nutrient limitation trends (Maavara et al., in preparation).

Appendix A

Supplementary Material of Chapter 2

Table A1. Comparison between model-derived rates for Seine River sediments and rates reported in the literature (all the values refer to sediments).

Location	Integrated rate in depth (μmol N cm^{-2} yr^{-1})	References
Denitrification		
River and stream	>302	(Seitzinger, 1988)
Four dam reservoirs, Poland	50-2200	(Tomaszek and Czerwieniec, 2000)
Millstone River/Sugar Creek, US	587-13850	(Laursen and Seitzinger, 2002)
Seine River, France	60-2500	(Billen et al., 2007)
Seine River, France	125-625	(Thouvenot-Korppoo et al., 2009)
Seine River, France	497-1248	(This study)
Anammox		
Yincungang and Henangeng Rivers, China	0.1-6	(Zhao et al., 2013)
Qinshui River, China	86-724	(Wang et al., 2013)
Seine River, France	33-78	(This study)
DNRA		
Nueces River Mouth, US	2.8	(Gardner et al., 2006)
Lake Taihu, China	219	(McCarthy et al., 2007)
Seine River, France	16-41	(This study)

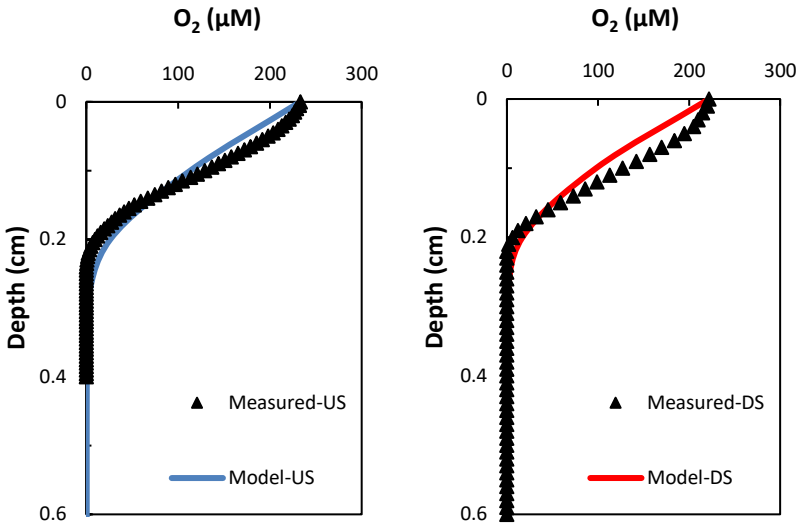

Figure A1. Measured (symbols) and modeled (full line) oxygen concentration profiles upstream (US) and downstream (DS) of the SAV wastewater treatment plant in October 2013.

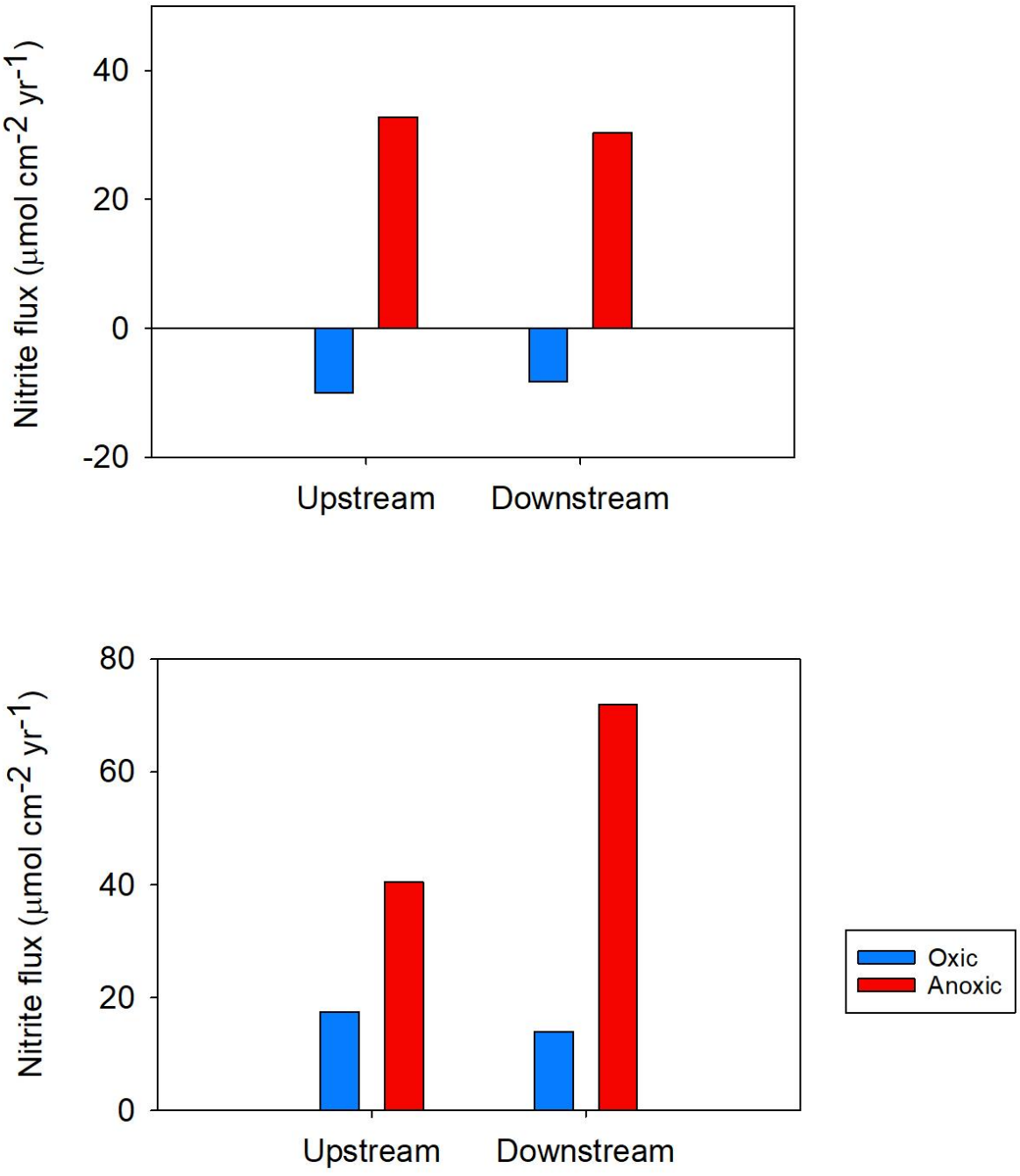

Figure A2. Model predicted benthic nitrite fluxes upstream and downstream of the SAV wastewater treatment plant in August 2012 and October 2013, in the presence (oxic) and absence (anoxic) of bottom water O_2.

Appendix B

Supplementary Material of Chapter 4

Table B1. Parameter ranges and probability distribution functions (PDFs) used in the Monte Carlo analysis.

Parameter	units	PDF	PDF parameters	Source
k_{Min}	yr^{-1}	Lognormal: $y=\frac{1}{x\sigma\sqrt{2\pi}}e^{\frac{-(lnx-\mu)}{2\sigma^2}}$	μ=1.58, σ=1.32	[1], [2], [8], [5], [4], [3], [6], [7], [8], [9]
k_{Bur}	yr^{-1}	Uniform	[0.5, 2.0]	Model calibration based on [10], [11], [12]
k_{Hyd}	yr^{-1}	Uniform	a=0.001, b=7.5	[3], [4], [5], [7], [8], [9]
Volume	km^3	Pareto: $y=(\frac{1}{\sigma})(1+k\frac{x-\theta}{\sigma})^{-1-\frac{1}{k}}$	σ =0.0556487, k =1.39388, $\theta=0$	[13]
Discharge	km^3yr^{-1}	Pareto: $y=(\frac{1}{\sigma})(1+k\frac{x-\theta}{\sigma})^{-1-\frac{1}{k}}$	σ =0.0511971, k =2.12464, $\theta=0$	[13]
Inflowing TN concentration	$mol\ km^{-3}$	Gamma: $y=\frac{1}{b^a\Gamma(a)}x^{a-1}e^{\frac{-x}{b}}$	μ=1.01352, σ=4.37103	[14] - [31]
Proportion DIN	-	Gamma: $y=\frac{1}{b^a\Gamma(a)}x^{a-1}e^{\frac{-x}{b}}$	a=4.5, b=0.055	Gamma PDF constrained using world average proportions of each species (DIN=0.225, DON=0.3, PON=0.475) [32-34]. Mean of Monte Carlo outputs equals the observed means, but the full range of proportions is possible in the outcome of each iteration.
Proportion DON	-	Gamma: $y=\frac{1}{b^a\Gamma(a)}x^{a-1}e^{\frac{-x}{b}}$	a=3, b=0.1	
Proportion PON	-	1-(Proportion DIN- Proportion DON)		

[1]: (Doan et al., 2015), [2]: (Romero et al., 2004), [3]: (Özkundakci et al., 2011), [4]: (Marcé et al., 2010), [5]: (Imteaz et al., 2003), [6]: (Cui et al., 2016), [7]:(Chung et al., 2014), [8]: (Bruce et al., 2006), [9]: (Schladow and Hamilton, 1997), [10]: (Knoll et al., 2014), [11]: (Grantz et al., 2014), [12]: (Kunz et al., 2011a), [13]: (Maavara et al., 2015), [14]: [Boyer, 2008], [15]: (Bhat et al., 2014), [16]: (Judd, 2008), [17]: (Gurung, 2005), [18]: (Lévesque and Page, 2011), [19]: (Sprague et al., 2002), [20]: (Vandermeulen and Gemza, 1991), [21]: (Ren et al., 2015), [22]: (Pahl, 2007), [23]: (Policht-latawiec, 2013), [24]: (Chen et al., 2017), [25]: (Windolf et al., 1996), [26]: (Hur and Cho, 2012), [27]: (Sun et al., 2013), [28]: (Edwards et al., 2000), [29]: (Jarvie et al., 1998), [30]: (Bhat et al., 2014), [31]: (Goolsby and Battaglin, 2001), [32]: (Seitzinger et al., 2005), [33]: (Meybeck, 1982), [34]: (Berner and Berner, 1995)

Table B2. Literature data on N fixation in reservoirs and lakes used to generate Figure 4.2. TN:TP represents the molar ratio of river input to the reservoir or lake, and % fixation is the relative contribution of N fixation to the total N influx (river input plus N fixation).

Reservoir/Lake	TN:TP	Fixation (%)	Reference
Rietvlei Dam (1976)	1.4	46.5	(Ashton, 1981); (Howarth et al., 1988)
Rietvlei Dam (1977)	2.2	23	(Ashton, 1981); (Howarth et al., 1988)
Lake Valencia	2.8	3.5	(Levine and Lewis, 1984); (Ashton, 1981)
Lake 227 (1990)	3.8	52	(Findlay et al., 1994)
Lake 227 (1991)	6.0	37	(Findlay et al., 1994)
Lake Clear	6.6	43	(Toetz and McFarland, 1987)
Lake S bergundasjon2	6.7	21	(Persson, 2003)
Lake 227 (1992)	8.2	42	(Findlay et al., 1994)
Fayetteville Dam	9.1	27	(Grantz et al., 2014)
Lake 227 (1979)	13.7	24	(Findlay et al., 1994)
Lake 227 (1975)	13.9	4	(Findlay et al., 1994)
Lake 227 (1976)	13.9	6	(Findlay et al., 1994)
Lake 227 (1980)	13.9	16	(Findlay et al., 1994)
Lake 227 (1981)	14.4	9	(Findlay et al., 1994)
Lake 227 (1977)	14.6	11	(Findlay et al., 1994)
Lake 227 (1983)	14.8	11	(Findlay et al., 1994)
Elmdale Dam	15	30	(Grantz et al., 2014)
Lake 227 (1987)	15.3	11	(Findlay et al., 1994)
Lake 227 (1978)	15.5	4	(Findlay et al., 1994)
Lake 227 (1986)	15.5	13	(Findlay et al., 1994)
Lake 227 (1982)	15.7	31	(Findlay et al., 1994)
Lake 227 (1984)	15.9	13	(Findlay et al., 1994)
Lake 227 (1988)	17.5	7	(Findlay et al., 1994)
Lake 227 (1989)	17.5	10	(Findlay et al., 1994)
Lake Mendota	18	7	(Howarth et al., 1988); (Mugidde, 2001);
Lake 227 (1985)	18.6	7	(Findlay et al., 1994)
Lake Washington	22.6	0.5	(Howarth et al., 1988); (Mugidde, 2001);
Lake Malawi	28	3.5	(Gondwe et al., 2008); (Schindler, 2012)
Lake 227 (1971)	29.2	0	(Findlay et al., 1994)
Lake 227 (1970)	29.7	0	(Findlay et al., 1994)

Table B3. Literature data from freshwater early diagenetic studies used to extract the value of K_{DEN} in Equation 4.6. DIN is the concentrations of dissolved inorganic nitrogen at the sediment-water interface (primarily as nitrate); f_C is the depth-integrated total C oxidation rate (or the sediment oxygen uptake rate); f_N is the depth-integrated denitrification rate. Denitrification rates were converted to $\mathrm{mmoles\ C\ m^{-2}d^{-1}}$. The data in the table are used to generate Figure B2.

DIN (μmol L^{-1})	$\mathbf{f_C}$ ($mmoles\ C\ m^{-2}d^{-1}$)	$\mathbf{f_N}$ ($mmoles\ C\ m^{-2}d^{-1}$)	**Reference**
130	10.2	6.4	(Seitzinger, 1994)
60	15.9	7.6	(Seitzinger, 1994)
55	21.7	6.1	(Seitzinger, 1994)
12.7	4.7	0.4	(Han et al., 2014)
13.1	5.3	0.7	(Han et al., 2014)
107	18.3	3.9	(Canavan et al., 2006)
168.5	$\frac{\mathrm{fN}}{\mathrm{fC}} = 0.25$ is reported	-	(Jones and Simon, 1981)
33.67	22.3	4.6	(McCarthy et al, 2007)
320.5	39.0	25.6	(Akbarzadeh et al., 2018)

Table B4. Model parameters of Equation 4.7 for years 1970 and 2000, and the four MEA scenarios in years 2030 and 2050.

Year – scenario	a	B	c	R^2
1970 & 2000 – burial	0.2827	0.2723	1.43	0.37
1970 & 2000 - denitrification	0.4524	0.4520	1.459	0.55
2030 AM – burial	0.2750	0.2668	1.501	0.37
2030 AM - denitrification	0.4511	0.4513	1.611	0.54
2030 TG – burial	0.2772	0.2677	1.471	0.36
2030 TG - denitrification	0.4503	0.4489	1.614	0.53
2030 GO – burial	0.2772	0.2677	1.469	0.36
2030 GO - denitrification	0.4503	0.4489	1.613	0.53
2030 OS – burial	0.2746	0.2640	1.395	0.36
2030 OS - denitrification	0.4593	0.4592	1.551	0.54
2050 AM – burial	0.2782	0.2694	1.389	0.35
2050 AM - denitrification	0.4436	0.4415	1.717	0.51
2050 TG – burial	0.2848	0.2735	1.299	0.37
2050 TG - denitrification	0.4383	0.4402	1.699	0.52
2050 GO – burial	0.2896	0.2800	1.334	0.37
2050 GO - denitrification	0.4409	0.4423	1.77	0.53
2050 OS – burial	0.2958	0.2825	1.193	0.38
2050 OS - denitrification	0.4459	0.4487	1.768	0.53

Table B5. Standard deviations of parameters in Equation 4.7 obtained from 5000 iterations for year 2000.

Parameter	a	b	c
Standard deviation for N burial	0.007	0.006	0.135
Standard deviation for denitrification	0.007	0.006	0.075

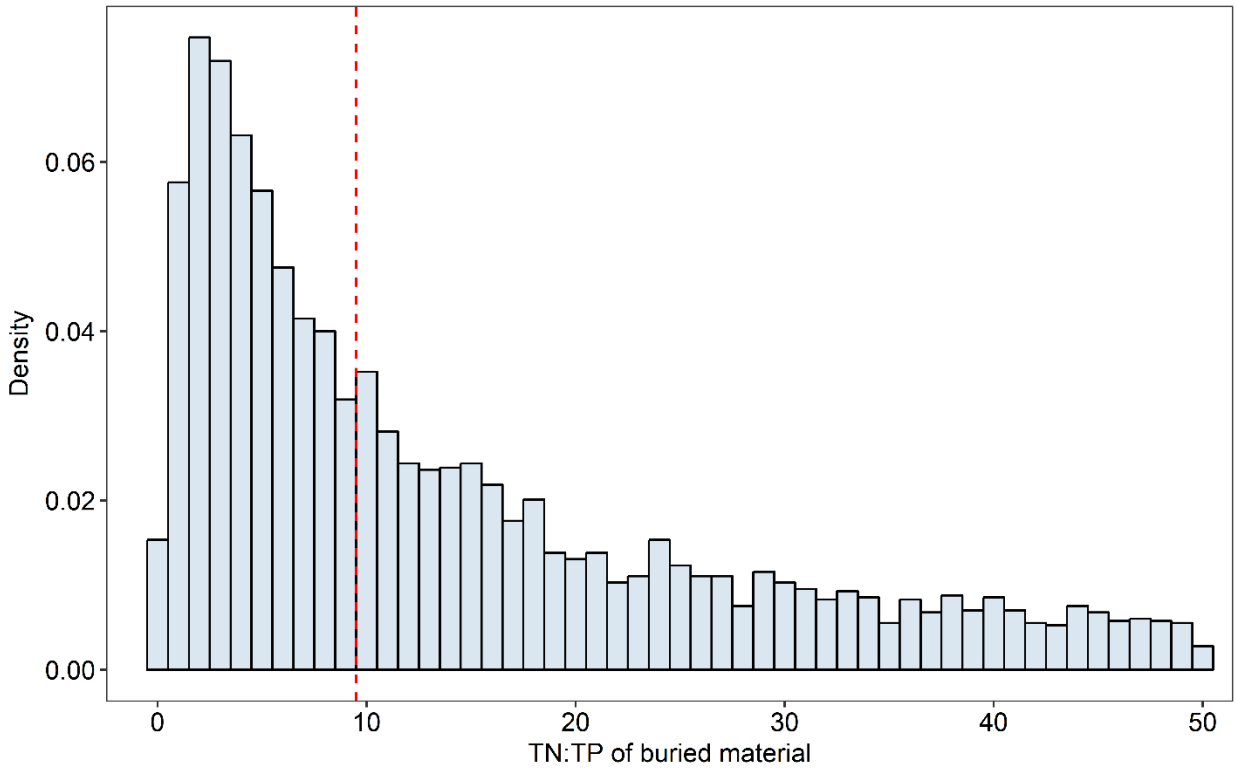

Figure B1. Distribution of molar TN:TP ratios of buried material in reservoir sediments generated by the Monte Carlo simulations for year 2000. The red dashed line shows the median (TN:TP = 9.5) of the distribution. The mode and mean of the distribution are 2.5 and 14.

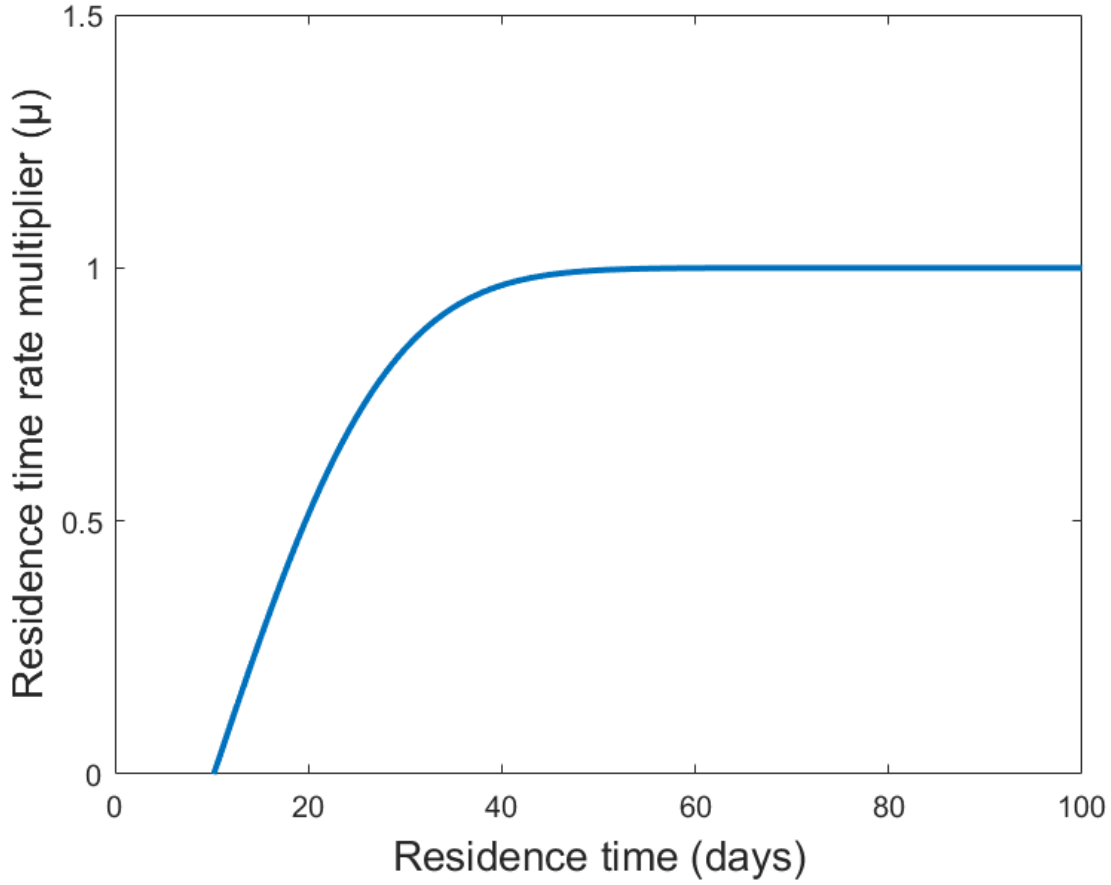

Figure B2. Residence time rate multiplier (μ) in Equations 4.3 and 4.4, as a function of the water residence time.

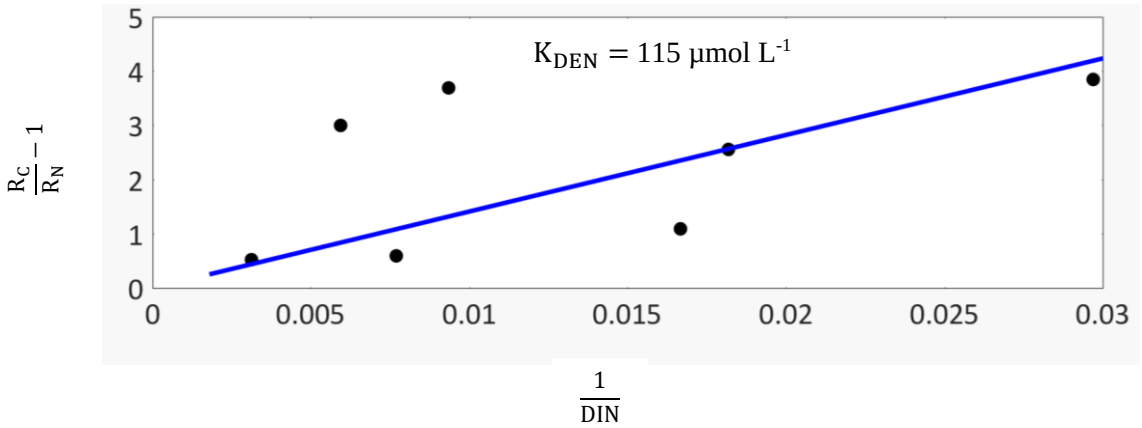

Figure B3. Calibration of K_{DEN} based on literature data for freshwater sediments assembled in Table B3; R_{C} is the depth-integrated total carbon mineralization rate; R_{N} is the depth-integrated denitrification rate for individual sediments. The slope of the graph yields K_{DEN}.

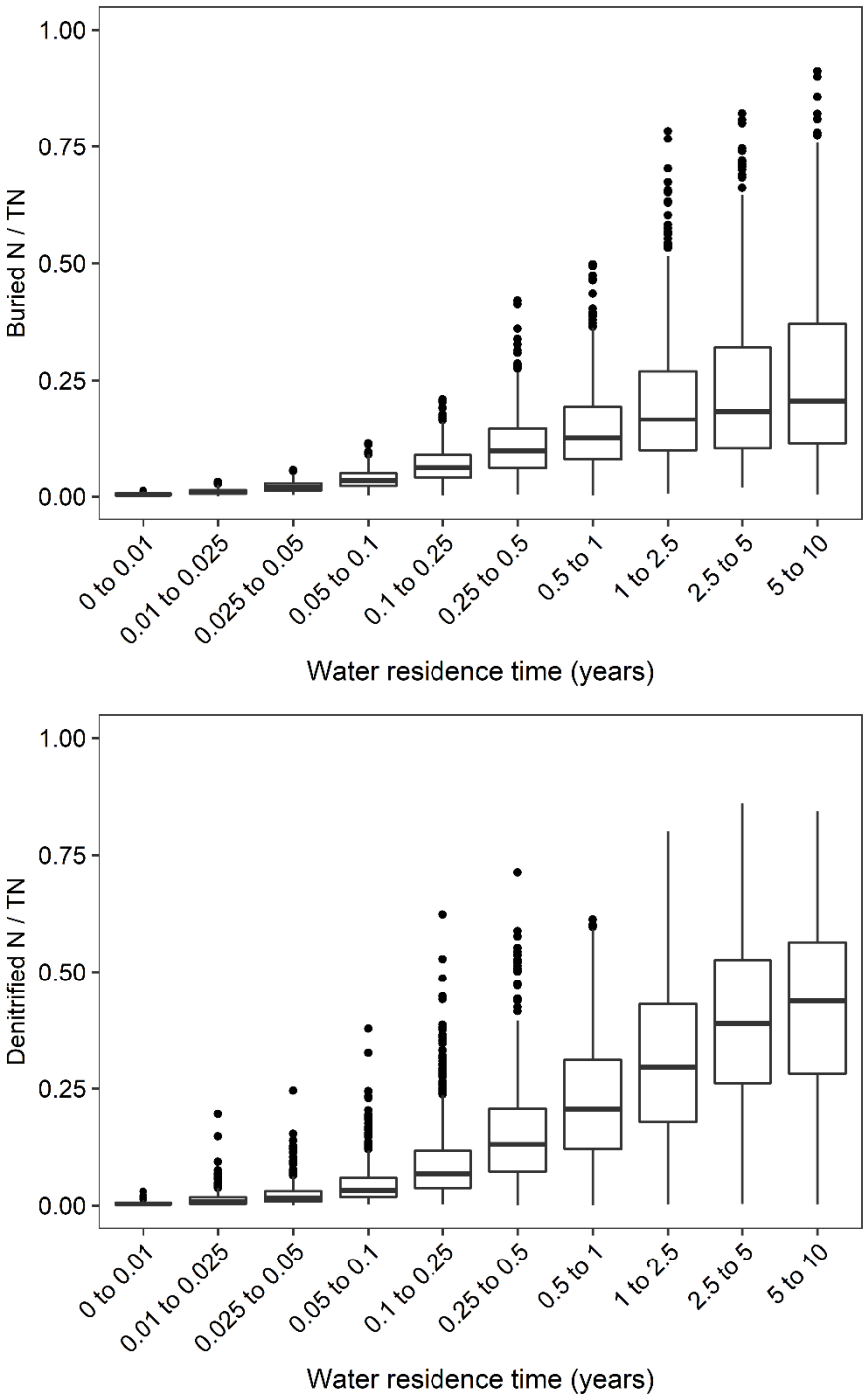

Figure B4. Relative burial and denitrification fluxes normalized to the TN influx (N fixation included) for year 2000, generated by 6000 Monte Carlo iterations, and binned by water residence time.

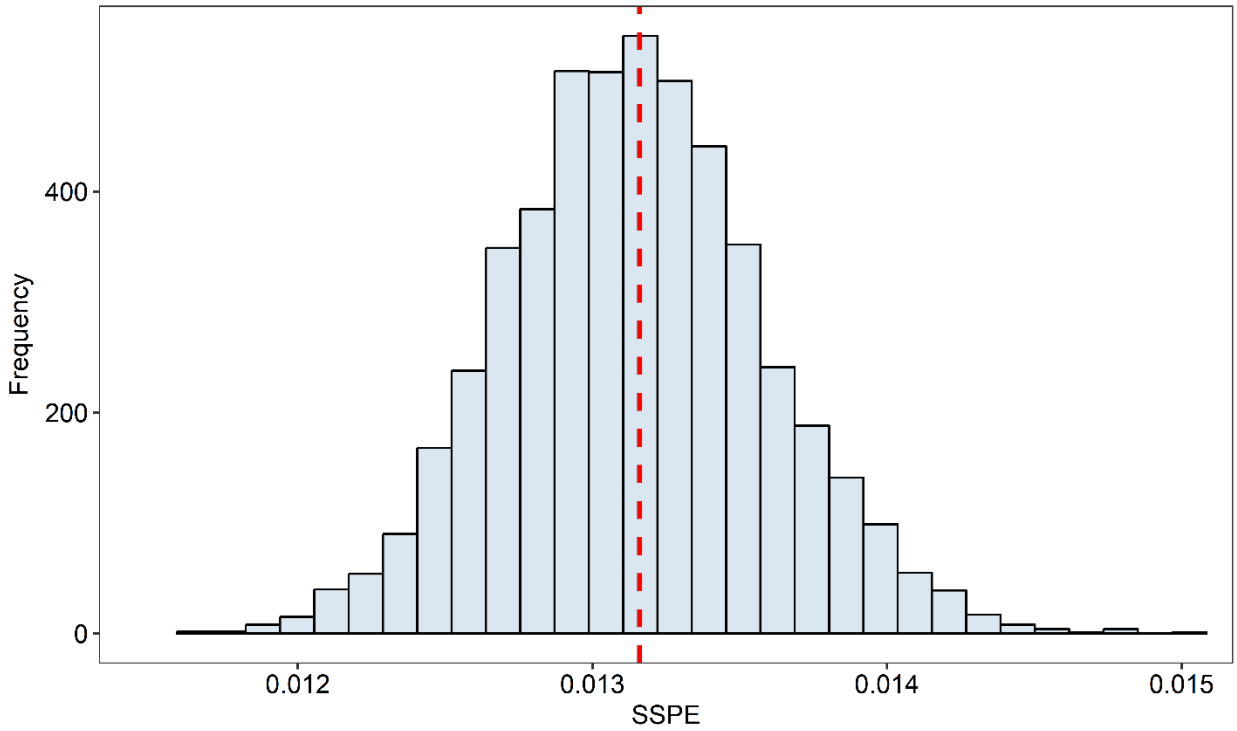

Fig B5. Distribution of the sum of squared prediction errors (SSPE) for N fixation obtained after 5000 iterations, with each iteration drawing 5000 samples from the virtual dataset of dams. The red dashed line shows the SSPE for the complete virtual dataset of dams.

References

Aissa-Grouz, N., Garnier, J., Billen, G., Mercier, B., Martinez, A., 2015. The response of river nitrification to changes in wastewater treatment (The case of the lower Seine River downstream from Paris). Ann. Limnol. - Int. J. Limnol. 51, 351–364. https://doi.org/10.1051/limn/2015031

Akbarzadeh, Z., Laverman, A.M., Rezanezhad, F., Raimonet, M., Viollier, E., Shafei, B., Van Cappellen, P., 2018. Benthic nitrite exchanges in the Seine River (France): An early diagenetic modeling analysis. Sci. Total Environ. 628–629, 580–593. https://doi.org/10.1016/j.scitotenv.2018.01.319

Alcamo, J., Vuuren, D. Van, Cramer, W., Alder, J., Bennett, E., Carpenter, S., Christensen, V., Foley, J., Masui, T., Morita, T., Neill, B.O., Peterson, G., Ringler, C., Schulze, K., Bouwman, L., Eickhout, B., Floerke, M., Lal, R., Takahashi, K., 2005. Changes in Ecosystem Services and Their Drivers across the Scenarios. Ecosyst. Hum. Well-being Scenar. Vol. 2 297–373.

Altmann, D., Stief, P., Amann, R., Beer, D. De, Schramm, A., 2003. Brief report In situ distribution and activity of nitrifying bacteria in freshwater sediment. Environ. Microbiol. 5, 798–803. https://doi.org/10.1046/j.1462-2920.2003.00469.x

Ashton, P.J., 1981. Nitrogen fixation and the nitrogen budget of a eutrophic impoundment. Water Res. 15, 823–833.

Beaulieu, J.J., Arango, C.P., Hamilton, S.K., Tank, J.L., 2007. The production and emission of nitrous oxide from headwater streams in the Midwestern United States. Glob. Chang. Biol. 14, 878–894. https://doi.org/10.1111/j.1365-2486.2007.01485.x

Berner, E.K., Berner, R.A., 1995. Global Environment: Water, Air, and Geochemical Cycles, second. ed. Prentice Hall, Upper Saddle River, NJ.

Berner, R.A., 1980. Early Diagenesis, A Theoretical Approach. Princeton University Press.

Betlach, M.R., Tiedje, J.M., 1981. Kinetic Explanation for Accumulation of Nitrite, Nitric Oxide, and Nitrous Oxide during Bacterial Denitrification. Appl. Environ. Microbiol. 42, 1074–1084. https://doi.org/Article

Beusen, A.H.W., Bouwman, A.F., Van Beek, L.P.H., Mogollón, J.M., Middelburg, J.J., 2015. Global riverine N and P transport to ocean increased during the twentieth century despite increased retention along the aquatic continuum. Biogeosciences Discuss. 12, 20123–20148. https://doi.org/10.5194/bgd-12-20123-2015

Beusen, A.H.W., Van Beek, L.P.H., Bouwman, A.F., Mogollón, J.M., Middelburg, J.J., 2015. Coupling global models for hydrology and nutrient loading to simulate nitrogen and phosphorus retention in surface water - Description of IMAGE-GNM and analysis of performance. Geosci. Model Dev. 8, 4045–4067. https://doi.org/10.5194/gmd-8-4045-2015

Bhat, S.A., Meraj, G., Yaseen, S., Pandit, A.K., 2014. Statistical Assessment of Water Quality Parameters for Pollution Source Identification in Sukhnag Stream: An Inflow Stream of Lake Wular (Ramsar Site), Kashmir Himalaya. J. Ecosyst. 2014, 1–18. https://doi.org/10.1155/2014/898054

Billen, G., Garnier, J., Némery, J., Sebilo, M., Sferratore, A., Barles, S., Benoit, P., Benoît, M., 2007. A long-term view of nutrient transfers through the Seine river continuum. Sci. Total Environ. 375, 80–97. https://doi.org/10.1016/j.scitotenv.2006.12.005

Boudreau, B.P., 2000. The mathematics of early diagenesis: From worms to waves. Rev. Geophys. 38, 389–416. https://doi.org/10.1029/2000RG000081

Boudreau, B.P., 1997. Diagenetic models and their implementation.Springer, Berlin, Germany.

Boudreau, B.P., 1996. A Method-of-lines code for carbon and nutrient diagenesis in aquatic sediments. Comput. Geosci. 22, 479–496.

Bouwman, a. F., Beusen, a. H.W., Billen, G., 2009. Human alteration of the global nitrogen and phosphorus soil balances for the period 1970-2050. Global Biogeochem. Cycles 23. https://doi.org/10.1029/2009GB003576

Boyer, J.M., 2008. Milton Reservoir Water-Quality Assessment Weld County, Colorado. AMEC Earth & Environmental.

Bruce, L.C., Hamilton, D., Imberger, J., Gal, G., Gophen, M., Zohary, T., Hambright, K.D., 2006. A numerical simulation of the role of zooplankton in C, N and P cycling in Lake Kinneret, Israel. Ecol. Modell. 193, 412–436. https://doi.org/10.1016/j.ecolmodel.2005.09.008

Canavan, R.W., Laverman, A.M., Slomp, C.P., 2007. Modeling nitrogen cycling in a coastal fresh water sediment. Hydrobiologia 584, 27–36. https://doi.org/10.1007/s10750-007-0583-z

Canavan, R.W., Slomp, C.P., Jourabchi, P., Van Cappellen, P., Laverman, A.M., van den Berg, G.A., 2006. Organic matter mineralization in sediment of a coastal freshwater lake and response to salinization. Geochim. Cosmochim. Acta 70, 2836–2855. https://doi.org/10.1016/j.gca.2006.03.012

Canfield, D.., Jørgensen, B.., Fossing, H., Glud, R., Gundersen, J., Ramsing, N.., Thamdrup, B., Hansen, J.., Nielsen, L.., Hall, P.O.., 1993. Pathways of organic carbon oxidation in three continental margin sediments. Mar. Geol. 113, 27–40. https://doi.org/10.1016/0025-3227(93)90147-N

Casciotti, K.L., 2016. Nitrite isotopes as tracers of marine N cycle processes. Philos. Trans. R. Soc. A Math. Phys. Eng. Sci. 374, 20150295. https://doi.org/10.1098/rsta.2015.0295

Casciotti, K.L., 2009. Inverse kinetic isotope fractionation during bacterial nitrite oxidation. Geochim. Cosmochim. Acta 73, 2061–2076. https://doi.org/10.1016/j.gca.2008.12.022

Casciotti, K.L., Buchwald, C., 2012. Insights on the marine microbial nitrogen cycle from isotopic approaches to nitrification. Front. Microbiol. 3, 1–14. https://doi.org/10.3389/fmicb.2012.00356

Cébron, A., Garnier, J., 2005. Nitrobacter and Nitrospira genera as representatives of nitrite-oxidizing

bacteria: Detection, quantification and growth along the lower Seine River (France). Water Res. 39, 4979–4992. https://doi.org/10.1016/j.watres.2005.10.006

Chen, L., Yang, Z., Liu, H., 2017. Sensitivity analysis for the total nitrogen pollution of the Danjiangkou Reservoir based on a 3-D water quality model. Front. Earth Sci. https://doi.org/10.1007/s11707-017-0650-3

Chen, N., Chen, Z., Wu, Y., Hu, A., 2014. Understanding gaseous nitrogen removal through direct measurement of dissolved N2 and N2O in a subtropical river-reservoir system. Ecol. Eng. 70, 56–67. https://doi.org/10.1016/j.ecoleng.2014.04.017

Chesterikoff, A., Garban, B., Billen, G., Poulin, M., 1992. Inorganic nitrogen dynamics in the river seine downstream from paris (france). Biogeochemistry 17, 147–164.

Chung, S.W., Imberger, J., Hipsey, M.R., Lee, H.S., 2014. The influence of physical and physiological processes on the spatial heterogeneity of a Microcystis bloom in a stratified reservoir. Ecol. Modell. 289, 133–149. https://doi.org/10.1016/j.ecolmodel.2014.07.010

Clevinger, C.C., Heath, R.T., Bade, D.L., 2014. Oxygen use by nitrification in the hypolimnion and sediments of Lake Erie. J. Great Lakes Res. 40, 202–207. https://doi.org/10.1016/j.jglr.2013.09.015

Clough, T.J., Bertram, J.E., Sherlock, R.R., Leonard, R.L., Nowicki, B.L., 2006. Comparison of measured and EF5-r-derived N2O fluxes from a spring-fed river. Glob. Chang. Biol. 12, 352–363. https://doi.org/10.1111/j.1365-2486.2005.01089.x

Cook, P.L.M., Aldridge, K.T., Lamontagne, S., Brookes, J.D., 2010. Retention of nitrogen, phosphorus and silicon in a large semi-arid riverine lake system. Biogeochemistry 99, 49–63. https://doi.org/10.1007/s10533-009-9389-6

Cooper, A.B., 1984. Activities of benthic nitrifiers in streams and their role in oxygen consumption. Microb. Ecol. 10, 317–334. https://doi.org/10.1007/BF02015557

Couture, R.-M., Shafei, B., Van Cappellen, P., Tessier, A., Gobeil, C., 2010. Non-steady state modeling of arsenic diagenesis in lake sediments. Environ. Sci. Technol. 44, 197–203. https://doi.org/10.1021/es902077q

Cowling, E.B., Erisman, J.W., Smeulders, S.M., Holman, S.C., Nicholson, B.M., 1998. Optimizing air quality management in Europe and North America: Justification for integrated management of both oxidized and reduced forms of nitrogen. Environ. Pollut. 102, 599–608. https://doi.org/10.1016/S0269-7491(98)80088-2

Crowe, S.A., Treusch, A.H., Forth, M., Li, J., Magen, C., Canfield, D.E., Thamdrup, B., Katsev, S., 2017. Novel anammox bacteria and nitrogen loss from Lake Superior. Sci. Rep. 7, 1–7. https://doi.org/10.1038/s41598-017-12270-1

Crutzen, P.J., Mosier, A.R., Smith, K.A., Winiwarter, W., 2007. N_2O release from agro-biofuel

production negates global warming reduction by replacing fossil fuels. Atmos. Chem. Phys. Discuss. 7, 11191–11205. https://doi.org/10.5194/acpd-7-11191-2007

Cui, Y., Zhu, G., Li, H., Luo, L., Cheng, X., Jin, Y., Trolle, D., 2016. Modeling the response of phytoplankton to reduced external nutrient load in a subtropical Chinese reservoir using DYRESM-CAEDYM. Lake Reserv. Manag. 32, 146–157. https://doi.org/10.1080/10402381.2015.1136365

Dai, S.B., Yang, S.L., Li, M., 2009. The sharp decrease in suspended sediment supply from China's rivers to the sea: Anthropogenic and natural causes. Hydrol. Sci. J. 54, 135–146. https://doi.org/10.1623/hysj.54.1.135

Dale, a. W., Sommer, S., Bohlen, L., Treude, T., Bertics, V.J., Bange, H.W., Pfannkuche, O., Schorp, T., Mattsdotter, M., Wallmann, K., 2011. Rates and regulation of nitrogen cycling in seasonally hypoxic sediments during winter (Boknis Eck, SW Baltic Sea): Sensitivity to environmental variables. Estuar. Coast. Shelf Sci. 95, 14–28. https://doi.org/10.1016/j.ecss.2011.05.016

Dale, A.W., Bru, V., Alperin, M., Regnier, P., 2009. An integrated sulfur isotope model for Namibian shelf sediments. https://doi.org/10.1016/j.gca.2008.12.015

Dale, A.W., Regnier, P., Knab, N.J., Jørgensen, B.B., Van Cappellen, P., 2008. Anaerobic oxidation of methane (AOM) in marine sediments from the Skagerrak (Denmark): II. Reaction-transport modeling. Geochim. Cosmochim. Acta 72, 2880–2894. https://doi.org/10.1016/j.gca.2007.11.039

David, M.B., Wall, L.G., Royer, T. V., Tank, J.L., 2006. Denitrification and the nitrogen budget of a reservoir in an agricultural landscape. Ecol. Appl. 16, 2177–2190. https://doi.org/10.1890/1051-0761(2006)016[2177:DATNBO]2.0.CO;2

Delconte, C.A., Sacchi, E., Racchetti, E., Bartoli, M., Mas-pla, J., Re, V., 2014. Science of the Total Environment Nitrogen inputs to a river course in a heavily impacted watershed : A combined hydrochemical and isotopic evaluation (Oglio River Basin , N Italy) 467, 924–938. https://doi.org/10.1016/j.scitotenv.2013.07.092

Devallois, V., Boyer, P., Boudenne, J.L., Coulomb, B., 2008. Modelling the vertical profiles of O2 and pH in saturated freshwater sediments. Ann. Limnol. - Int. J. Limnol. 44, 275–288. https://doi.org/10.1051/limn:2008011

Diaz, R.J., Rosenberg, R., 2008. Spreading Dead Zones and Consequences for Marine Ecosystems. Science (80-.). 321, 926–929. https://doi.org/10.1126/science.1156401

Doan, P.T.K., Nèmery, J., Schmid, M., Gratiot, N., 2015. Eutrophication of turbid tropical reservoirs: Scenarios of evolution of the reservoir of Cointzio, Mexico. Ecol. Inform. 29, 192–205. https://doi.org/10.1016/j.ecoinf.2015.01.006

Driscoll, C., Whitall, D., Aber, J., Boyer, E., Castro, M., Cronan, C., Goodale, C.L., Groffman, P., Hopkinson, C., Lambert, K., Lawrence, G., Ollinger, S., 2003. Nitrogen Pollution in the

Northeastern United States: Sources, Effects, and Management Options. Bioscience 53.

Edwards, A.C., Cook, Y., Smart, R., Wade, A.J., 2000. Concentrations of nitrogen and phosphorus in streams draining the mixed land-use Dee Catchment, north-east Scotland. J. Appl. Ecol. 37, 159–170. https://doi.org/10.1046/j.1365-2664.2000.00500.x

Erisman, J.W., Galloway, J.N., Seitzinger, S., Bleeker, A., Dise, N.B., Petrescu, A.M.R., Leach, A.M., de Vries, W., 2013. Consequences of human modification of the global nitrogen cycle. Philos. Trans. R. Soc. B Biol. Sci. 368, 20130116–20130116. https://doi.org/10.1098/rstb.2013.0116

Fekete, B.M., Wisser, D., Kroeze, C., Mayorga, E., Bouwman, L., Wollheim, W.M., Vörösmarty, C., 2010. Millennium Ecosystem Assessment scenario drivers (1970-2050): Climate and hydrological alterations. Global Biogeochem. Cycles 24. https://doi.org/10.1029/2009GB003593

Findlay, D.L., Hecky, R.E., Hendzel, L.L., Stainton, M.P., Regehr, G.W., 1994. -Fixation and Heterocyst Abundance and its Relevance to the Nitrogen Budget of Lake 227. Can. J. Fish. Aquat. Sci. 51, 2254–2266. https://doi.org/10.1139/f94-229

Forbes, M.G., Doyle, R.D., Scott, J.T., Stanley, J.K., Huang, H., Brooks, B.W., 2008. Physical Factors Control Phytoplankton Production and Nitrogen Fixation in Eight Texas Reservoirs. Ecosystems 11, 1181–1197. https://doi.org/10.1007/s10021-008-9188-2

Galloway, J.N., Dentener, F.J., Capone, D.G., Boyer, E.W., Howarth, R.W., Seitzinger, S.P., Asner, G.P., Cleveland, C.C., Green, P.A., Holland, E.A., Karl, D.M., Michaels, A.F., Porter, J.H., Townsend, A.R., Vo, C.J., 2004. Nitrogen cycles : past , present , and future.

Galloway, N., Schlesinger, W.H., Ii, H.L., Schnoor, L., Tg, N., 1995. Nitrogen fixation : Anthropogenic enhancement-environmental response 9, 235–252.

Garban, B., Ollivon, D., Poulin, M., Gaultier, V., Chesterikoff, A., 1995. Exchanges at the sediment-water interface in the river Seine, downstream from Paris. Water Res. 29, 473–481. https://doi.org/10.1016/0043-1354(94)00181-6

García-Ruiz, R., Pattinson, S.N., Whitton, B.A., 1998. Kinetic parameters of denitrification in a river continuum. Appl. Environ. Microbiol. 64, 2533–2538.

Gardner, W.S., McCarthy, M.J., 2009. Nitrogen dynamics at the sediment–water interface in shallow, sub-tropical Florida Bay: why denitrification efficiency may decrease with increased eutrophication. Biogeochemistry 95, 185–198. https://doi.org/10.1007/s10533-009-9329-5

Gardner, W.S., Mccarthy, M.J., An, S., Sobolev, D., Sell, K.S., Brock, D., 2006. Nitrogen Fixation and Dissimilatory Nitrate Reduction to Ammonium (DNRA) Support Nitrogen Dynamics in Texas Estuaries 51, 558–568.

Garnier, J., Bruno, L., Sanchez, N., Philippon, 1999. Biogeochemical mass-balances (C, N, P, Si) in three large. Biogeochemistry 47, 119–146.

Garnier, J., Cébron, A., Tallec, G., Billen, G., Sebilo, M., Martinez, A., 2006. Nitrogen behaviour and nitrous oxide emission in the tidal Seine River estuary (France) as influenced by human activities in the upstream watershed. Biogeochemistry 77, 305–326. https://doi.org/10.1007/s10533-005-0544-4

Gin, K.Y.-H., Gopalakrishnan, A.P., 2010. Sediment Oxygen Demand and Nutrient Fluxes for a Tropical Reservoir in Singapore. J. Environ. Eng. 136, 78–85. https://doi.org/10.1061/(ASCE)EE.1943-7870.0000119

Gondwe, M.J., Guildford, S.J., Hecky, R.E., 2008. Planktonic nitrogen fixation in Lake Malawi/Nyasa. Hydrobiologia 596, 251–267. https://doi.org/10.1007/s10750-007-9101-6

Goolsby, D.A., Battaglin, W.A., 2001. Long-term changes in consentrations and flux fo nitrogen in the Mississippi River Basin, USA. Hydrol. Process. 15, 1209–1226. https://doi.org/10.1002/hyp.210

Granger, J., Wankel, S.D., 2016. Isotopic overprinting of nitrification on denitrification as a ubiquitous and unifying feature of environmental nitrogen cycling. Proc. Natl. Acad. Sci. 113, E6391–E6400. https://doi.org/10.1073/pnas.1601383113

Grantz, E.M., Haggard, B.E., Scott, J.T., 2014. Stoichiometric imbalance in rates of nitrogen and phosphorus retention, storage, and recycling can perpetuate nitrogen deficiency in highly-productive reservoirs. Limnol. Oceanogr. 59, 2203–2216. https://doi.org/10.4319/lo.2014.59.6.2203

Green, P. a., Vörösmarty, C.J., Meybeck, M., Galloway, J.N., Peterson, B.J., Boyer, E.W., 2004. Pre-industrial and contemporary fluxes of nitrogen through rivers: a global assessment based on typology. Biogeochemistry 68, 71–105. https://doi.org/10.1023/B:BIOG.0000025742.82155.92

Gruber, N., Galloway, J.N., 2008. An Earth-system perspective of the global nitrogen cycle. Nature 451, 293–6. https://doi.org/10.1038/nature06592

Guildford, S.J., Hecky, R.E., 2000. Total nitrogen, total phosphorus, and nutrient limitation in lakes and oceans: Is there a common relationship? Limnol. Oceanogr. 45, 1213–1223. https://doi.org/10.4319/lo.2000.45.6.1213

Gupta, H., Kao, S.J., Dai, M., 2012. The role of mega dams in reducing sediment fluxes: A case study of large Asian rivers. J. Hydrol. 464–465, 447–458. https://doi.org/10.1016/j.jhydrol.2012.07.038

Gurung, R.P., 2005. Modelling of eutrophication in Roxo reservoir, Alentejo, Portugal: a system dynamic based approach.

Hall, G.H., Jeffries, C., 1984. The contribution of nitrification in the water column and profundal sediments to the total oxygen deficit of the hypolimnion of a mesotrophic lake (Grasmere, English Lake District). Microb. Ecol. 10, 37–46. https://doi.org/10.1007/BF02011593

Han, H., Lu, X., Burger, D.F., Joshi, U.M., Zhang, L., 2014. Nitrogen dynamics at the sediment–water interface in a tropical reservoir. Ecol. Eng. 73, 146–153. https://doi.org/10.1016/j.ecoleng.2014.09.016

Harrison, J. a., Maranger, R.J., Alexander, R.B., Giblin, A.E., Jacinthe, P.-A., Mayorga, E., Seitzinger, S.P., Sobota, D.J., Wollheim, W.M., 2009. The regional and global significance of nitrogen removal in lakes and reservoirs. Biogeochemistry 93, 143–157. https://doi.org/10.1007/s10533-008-9272-x

Höhener, P., Gächter, R., Sciences, A., Science, E., Re-, L., 1994. Nitrogen cycling across the sediment-water interface in an eutrophic, artificially oxygenated lake. Aquat. Sci. 56, 115–132. https://doi.org/10.1007/BF00877203

Horne, a. J., Galat, D.L., 1985. Nitrogen fixation in an oligotrophic. saline desert lake: Pyramid Lake, Nevada. Limnol. Oceanogr. 30, 1229–1239. https://doi.org/10.4319/lo.1985.30.6.1229

Horváth, H., Mátyás, K., Süle, G., Présing, M., 2013. Contribution of nitrogen fixation to the external nitrogen load of a water quality control reservoir (Kis-Balaton Water Protection System, Hungary). Hydrobiologia 702, 255–265. https://doi.org/10.1007/s10750-012-1329-0

Howarth, R.W., Marino, R., Cole, J.J., 1988. Nitrogen fixation in freshwater, estuarine, and marine ecosystems. 2. Riogeochemical control. Limnol. Ocean. 33, 688–701. https://doi.org/10.4319/lo.1988.33.4_part_2.0688

Hur, J., Cho, J., 2012. Prediction of BOD, COD, and total nitrogen concentrations in a typical urban river using a fluorescence excitation-emission matrix with PARAFAC and UV absorption indices. Sensors 12, 972–986. https://doi.org/10.3390/s120100972

Imteaz, M.A., Asaeda, T., Lockington, D.A., 2003. Modelling the effects of inflow parameters on lake water quality. Environ. Model. Assess. 8, 63–70. https://doi.org/10.1023/A:1023905532180

Jacob, J., Sanders, T., Dähnke, K., 2016. Nitrite consumption and associated isotope changes during a river flood event. Biogeosciences 13, 5649–5659. https://doi.org/10.5194/bg-13-5649-2016

Jankowski, K., Schindler, D.E., Holtgrieve, G.W., 2012. Assessing nonpoint-source nitrogen loading and nitrogen fixation in lakes using δ15N and nutrient stoichiometry. Limnol. Oceanogr. 57, 671–683. https://doi.org/10.4319/lo.2012.57.3.0671

Jarvie, H.P., Whitton, B.A., Neal, C., 1998. Nitrogen and phosphorus in east coast British rivers: Speciation, sources and biological significance. Sci. Total Environ. https://doi.org/10.1016/S0048-9697(98)00109-0

Jones, J.G., Simon, B.M., 1981. Differences in Microbial Decomposition Processes in Profundal and Littoral Lake Sediments, with Particular Reference to the Nitrogen Cycle. Microbiology 123, 297–312. https://doi.org/10.1099/00221287-123-2-297

Judd, H.L., 2008. Newcastle Reservoir TMDL. Utah Department of Environmental Quality, Division of Water Quality, TMDL Section Cottonwood Wash TMDL.

Kaiser, D., Kowalski, N., Böttcher, M., Yan, B., Unger, D., 2015. Benthic Nutrient Fluxes from Mangrove Sediments of an Anthropogenically Impacted Estuary in Southern China. J. Mar. Sci.

Eng. 3, 466–491. https://doi.org/10.3390/jmse3020466

Kanta, S., Plangklang, B., Subsingha, W., 2014. World ' s largest Science , Technology & Medicine Open Access book publisher c. Energy Procedia 56, 604–609. https://doi.org/10.5772/711

Keffala, C., Galleguillos, M., Ghrabi, A., Vasel, J.L., 2011. Investigation of nitrification and denitrification in the sediment of wastewater stabilization ponds. Water. Air. Soil Pollut. 219, 389–399. https://doi.org/10.1007/s11270-010-0715-3

Kelso, B.H.L., Smith, R. V., Laughlin, R.J., Lennox, S.D., 1997. Dissimilatory nitrate reduction in anaerobic sediments leading to river nitrite accumulation. Appl. Environ. Microbiol. 63, 4679–4685.

Knobeloch, L., Salna, B., Hogan, A., Postle, J., Anderson, H., 2000. Blue Babies and Nitrate-Contaminated Well Water. Environ. Health Perspect. 108, 675–678. https://doi.org/10.1289/ehp.00108675

Knoll, L.B., Vanni, M.J., Renwick, W.H., Kollie, S., 2014. Burial rates and stoichiometry of sedimentary carbon, nitrogen and phosphorus in Midwestern US reservoirs. Freshw. Biol. 59, 2342–2353. https://doi.org/10.1111/fwb.12438

Koszelnik, P., Tomaszek, J.A., Gruca-Rokosz, R., 2007a. The significance of denitrification in relation to external loading and nitrogen retention in a mountain reservoir. Mar. Freshw. Res. 58, 818–826. https://doi.org/10.1071/MF07012

Koszelnik, P., Tomaszek, J.A., Gruca-Rokosz, R., 2007b. The significance of denitrification in relation to external loading and nitrogen retention in a mountain reservoir. Mar. Freshw. Res. 58, 818–826. https://doi.org/10.1071/MF07012

Krumins, V., Gehlen, M., Arndt, S., Van Cappellen, P., Regnier, P., 2013. Dissolved inorganic carbon and alkalinity fluxes from coastal marine sediments: Model estimates for different shelf environments and sensitivity to global change. Biogeosciences 10, 371–398. https://doi.org/10.5194/bg-10-371-2013

Kunz, M.J., Anselmetti, F.S., West, A., Wehrli, B., Vollenweider, A., Thüring, S., Senn, D.B., 2011a. Sediment accumulation and carbon, nitrogen, and phosphorus deposition in the large tropical reservoir Lake Kariba (Zambia/Zimbabwe). J. Geophys. Res. Biogeosciences 116, 1–13. https://doi.org/10.1029/2010JG001538

Kunz, M.J., Wüest, A., Wehrli, B., Landert, J., Senn, D.B., 2011b. Impact of a large tropical reservoir on riverine transport of sediment, carbon, and nutrients to downstream wetlands. Water Resour. Res. 47, 1–16. https://doi.org/10.1029/2011WR010996

LaBolle, E.M., Fogg, G.E., Eweis, J.B., Gravner, J., Leaist, D.G., 2008. Isotopic fractionation by diffusion in groundwater. Water Resour. Res. 44, 1–15. https://doi.org/10.1029/2006WR005264

Laursen, A.E., Seitzinger, S.P., 2002. Measurement of denitrification in rivers: an integrated, whole reach

approach. Hydrobiologia 485, 67–81. https://doi.org/10.1023/A:1021398431995

Laverman, A.M., Garnier, J. a, Mounier, E.M., Roose-Amsaleg, C.L., 2010. Nitrous oxide production kinetics during nitrate reduction in river sediments. Water Res. 44, 1753–64. https://doi.org/10.1016/j.watres.2009.11.050

Laverman, A.M., Meile, C., Van Cappellen, P., Wieringa, E.B.A., 2007. Vertical distribution of denitrification in an estuarine sediment: integrating sediment flowthrough reactor experiments and microprofiling via reactive transport modeling. Appl. Environ. Microbiol. 73, 40–47. https://doi.org/10.1128/AEM.01442-06

Lecroart, P., Schmidt, S., Anschutz, P., Jouanneau, J.-M., 2007. Modeling sensitivity of biodiffusion coefficient to seasonal bioturbation. J. Mar. Res. 65, 417–440. https://doi.org/10.1357/002224007781567630

Lehner, B., Liermann, C.R., Revenga, C., Vörömsmarty, C., Fekete, B., Crouzet, P., Döll, P., Endejan, M., Frenken, K., Magome, J., Nilsson, C., Robertson, J.C., Rödel, R., Sindorf, N., Wisser, D., 2011. High-resolution mapping of the world's reservoirs and dams for sustainable river-flow management. Front. Ecol. Environ. 9, 494–502. https://doi.org/10.1890/100125

Lerat, Y., 1990. Seasonal changes in pore water concentrations of nutrients and their diffusive fluxes at the sediment-water. J. Exp. Mar. Bio. Ecol. 135, 135–160. https://doi.org/10.1016/0022-0981(90)90012-2

Lévesque, L., Page, E., 2011. State of Lake Winnipeg : 1999 to 2007. Environment Canada, Manitoba Water Stewardship.

Levine, S.N., Lewis, W.M., 1984. Diel variation of nitrogen-fixation in Lake Valencia, Venezuela. Limnol. Oceanogr. 29, 887–893.

Levine, S.N., Schindler, D.W., 1999. Influence of nitrogen to phosphorus supply ratios and physicochemical conditions on cyanobacteria and phytoplankton species composition in the Experimental Lakes Area, Canada. Can. J. Fish. Aquat. Sci. 56, 451–466. https://doi.org/10.1139/f98-183

Liu, C., Kroeze, C., Hoekstra, A.Y., Gerbens-Leenes, W., 2012. Past and future trends in grey water footprints of anthropogenic nitrogen and phosphorus inputs to major world rivers. Ecol. Indic. 18, 42–49. https://doi.org/10.1016/j.ecolind.2011.10.005

Maavara, T., Dürr, H.H., Van Cappellen, P., 2014. Global Biogeochemical Cycles. AGU Publ. 1–14. https://doi.org/10.1002/2014GB004875.Received

Maavara, T., Lauerwald, R., Regnier, P., Van Cappellen, P., 2017. Global perturbation of organic carbon cycling by river damming. Nat. Commun. 8. https://doi.org/10.1038/ncomms15347

Maavara, T., Parsons, C.T., Ridenour, C., Stojanovic, S., Dürr, H.H., Powley, H.R., Van Cappellen, P.,

2015. Global phosphorus retention by river damming. Proc. Natl. Acad. Sci. U. S. A. 112, 15603–8. https://doi.org/10.1073/pnas.1511797112

Maberly, S.C., King, L., Dent, M.M., Jones, R.I., Gibson, C.E., 2002. Nutrient limitation of phytoplankton and periphyton growth in upland lakes. Freshw. Biol. 47, 2136–2152. https://doi.org/10.1046/j.1365-2427.2002.00962.x

Mackenzie, F.T., Ver, L.M., Lerman, A., 2002. Century-scale nitrogen and phosphorus controls of the carbon cycle. Chem. Geol. 190, 13–32. https://doi.org/10.1016/S0009-2541(02)00108-0

Marcé, R., Moreno-Ostos, E., García-Barcina, J.M., Armengol, J., 2010. Tailoring dam structures to water quality predictions in new reservoir projects: Assisting decision-making using numerical modeling. J. Environ. Manage. 91, 1255–1267. https://doi.org/10.1016/j.jenvman.2010.01.014

Massoudieh, A., Bombardelli, F.A., Ginn, T.R., 2010. A biogeochemical model of contaminant fate and transport in river waters and sediments. J. Contam. Hydrol. 112, 103–117. https://doi.org/10.1016/j.jconhyd.2009.11.001

Mayorga, E., Seitzinger, S.P., Harrison, J.A., Dumont, E., Beusen, A.H.W., Bouwman, A.F., Fekete, B.M., Kroeze, C., Van Drecht, G., 2010. Global Nutrient Export from WaterSheds 2 (NEWS 2): Model development and implementation. Environ. Model. Softw. 25, 837–853. https://doi.org/10.1016/j.envsoft.2010.01.007

McCarthy, M.J., Lavrentyev, P.J., Yang, L., Zhang, L., Chen, Y., Qin, B., Gardner, W.S., 2007. Nitrogen dynamics and microbial food web structure during a summer cyanobacterial bloom in a subtropical, shallow, well-mixed, eutrophic lake (Lake Taihu, China). Hydrobiologia 581, 195–207. https://doi.org/10.1007/s10750-006-0496-2

Meile, C., Van Cappellen, P., 2003. Global estimates of enhanced solute transport in marine sediments. Limnol. Oceanogr. 48, 777–786. https://doi.org/10.4319/lo.2003.48.2.0777

Meybeck, M., 1982. Carbon, nitrogen, and phosphorus transport by world rivers. Am. J. Sci. 282, 401–450. https://doi.org/10.2475/ajs.282.4.401

Meyer, R.L., Allen, D.E., Schmidt, S., 2008. Nitrification and denitrification as sources of sediment nitrous oxide production: A microsensor approach. Mar. Chem. 110, 68–76. https://doi.org/10.1016/j.marchem.2008.02.004

Meyer, R.L., Risgaard-Petersen, N., Allen, D.E., 2005. Correlation between anammox activity and microscale distribution of nitrite in a subtropical mangrove sediment. Appl. Environ. Microbiol. 71, 6142–9. https://doi.org/10.1128/AEM.71.10.6142-6149.2005

Möbius, J., 2013. Isotope fractionation during nitrogen remineralization (ammonification): Implications for nitrogen isotope biogeochemistry. Geochim. Cosmochim. Acta 105, 422–432. https://doi.org/10.1016/j.gca.2012.11.048

Mordy, C.W., Eisner, L.B., Proctor, P., Stabeno, P., Devol, A.H., Shull, D.H., Napp, J.M., Whitledge, T., 2010. Temporary uncoupling of the marine nitrogen cycle: Accumulation of nitrite on the Bering Sea shelf. Mar. Chem. 121, 157–166. https://doi.org/10.1016/j.marchem.2010.04.004

Mozeto, A. a., Silvério, P.F., Soares, A., 2001. Estimates of benthic fluxes of nutrients across the sediment-water interface (Guarapiranga reservoir, Sao Paulo, Brazil). Sci. Total Environ. 266, 135–142. https://doi.org/10.1016/S0048-9697(00)00726-9

Mugidde, R., 2001. Status and Planktonic Nitrogen Fixation in Lake Victoria, Africa. Methods 196.

Mugidde, R., Hecky, R.E., Hendzel, L.L., Taylor, W.D., 2003. Pelagic Nitrogen Fixation in Lake Victoria (East Africa). J. Great Lakes Res. 29, 76–88. https://doi.org/10.1016/S0380-1330(03)70540-1

Naeher, S., Huguet, A., Roose-Amsaleg, C.L., Laverman, A.M., Fosse, C., Lehmann, M.F., Derenne, S., Zopfi, J., 2015. Molecular and geochemical constraints on anaerobic ammonium oxidation (anammox) in a riparian zone of the Seine Estuary (France). Biogeochemistry. https://doi.org/10.1007/s10533-014-0066-z

Ndegwa, P.M., Hristov, A.N., Arogo, J., Sheffield, R.E., 2008. A review of ammonia emission mitigation techniques for concentrated animal feeding operations. Biosyst. Eng. 100, 453–469. https://doi.org/10.1016/j.biosystemseng.2008.05.010

Némery, J., Gratiot, N., Doan, P.T.K., Duvert, C., Alvarado-Villanueva, R., Duwig, C., 2016. Carbon, nitrogen, phosphorus, and sediment sources and retention in a small eutrophic tropical reservoir. Aquat. Sci. 78, 171–189. https://doi.org/10.1007/s00027-015-0416-5

Nõges, T., Laugaste, R., Nõges, P., Tõnno, I., 2008. Critical N:P ratio for cyanobacteria and N2-fixing species in the large shallow temperate lakes Peipsi and Võrtsjärv, North-East Europe. Hydrobiologia 599, 77–86. https://doi.org/10.1007/s10750-007-9195-x

Oenema, O., Bleeker, A., Braathen, N.A., Budňáková, M., Bull, K., Čermák, P., Geupel, M., Hicks, K., Hoft, R., Kozlova, N., Leip, A., Spranger, T., Valli, L., Velthof, G., Winiwarter, W., 2011. Nitrogen in current European policies. Eur. Nitrogen Assess. 62–81.

Özkundakci, D., Hamilton, D., Trolle, D., 2011. Modelling the response of a highly eutrophic lake to reductions in external and internal nutrient loading. New Zeal. J. Mar. Freshw. Res. 45, 165–185. https://doi.org/10.1080/00288330.2010.548072

Paerl, H.W., Tucker, C.S., 1995. Ecology of Blue-Green Algae in Aquaculture Ponds. J. World Aquac. Soc. 26, 109–131. https://doi.org/10.1111/j.1749-7345.1995.tb00235.x

Pahl, R., 2007. Trends in Nutrient Loads to Lahontan Reservoir.

Paraska, D.W., Hipsey, M.R., Salmon, S.U., 2014. Sediment diagenesis models: Review of approaches, challenges and opportunities. Environ. Model. Softw. 61, 297–325. https://doi.org/10.1016/j.envsoft.2014.05.011

Pauer, J., 2000. Nitrification in the water column and sediment of a hypereutrophic lake and adjoining river system. Water Res. 34, 1247–1254. https://doi.org/10.1016/S0043-1354(99)00258-4

Peña, M.A., Katsev, S., Oguz, T., Gilbert, D., 2010. Modeling dissolved oxygen dynamics and hypoxia. Biogeosciences 7, 933–957. https://doi.org/10.5194/bg-7-933-2010

Persson, G., 2003. Nitrogen retention in lakes in Sweden; a review. Dep Environ. assessment, SLU Rapp.

Philips, S., Laanbroek, H.J., Verstraete, W., 2002. Origin, causes and effects of increased nitrite concentrations in aquatic environments. Rev. Environ. Sci. Bio/Technology 1, 115–141. https://doi.org/10.1023/A:1020892826575

Pinto, P. de T., Litchman, E., 2010. Interactive effects of N:P ratios and light on nitrogen-fixer abundance. Oikos 119, 567–575. https://doi.org/10.1111/j.1600-0706.2009.17924.x

Poff, N.L., Hart, D.D., 2002. How Dams Vary and Why It Matters for the Emerging Science of Dam Removal. Bioscience 52, 659. https://doi.org/10.1641/0006-3568(2002)052[0659:HDVAWI]2.0.CO;2

Policht-latawiec, A., 2013. Assessment of water inflowing, stored and flowing away from Mściwojów reservoir 107–115.

Quan, T.M., Falkowski, P.G., 2009. Redox control of N:P ratios in aquatic ecosystems. Geobiology 7, 124–139. https://doi.org/10.1111/j.1472-4669.2008.00182.x

Rabalais, N.N., Díaz, R.J., Levin, L.A., Turner, R.E., Gilbert, D., Zhang, J., 2010. Dynamics and distribution of natural and human-caused hypoxia. Biogeosciences 7, 585–619. https://doi.org/10.5194/bg-7-585-2010

Raimonet, M., Cazier, T., Rocher, V., Laverman, A.M., 2017. Nitrifying Kinetics and the Persistence of Nitrite in the Seine River, France. J. Environ. Qual. 595, 585–595. https://doi.org/10.2134/jeq2016.06.0242

Raimonet, M., Vilmin, L., Flipo, N., Rocher, V., Laverman, A.M., 2015. Modelling the fate of nitrite in an urbanized river using experimentally obtained nitrifier growth parameters. Water Res. 73, 373–387. https://doi.org/10.1016/j.watres.2015.01.026

Ramírez-Zierold, J.A., Merino-Ibarra, M., Monroy-Ríos, E., Olson, M., Castillo, F.S., Gallegos, M.E., Vilaclara, G., 2010. Changing water, phosphorus and nitrogen budgets for Valle de Bravo reservoir, water supply for Mexico City Metropolitan Area. Lake Reserv. Manag. 26, 23–34. https://doi.org/10.1080/07438140903539790

Ren, C., Wang, L., Zheng, B., Holbach, A., 2015. Total nitrogen sources of the three Gorges reservoir - A spatio-temporal approach. PLoS One 10, 1–17. https://doi.org/10.1371/journal.pone.0141458

Revsbech, N.P., 1989. An oxygen microsensor with a guard cathode. Limnol. Oceanogr. 34, 474–478. https://doi.org/10.4319/lo.1989.34.2.0474

Revsbech, N.P., Jørgensen, B.B., 1986. Microelectrodes: Their Use in Microbial Ecology, in: Marshall, K.C. (Ed.), Advances in Microbial Ecology, Advances in Microbial Ecology. Springer US, pp. 293–352.

Richardson, D., Felgate, H., Watmough, N., Thomson, A., Baggs, E., 2009. Mitigating release of the potent greenhouse gas N2O from the nitrogen cycle – could enzymic regulation hold the key? Trends Biotechnol. 27, 388–397. https://doi.org/10.1016/j.tibtech.2009.03.009

Rocher, V., Garcia-Gonzalez, E., Paffoni, C., Thomas, W., 2015. La production de nitrites lors de la dénitrification des eaux usées : un sujet sensible et complexe !L'Eau, l'Industrie, les Nuisances 344, 80–83.

Rodier, J., 1984. In: Dunod (Ed.), L'analyse de l'eau (eaux naturelles, eaux re´ siduaires, eau de mer), seventh ed, Paris, 1364pp.

Romero, J.R., Antenucci, J.P., Imberger, J., 2004. One- and three-dimensional biogeochemical simulations of two differing reservoirs. Ecol. Modell. 174, 143–160. https://doi.org/10.1016/j.ecolmodel.2004.01.005

Rong, N., Shan, B., Wang, C., 2016. Determination of Sediment Oxygen Demand in the Ziya River Watershed, China: Based on Laboratory Core Incubation and Microelectrode Measurements. Int. J. Environ. Res. Public Health 13, 232. https://doi.org/10.3390/ijerph13020232

Rooze, J., Meile, C., 2016. The effect of redox conditions and bioirrigation on nitrogen isotope fractionation in marine sediments. Geochim. Cosmochim. Acta 184, 227–239. https://doi.org/10.1016/j.gca.2016.04.040

Rosamond, M.S., Thuss, S.J., Schiff, S.L., 2012. Dependence of riverine nitrous oxide emissions on dissolved oxygen levels. Nat. Geosci. 5, 715–718. https://doi.org/10.1038/ngeo1556

Rysgaard, S., Risgaard-Petersen, N., Sloth, N.P., Jensen, K., Nielsen, L.P., 1994. Oxygen regulation of nitrification and denitrification in freshwater sediments. Limnol. Oceanogr. 39, 1643–1652.

Schindler, D.W., 2012. The dilemma of controlling cultural eutrophication of lakes. Proc. Biol. Sci. 279, 4322–33. https://doi.org/10.1098/rspb.2012.1032

Schindler, D.W., Hecky, R.E., Findlay, D.L., Stainton, M.P., Parker, B.R., Paterson, M.J., Beaty, K.G., Lyng, M., Kasian, S.E.M., 2008. Eutrophication of lakes cannot be controlled by reducing nitrogen input: Results of a 37-year whole-ecosystem experiment. Proc. Natl. Acad. Sci. 105, 11254–11258. https://doi.org/10.1073/pnas.0805108105

Schladow, S.G., Hamilton, D.P., 1997. Prediction of water quality in lakes and reservoirs: Part II - Model calibration, sensitivity analysis and application. Ecol. Modell. 96, 111–123. https://doi.org/10.1016/S0304-3800(96)00063-4

Schlesinger, W.H., Reckhow, K.H., Bernhardt, E.S., 2006. Global change: The nitrogen cycle and rivers.

Water Resour. Res. 42, 5–6. https://doi.org/10.1029/2005WR004300

Scott, J.T., Stanley, J.K., Doyle, R.D., Forbes, M.G., Brooks, B.W., 2009. River–reservoir transition zones are nitrogen fixation hot spots regardless of ecosystem trophic state. Hydrobiologia 625, 61–68. https://doi.org/10.1007/s10750-008-9696-2

Seitzinger, S., 1994. Linkages between organic matter mineralization and denitrification in eight riparian wetlands. Biogeochemistry 25, 19–39. https://doi.org/10.1007/BF00000510

Seitzinger, S.P., 1988. Denitrification in freshwater and coastal marine ecosystems: Ecological and geochemical significance. Limnol. Oceanogr. 33, 702–724. https://doi.org/10.4319/lo.1988.33.4_part_2.0702

Seitzinger, S.P., Harrison, J.A., Dumont, E., Beusen, A.H.W., Bouwman, A.F., 2005. Sources and delivery of carbon, nitrogen, and phosphorus to the coastal zone: An overview of Global Nutrient Export from Watersheds (NEWS) models and their application. Global Biogeochem. Cycles 19, 1–11. https://doi.org/10.1029/2005GB002606

Seitzinger, S.P., Mayorga, E., Bouwman, A.F., Kroeze, C., Beusen, A.H.W., Billen, G., Van Drecht, G., Dumont, E., Fekete, B.M., Garnier, J., Harrison, J.A., 2010. Global river nutrient export: A scenario analysis of past and future trends. Global Biogeochem. Cycles 24. https://doi.org/10.1029/2009GB003587

Shen, L., Liu, S., He, Z., Lian, X., Huang, Q., He, Y., Lou, L., Xu, X., Zheng, P., Hu, B., 2015. Depth-specific distribution and importance of nitrite-dependent anaerobic ammonium and methane-oxidising bacteria in an urban wetland. Soil Biol. Biochem. 83, 43–51. https://doi.org/10.1016/j.soilbio.2015.01.010

Sigman, D.M., DiFiore, P.J., Hain, M.P., Deutsch, C., Wang, Y., Karl, D.M., Knapp, A.N., Lehmann, M.F., Pantoja, S., 2009. The dual isotopes of deep nitrate as a constraint on the cycle and budget of oceanic fixed nitrogen. Deep. Res. Part I Oceanogr. Res. Pap. 56, 1419–1439. https://doi.org/10.1016/j.dsr.2009.04.007

Søballe, D.M., Kimmel, B.L., 1987. A Large-Scale Comparison of Factors Influencing Phytoplankton Abundance in Rivers , Lakes , and Impoundments 68, 1943–1954.

Soetaert, K., Middelburg, J.J., Herman, P.M.J., Buis, K., 2000. On the coupling of benthic and pelagic biogeochemical models. Earth Sci. Rev. 51, 173–201. https://doi.org/10.1016/S0012-8252(00)00004-0

Sprague, L.A., Kimbrough, R.A., Ranalli, A.J., 2002. What happens to nutrients in offstream reservoirs in the lower South Platte River Basin. Usgs NAWQA, 1–6.

Stein, L.Y., 2015. Microbiology: Cyanate fuels the nitrogen cycle. Nature 524, 43–44. https://doi.org/10.1038/nature14639

Stief, P., Beer, D., Neumann, D., 2002. Small-Scale Distribution of Interstitial Nitrite in Freshwater Sediment Microcosms: The Role of Nitrate and Oxygen Availability, and Sediment Permeability. Microb. Ecol. 43, 367–377. https://doi.org/10.1007/s00248-002-2008-x

Stief, P., de Beer, D., 2006. Probing the microenvironment of freshwater sediment macrofauna: Implications of deposit-feeding and bioirrigation for nitrogen cycling. Limnol. Oceanogr. 51, 2538–2548. https://doi.org/10.4319/lo.2006.51.6.2538

Straškraba, M., Tundisi, J.G., Duncan, A. (Annie), 1993. Comparative Reservoir Limnology and Water Quality Management. Springer Netherlands, Dordrecht. https://doi.org/10.1007/978-94-017-1096-1

Strauss, E. a, Richardson, W.B., Bartsch, L. a., Cavanaugh, J.C., Bruesewitz, D. a., Imker, H., Heinz, J. a, Soballe, D.M., 2004. Nitrification in the Upper Mississippi River: patterns , controls , and contribution to the NO3- budget. J. North Am. Benthol. Soc. 23, 1–14. https://doi.org/10.1899/0887-3593(2004)023<0001:NITUMR>2.0.CO;2

Strous, M., Kuenen, J.G., Jetten, M.S.M., 1999. Key physiology of anaerobic ammonium oxidation. Appl. Environ. Microbiol. 65, 3248–3250.

Sun, R., Chen, L., Chen, W., Ji, Y., 2013. Effect of land-use patterns on total nitrogen concentration in the upstream regions of the haihe river basin, China. Environ. Manage. 51, 45–58. https://doi.org/10.1007/s00267-011-9764-7

Sweerts, J.-P.R.A., Beer, D. de, 1989. Microelectrode Measurements of Nitrate Gradients in the Littoral and Profundal Sediments of a Meso-Eutrophic Lake (Lake Vechten, The Netherlands). Appl. Environ. Microbiol. 55, 754–757.

Thamdrup, B., 2012. New Pathways and Processes in the Global Nitrogen Cycle. Annu. Rev. Ecol. Evol. Syst. 43, 407–428. https://doi.org/10.1146/annurev-ecolsys-102710-145048

Thamdrup, B.O., Dalsgaard, T., 2008. Nitrogen cycling in sediments. In Microbial Ecology of the Oceans (ed. D. L. Kirchman), 2nd Edition, pp. 527-568. Jhon Wiley & sons Inc., Hoboken , New Jeresy.

Thouvenot-Korppoo, M., Billen, G., Garnier, J., 2009. Modelling benthic denitrification processes over a whole drainage network. J. Hydrol. 379, 239–250. https://doi.org/10.1016/j.jhydrol.2009.10.005

Thouvenot, M., Billen, G., Garnier, J., 2007. Modelling nutrient exchange at the sediment–water interface of river systems. J. Hydrol. 341, 55–78. https://doi.org/10.1016/j.jhydrol.2007.05.001

Toetz, D., McFarland, M., 1987. Lake loading (N:P) and lacustrine nitrogen fixation. Water Resour. Bull. AWRA 23, 239–241.

Tomaszek, J.A., Czerwieniec, E., 2003. Dentrification and oxygen consumption in bottom sediments: Factors influencing rates of the processes. Hydrobiologia 504, 59–65. https://doi.org/10.1023/B:HYDR.0000008508.81690.10

Tomaszek, J.A., Czerwieniec, E., 2000. In situ chamber denitrification measurements in reservoir

sediments: an example from southeast Poland. Ecol. Eng. 16, 61–71. https://doi.org/10.1016/S0925-8574(00)00090-2

Tomaszek, J.A., Koszelnik, P., 2003. A simple model of nitrogen retention in reservoirs. Hydrobiologia 504, 51–58. https://doi.org/10.1023/B:HYDR.0000008507.66924.23

Torres, E., Couture, R.M., Shafei, B., Nardi, A., Ayora, C., Van Cappellen, P., 2015. Reactive transport modeling of early diagenesis in a reservoir lake affected by acid mine drainage: Trace metals, lake overturn, benthic fluxes and remediation. Chem. Geol. 419, 75–91. https://doi.org/10.1016/j.chemgeo.2015.10.023

Trimmer, M., Nicholls, J.C., Morley, N., Davies, C. a, Aldridge, J., 2005. Biphasic Behavior of Anammox Regulated by Nitrite and Nitrate in an Estuarine Sediment Biphasic Behavior of Anammox Regulated by Nitrite and Nitrate in an Estuarine Sediment. Society 71, 1923–1930. https://doi.org/10.1128/AEM.71.4.1923

Trinh, A.D., Meysman, F., Rochelle-Newall, E., Bonnet, M.P., 2012. Quantification of sediment-water interactions in a polluted tropical river through biogeochemical modeling. Global Biogeochem. Cycles 26, 1–15. https://doi.org/10.1029/2010GB003963

Udert, K.M., Larsen, T.A., Gujer, W., 2005. Chemical Nitrite Oxidation in Acid Solutions as a Consequence of Microbial Ammonium Oxidation. Environ. Sci. Technol. 39, 4066–4075. https://doi.org/10.1021/es048422m

Van Cappellen, P., Gaillard, J.-F., 1996. Biogochemical dynamics in aquatic sediments. Rev. Mineral. 34, 335–376.

Van Cappellen, P., Gaillard, J.-F., Rabouille, C., 1993. Biogeochemical transformations in sediments: Kinetic models of early diagenesis. Interact. C, N, P S Biogeochem. Cycles Glob. Chang. 4, 401–445. https://doi.org/10.1007/978-3-642-76064-8_17

Van Cappellen, P., Maavara, T., 2016. Rivers in the Anthropocene: Global scale modifications of riverine nutrient fluxes by damming. Ecohydrol. Hydrobiol. 16, 106–111. https://doi.org/10.1016/j.ecohyd.2016.04.001

Van Cappellen, P., Wang, Y., 1995. Metal cycling in sediments: Modeling the interplay of reaction and transport. In Metal Contaminated Aquatic Sediments (ed.H.E.Allen), pp. 21-64. Ann Arbor Press, Chelsea.

Van Den Berg, G.A., Gustav Loch, J.P., Van Der Heijdt, L.M., Zwolsman, J.J.G., 2000. Redox processes in recent sediments of the river Meuse, The Netherlands. Biogeochemistry 48, 217–235. https://doi.org/10.1023/A:1006268325889

Vandermeulen, H., Gemza, A., 1991. Fanshawe lake: the need for water quality management in southern ontario reservoirs. Water Resources Branch, Ontario Ministry of the Environment.

Vanni, M.J., Renwick, W.H., Bowling, A.M., Horgan, M.J., Christian, A.D., 2011. Nutrient stoichiometry of linked catchment-lake systems along a gradient of land use. Freshw. Biol. 56, 791–811. https://doi.org/10.1111/j.1365-2427.2010.02436.x

Vilmin, L., Aissa-Grouz, N., Garnier, J., Billen, G., Mouchel, J.-M., Poulin, M., Flipo, N., 2015. Impact of hydro-sedimentary processes on the dynamics of soluble reactive phosphorus in the Seine River. Biogeochemistry 122, 229–251. https://doi.org/10.1007/s10533-014-0038-3

Vilmin, L., Escoffier, N., Groleau, A., Poulin, M., Flipo, N., 2014. Modelling algae growth and dissolved oxygen in the Seine River downstream the Paris urban area : contribution of high frequency measurements 16, 7748.

von der Wiesche, M., Wetzel, A., 1998. Temporal and spatial dynamics of nitrite accumulation in the River Lahn. Water Res. 32, 1653–1661. https://doi.org/10.1016/S0043-1354(97)00376-X

Vörösmarty, C.J., Meybeck, M., Fekete, B., Sharma, K., Green, P., Syvitski, J.P.M., 2003. Anthropogenic sediment retention: Major global impact from registered river impoundments. Glob. Planet. Change 39, 169–190. https://doi.org/10.1016/S0921-8181(03)00023-7

Vrede, T., Ballantyne, A., Mille-Lindblom, C., Algesten, G., Gudasz, C., Lindahl, S., Brunberg, A.K., 2009. Effects of N : P loading ratios on phytoplankton community composition, primary production and N fixation in a eutrophic lake. Freshw. Biol. 54, 331–344. https://doi.org/10.1111/j.1365-2427.2008.02118.x

Wang, Y., Li, Z., Zhou, L., Feng, L., Fan, N., Shen, J., 2013. Effects of macrophyte-associated nitrogen cycling bacteria on denitrification in the sediments of the eutrophic Gonghu Bay, Taihu Lake. Hydrobiologia 700, 329–341. https://doi.org/10.1007/s10750-012-1241-7

Wang, Y., Van Cappellen, P., 1996. A multicomponent reactive transport model of early diagenesis: Application to redox cycling in coastal marine sediments. Geochim. Cosmochim. Acta 60, 2993–3014. https://doi.org/10.1016/0016-7037(96)00140-8

Ward, B.B., 2013. Nitrification, in: Reference Module in Earth Systems and Environmental Sciences. Elsevier, pp. 1–8. https://doi.org/10.1016/B978-0-12-409548-9.00697-7

Windolf, J., Jeppesen, E., Jensen, J., Kristensen, P., 1996. Modelling of seasonal variation in nitrogen retention and in-lake concentration: A four-year mass balance study in 16 shallow Danish lakes. Biogeochemistry 33. https://doi.org/10.1007/BF00000968

Wollheim, W.M., Vörösmarty, C.J., Bouwman, A.F., Green, P., Harrison, J., Linder, E., Peterson, B.J., Seitzinger, S.P., Syvitski, J.P.M., 2008. Global N removal by freshwater aquatic systems using a spatially distributed, within-basin approach. Global Biogeochem. Cycles 22. https://doi.org/10.1029/2007GB002963

Yoshinaga, I., Amano, T., Yamagishi, T., Okada, K., Ueda, S., Sako, Y., Suwa, Y., 2011. Distribution

and Diversity of Anaerobic Ammonium Oxidation (Anammox) Bacteria in the Sediment of a Eutrophic Freshwater Lake, Lake Kitaura, Japan. Microbes Environ. 26, 189–197. https://doi.org/10.1264/jsme2.ME10184

Yu, Y., Wu, J., Wang, X.Y., Zhang, Z.M., 2012. Degradation of Inorganic Nitrogen in Beiyun River of Beijing, China. Procedia Environ. Sci. 13, 1069–1075. https://doi.org/10.1016/j.proenv.2012.01.100

Zarfl, C., Lumsdon, A.E., Berlekamp, J., Tydecks, L., Tockner, K., 2015. A global boom in hydropower dam construction. Aquat. Sci. 77, 161–170. https://doi.org/10.1007/s00027-014-0377-0

Zhao, Y., Xia, Y., Kana, T.M., Wu, Y., Li, X., Yan, X., 2013. Seasonal variation and controlling factors of anaerobic ammonium oxidation in freshwater river sediments in the Taihu Lake region of China. Chemosphere 93, 2124–2131. https://doi.org/10.1016/j.chemosphere.2013.07.063

Zhu, G., Wang, S., Wang, W., Wang, Y., Zhou, L., Jiang, B., Op Den Camp, H.J.M., Risgaard-Petersen, N., Schwark, L., Peng, Y., Hefting, M.M., Jetten, M.S.M., Yin, C., 2013. Hotspots of anaerobic ammonium oxidation at land-freshwater interfaces. Nat. Geosci. 6, 103–107. https://doi.org/10.1038/ngeo1683